

การตรวจวัดแบบจำเพาะสูงของไบโอเจนิคแอมิน โดยใช้อนุภาคระดับนาโนเมตรของซิลิกาตัดแปร  
ด้วยฟลูออเรสเซนต์โพรบ

นางสาวเปรมฤดี พรหมเดช

จุฬาลงกรณ์มหาวิทยาลัย  
CHULALONGKORN UNIVERSITY

บทคัดย่อและแฟ้มข้อมูลฉบับเต็มของวิทยานิพนธ์ตั้งแต่ปีการศึกษา 2554 ที่ให้บริการในคลังปัญญาจุฬาฯ (CUIR)  
เป็นแฟ้มข้อมูลของนิสิตเจ้าของวิทยานิพนธ์ ที่ส่งผ่านทางบัณฑิตวิทยาลัย

The abstract and full text of theses from the academic year 2011 in Chulalongkorn University Intellectual Repository (CUIR)  
are the thesis authors' files submitted through the University Graduate School.

วิทยานิพนธ์นี้เป็นส่วนหนึ่งของการศึกษาตามหลักสูตรปริญญาวิทยาศาสตรมหาบัณฑิต

สาขาวิชาเคมี ภาควิชาเคมี

คณะวิทยาศาสตร์ จุฬาลงกรณ์มหาวิทยาลัย

ปีการศึกษา 2558

ลิขสิทธิ์ของจุฬาลงกรณ์มหาวิทยาลัย

HIGHLY SPECIFIC DETECTION OF BIOGENIC AMINES USING FLUORESCENCE-PROBE-MODIFIED SILICA NANOPARTICLES

Miss Premrudee Promdet



A Thesis Submitted in Partial Fulfillment of the Requirements  
for the Degree of Master of Science Program in Chemistry  
Department of Chemistry  
Faculty of Science  
Chulalongkorn University  
Academic Year 2015  
Copyright of Chulalongkorn University





## 5572049523 : MAJOR CHEMISTRY

KEYWORDS: O-PHTHALIC HEMITHIOACETAL / FRET / PET

PREMRUDEE PROMDET: HIGHLY SPECIFIC DETECTION OF BIOGENIC AMINES USING FLUORESCENCE-PROBE-MODIFIED SILICA NANOPARTICLES. ADVISOR: ASST. PROF. BOOSAYARAT TOMAPATANAGET, Ph.D., 118 pp.

A goal of this research is to design and synthesize chemosensors for detection of catecholamine and histidine in water solution. To enhance water solubility, silica nanosphere (SNPs) and mesoporous silica nanoparticles (MSNs) were applied as a solid support which was modified by *o*-phthalic hemithioacetal (OPTA) to detect primary amine and give high fluorescence emission of isoindole product as a donor fluorophore in the detection system. Moreover, CB and ZnC2 were designed and synthesized as acceptor fluorophores to specifically detect catecholamine and histidine, respectively. Studies on the specific detection of SNPs-OPTA and MSNs-OPTA toward various biogenic amines in phosphate buffer solution, pH 7.4 were found that all biogenic amines enable to form an isoindole product which displayed the emission band at 450 nm ( $\lambda_{\text{ex}} = 345\text{nm}$ ). Interestingly, histidine showed the highest fluorescence intensity of isoindole product. According to studies on the factors which influence on the binding ability of this system, it was proposed that the imidazole in histidine played important role as a self-catalyst in isoindole product formation. To discriminate the catecholamine, CB was applied to detect various biogenic amines in SNPs-OPTA solution. Interestingly, only dopamine and norepinephrine showed a significant influence on the fluorescence quenching of coumarin at 550 nm. Therefore, this new fluorescence sensor system to discriminate the catecholamine under photoinduced electron transfer (PET) process has been successfully developed. For detection of histidine, the fluorescence self-quenching of isoindole product and ZnC2 was observed as a hypothesis of orderly packing of naphthalimide based ZnC2 on the surface of silica (SNPs-OPTA). To avoid this effect, the system consisting of CTAB (SNPs-OPTA\_CTAB) was applied. The fluorescence responses of isoindole in SNPs-OPTA\_CTAB by varying amount of ZnC2 exhibited the promoting of energy transfer and the system showed high fluorescence intensity at 550 nm belonging to ZnC2 in case of histidine. It was clear that SNPs-OPTA and MSNs-OPTA offered the highly promising selectivity for histidine detection without the assistant of the acceptor fluorophore. However, the Fluorescence Resonance Energy Transfer (FRET) process is an expected benefit for higher wavelength of emission band to avoid the interference from biological matrix in sensing purpose.

Department: Chemistry

Student's Signature .....

Field of Study: Chemistry

Advisor's Signature .....

Academic Year: 2015

## ACKNOWLEDGEMENTS

I would like to thank my research advisor, Assistant Professor Dr. Boosayarat Tomapatanaget, for her valuable guidance, helpful suggestion and constant encouragement throughout this research. Furthermore, I would like to thank Professor Dr. Vinich Promarak and Dr. Duangratchaneekorn Muenmart from Vidyasirimedhi Institute of Science and Technology (VISTEC) for dynamic light scattering and zeta potential measurements, Dr. Gamolwan Tumcharern from National Nanotechnology Center (NANOTEC) for particle analysis under X-ray photoelectron spectroscopy (XPS). In addition, I would like to thank and pay my respect to Associate Professor Dr. Vudhichai Parasuk, Assistant Professor Dr. Anawat Ajavakom and Assistant Professor Dr. Jomjai Suksai for their valuable advices, useful suggestion and valuable comments as thesis committee.

This accomplishment could not occur without the support from Chulalongkorn University. Special thanks are due to Professor Dr. Thawatchai Tuntulani for financial support, beneficial suggestion and all members of Supramolecular Chemistry Research Unit at the department of Chemistry, Chulalongkorn University for their support and giving consultant throughout my research. Furthermore, I would like to thank the Development and Promotion of Science and Technology Talents Project (DPST), and Thailand Research Fund (TRF) for financial support.

Finally, I would like to thank all members of my family for their love, care, kindness, encouragement and financial support throughout my life.

## CONTENTS

	Page
THAI ABSTRACT .....	iv
ENGLISH ABSTRACT.....	v
ACKNOWLEDGEMENTS.....	vi
CONTENTS.....	vii
LIST OF FIGURES .....	xii
LIST OF SCHEMES.....	xviii
LIST OF TABLES.....	xix
LIST OF ABBREVIATIONS AND SYMBOLS .....	xxi
CHAPTER I INTRODUCTION.....	1
1.1 Mesoporous silica .....	2
1.2 Organically Functionalized Mesoporous Silica Phases [34] .....	2
1.2.1 Grafting (Post synthetic Functionalization of Silica).....	3
1.2.2 Co-condensation (Direct Synthesis).....	3
1.2.3 Preparation of Periodic Mesoporous Organosilicas (PMOs) .....	4
1.3 Functionalized silica materials applied for detection of biogenic amines .....	5
1.4 Determination of catecholamine by fluorescence spectrophotometry.....	9
1.5 Histidine fluorescent sensor by metal complexes.....	13
1.6 Ratio metric sensor under FRET mechanism .....	17
1.7 Concept of this study .....	25
1.8 Objective and scope of the research .....	27
CHAPTER II EXPERIMENTAL .....	28
2.1 General Procedure .....	28
2.1.1 Analytical measurements.....	28
2.1.2 Materials .....	28
2.2 Synthesis .....	29
2.2.1 Synthesis of SNPs-OPTA and SNPs-OPTA_CTAB .....	29
2.2.1.1 Preparation of silica nanospheres (SNPs) .....	29
2.2.1.2 Synthesis of SNPs-SH nanoparticles.....	29

	Page
2.2.1.3 Synthesis of SNPs-OPTA nanoparticles .....	29
2.2.1.4 Synthesis of SNPs-OPTA_CTAB nanoparticles.....	30
2.2.2 Characterization of SNPs and the modified SNPs .....	30
2.2.2.1 Size and morphology of silica nanoparticles.....	30
2.2.2.2 Study on accessible thiol density.....	30
2.2.3 Synthesis of MSNs-OPTA.....	31
2.2.3.1 Preparation of mesoporous silica nanoparticles (MSNs) .....	31
2.2.3.2 Synthesis of MSNs-SH nanoparticles .....	32
2.2.3.3 Synthesis of MSNs-OPTA nanoparticles .....	32
2.2.4 Characterization of MSNs and the modified MSNs.....	32
2.2.4.1 Size and morphology of mesoporous silica nanoparticles .....	32
2.2.4.2 Surface area and accessible thiol density .....	32
2.2.5 Synthesis of CB .....	33
2.2.5.1 Synthesis of A1 .....	33
2.2.5.2 Synthesis of CB .....	34
2.2.6 Synthesis of ZnC2.....	35
2.2.6.1 Synthesis of (2-Aminoethyl) carbamic acid tert-butyl ester, B1 ..	35
2.2.6.2 Synthesis of tert-Butyl 2-(bis(pyridin-2-ylmethyl)amino) ethylcarbamate, B2 .....	36
2.2.6.3 Synthesis of N-Bis-pyridin-2-ylmethylethane-1,2-diamine, B3 ..	36
2.2.6.4 Synthesis of C1 .....	37
2.2.6.5 Synthesis of C2.....	38
2.2.6.6 Synthesis of ZnC2 .....	39
2.2.7 Synthesis of ZnD2 .....	40
2.2.7.1 Synthesis of D1 .....	40
2.2.7.2 Synthesis of D2 .....	40
2.2.7.3 Synthesis of ZnD2.....	41
2.2.8 Synthesis of E1 .....	42
2.3 Complexation studies by fluorescence spectroscopy.....	43



	Page
2.3.1 Apparatus.....	43
2.3.2 Chemical.....	43
2.3.3 Experimental procedure.....	44
2.3.4 Complexation studies.....	44
2.3.4.1 Complexation studies in homogeneous solution of isoindole product with various biogenic amines .....	44
2.3.4.2 Complexation studies of SNPs-OPTA and CB with various biogenic amines .....	44
2.3.4.3 Complexation studies of SNPs-OPTA_CTAB and ZnC2.....	45
2.3.4.3A Energy transfer studies of ZnC2 in both SNPs-OPTA and SNPs-OPTA_CTAB systems .....	45
2.3.4.3B Complexation studies of SNPs-OPTA_CTAB and ZnC2 with various biogenic amines.....	46
2.3.4.3C Naked-eye studies of SNPs-OPTA_CTAB and SNPs- OPTA_CTAB consisting of ZnC2 with various biogenic amines.....	47
2.3.4.4 Complexation studies of MSNs-OPTA with various biogenic amines .....	49
2.3.4.4A Fluorescence responses of MSNs-OPTA in various biogenic amines.....	49
2.3.4.4B Naked-eye studies of MSNs-OPTA in various biogenic amines.....	49
2.3.4.4C Complexation study of sensor MSNs-OPTA with histidine by fluorescence spectrophotometric titration technique .....	50
2.3.4.4D Kinetic study of isoindole formation in MSNs-OPTA toward various biogenic amines.....	51
2.3.4.4E Study of the proposed mechanism of histidine in forming isiondole product .....	52
2.3.4.5 Complexation studies of MSNs-OPTA-CTAB and receptor molecules (ZnD2 and E2) with various biogenic amines.....	52
2.3.4.5A Suspension ability .....	52

	Page
2.3.4.5B Zeta potential and size distribution .....	53
2.3.4.5C Complexation studies of D2 toward various metal ions .....	54
2.3.4.5D Complexation studies of MSNs-OPTA-CTAB and ZnD2 prepared in buffer solution.....	55
2.3.4.5E Energy transfer studies of isoindole product of histidine in MSNs-OPTA-CTAB by D2 as a receptor...55	
2.3.4.5F Complexation studies of MSNs-OPTA and D2 with various biogenic amines .....	56
2.3.4.5G Energy transfer studies of isoindole product of histidine in MSNs-OPTA-CTAB by E2 as a receptor ...57	
CHAPTER III RESULTS AND DISCUSSIONS.....	58
3.1 Design and synthesis of biogenic amine base sensor .....	58
3.2 Synthesis and characterization.....	60
3.2.1 Synthesis of SNPs-OPTA and SNPs-OPTA_CTAB .....	60
3.2.2 Characterization of SNPs-OPTA .....	61
3.2.2.1 Size and morphology of the silica nanoparticles.....	61
3.2.2.2 Surface area and accessible thiol density .....	61
3.2.3 Synthesis of MSNs-OPTA.....	63
3.2.4 Characterization of MSNs-OPTA.....	64
3.2.4.1 Size and morphology of the mesoporous silica nanoparticles.....	64
3.2.4.2 Surface area and accessible thiol density .....	65
3.2.5 Synthesis and Characterization of CB .....	67
3.2.6 Synthesis and Characterization of ZnC2.....	68
3.2.7 Synthesis and Characterization of ZnD2.....	73
3.2.8 Synthesis and Characterization of E2.....	74
3.3 Complexation studies.....	75
3.3.1 Complexation studies in homogeneous solution of isoindole product with various biogenic amines .....	75

	Page
3.3.2 Complexation studies of SNPs-OPTA and CB with various biogenic amines.....	77
3.3.3 Complexation studies of SNPs-OPTA_CTAB and ZnC2 with biogenic amines.....	82
3.3.4 Complexation studies of MSNs-OPTA with various biogenic amines.....	85
3.3.5 Complexation studies of MSNs-OPTA-CTAB and receptor molecules (ZnD2 and E2) with various biogenic amines .....	90
3.3.5.1 Particle properties by varying concentration of CTAB.....	90
3.3.5.2 Complexation studies .....	94
CHAPTER IV CONCLUSION .....	99
REFERENCES .....	102
APPENDIX.....	109
VITA.....	118



## LIST OF FIGURES

<b>Figure 1.1</b>	Formation of mesoporous silica through liquid-crystal template mechanism .....	2
<b>Figure 1.2</b>	Grafting (post synthetic functionalization) for organic modification of mesoporous pure silica phases with terminal organosilanes of the type $(R'O)_3SiR$ , R = organic functional group .....	3
<b>Figure 1.3</b>	Co-condensation method (direct synthesis) for the organic modification of mesoporous pure silica phases, R = organic functional group .....	4
<b>Figure 1.4</b>	Preparation of Periodic Mesoporous that are constructed from bisilylated organic bridging units, R = bridge .....	5
<b>Figure 1.5</b>	The binding event of the fluorescent particles to dopamine in aqueous environment at neutral pH .....	5
<b>Figure 1.6</b>	Relative emission intensity of the fluorescent particles (0.3 mg/mL, sodium phosphate buffer, pH = 7.0, 32 °C, $\lambda_{em} = 432$ nm, $\lambda_{ex} = 342$ nm) in the presence of various concentrations of catechol, dopamine, or propylamine .....	6
<b>Figure 1.7</b>	Representation of the <i>o</i> -phthalic hemithioacetal (OPTA) functionalized mesoporous silica material and their fluorescent detection of amines. (R = siloxy, propyl, phenyl, or pentafluorophenyl groups), R'-NH <sub>2</sub> = dopamine or glucosamine .....	7
<b>Figure 1.8</b>	Kinetic measurements of the fluorescence detection of dopamine (a) and glucosamine (b) with OPTA-derivatized mesoporous silica grafted with secondary functional groups, such as silanol (M1: solid line), propyl (M2: dotted line), phenyl (M3: dashed line), and pentafluorophenyl (M4: dash-dotted line) groups. Fluorescence increase of OPTA-MX (X = 1 (●); 2 (○); 3 (▽); 4 (△) as a function of dopamine (c) and glucosamine (d) concentrations .....	8
<b>Figure 1.9</b>	Binding event between fluorescent sensor 1 and catecholamines under physiological conditions .....	9
<b>Figure 1.10</b>	Fluorescent sensor 2 recognizes L-DOPA through a combination of reversible interactions .....	11

- Figure 1.11** Normalized peak emission intensity of **2** in the presence of catechol, L-DOPA, and its natural precursors in buffered aqueous solutions (0.1 M MOPS, pH 7.2) with excitation wavelength of 430 nm ..... 11
- Figure 1.12** Structure of sensor **3** and propose binding mode of sensor **4** with dopamine ..... 12
- Figure 1.13** Fluorescence spectra of a) sensor **4** (3  $\mu$ M) upon the addition of dopamine in MeOH (excitation at 397 nm) b) sensor **3** (3  $\mu$ M) upon the addition of dopamine in 50% MeOH in 0.05 M HEPES buffer at pH 7.4 (excitation at 367 nm)..... 13
- Figure 1.14** Bond lengths and angles in one molecule of di(histidino)zinc..... 14
- Figure 1.15** Multipoint molecular recognition of tryptophane (trp) by the  $[\text{Zn}(\mathbf{5})]^{2+}$  system..... 14
- Figure 1.16** Titration of the  $[\text{Zn}(\mathbf{5})]^{2+}$  receptor with tryptophane (trp,  $\nabla$ ) and phenylalanine (phe,  $\blacktriangledown$ ) in methanolic solution..... 15
- Figure 1.17** Multipoint molecular recognition of tryptophane (trp) by the  $[\text{Zn}_2(\mathbf{6})]^{2+}$  system ..... 16
- Figure 1.18** Variation of the relative fluorescence intensity ( $IF$ , left vertical axis) and of the absorbance at 300 nm ( $A$ , right vertical axis) during the titration of  $9 \times 10^{-6}$  M  $[\text{Zn}_2(\mathbf{6})]^{2+}$ , buffered at pH 9.6, with imidazole, histidine and acetate: ( $\Delta$ )  $IF$  (imidazole); ( $\blacktriangle$ )  $A$  (imidazole); ( $\circ$ )  $IF$  (acetate); ( $\bullet$ )  $A$  (acetate); ( $\diamond$ )  $IF$  (L-histidine).  $n$  = number of equivalents of the added substrate ..... 17
- Figure 1.19** Structure of **8a** and **8b**, and schematic representation of the complexation between sensor **8b** and  $\text{Cu}^{2+}$  ions ..... 18
- Figure 1.20** A) Changes in the fluorescence spectrum of the **8b** (3  $\mu$ M) in 20% acetonitrile containing neutralmicelles TX-100 (2mM) with increase in addition of  $\text{Cu}^{2+}$  ions,  $[\text{Cu}^{2+}]$  (a) 0 and (j) 20  $\mu$ M (excitation wavelength = 339 nm) B) Relative changes in the fluorescence intensity of the **8b** (3  $\mu$ M) in the presence of various metal ions. Inset shows visual observation of fluorescence changes: (a) **8b** alone; (b-d) **8b** in the presence of  $\text{Cu}^{2+}$ ,  $\text{Li}^+$ ,  $\text{Hg}^{2+}$ , respectively; (e) equivalent mixture of various metal ions without  $\text{Cu}^{2+}$  ions; (f) equivalent mixture of various metal ions with  $\text{Cu}^{2+}$  ions..... 19
- Figure 1.21** A) The sensing mechanism of NRFTP for detection of cysteine. B) The emission spectra of NRFTP incubated with varying concentrations of cysteine. C) Confocal images of HeLa cells: (a-c)

	bright-field and fluorescence images of HeLa cells incubated with NRFTP; (d) overlay the images of panels a-c; (e-g) bright-field and fluorescence images of HeLa cells incubated with <i>N</i> -ethylmaleimide and then with NRFTP; (h) overlay the images of panels e-g .....	20
<b>Figure 1.22</b>	The proposed structure of the <b>PBA–DA–CA</b> complex inducing the FRET process .....	21
<b>Figure 1.23</b>	Fluorescence spectra of sensor <b>PBA</b> (1 mM) in buffer solution (100 mM Na <sub>2</sub> S <sub>2</sub> O <sub>3</sub> , 50 mM HEPES, 20 mM NaCl, pH 7.4) with various biogenic amines and inset: the relative fluorescence intensity of sensor <b>PBA</b> ( $\lambda_{\text{ex}} = 340$ nm) in the presence of various biogenic amines .....	22
<b>Figure 1.24</b>	Fluorescence spectra of the mixed sensors of <b>PBA</b> (1 mM) and <b>CA</b> (30 mM) in buffer solution (100 mM Na <sub>2</sub> S <sub>2</sub> O <sub>3</sub> , 50 mM HEPES, 20 mM NaCl, pH 7.4) with various biogenic amines and inset: relative fluorescence intensity of the mixed sensors of <b>PBA</b> and <b>CA</b> ( $\lambda_{\text{ex}} = 340$ nm) in the presence of various biogenic amines.....	22
<b>Figure 1.25</b>	Structure of <b>NB</b> and <b>CC</b> , and conceptual hypothesis of the dual fluorescence response mechanism.....	23
<b>Figure 1.26</b>	Fluorescence spectra of sensor <b>NB</b> ( $1 \times 10^{-5}$ M) in 1:9 v/v of DMSO: phosphate buffer at 0.01 M, pH 7.4 in the presence of 100 equivalents of various guests and the inset shows the fluorescence spectrum of sensor <b>NB</b> and <b>EPI</b> .....	24
<b>Figure 1.27</b>	Concept for detection of catecholamine .....	26
<b>Figure 1.28</b>	Concept for detection of histidine .....	26
<b>Figure 2.2</b>	The structures of various biogenic amines .....	43
<b>Figure 3.1</b>	TEM images of a) SNPs, b) SNPs-SH and c) SNPs-OPTA.....	61
<b>Figure 3.2</b>	Standard addition curve of 2-thiolpyridone for the investigation of accessible thiol group on SNPs-SH, in Tris buffer solution, pH 5, $\lambda_{\text{ab}} = 345$ nm.....	62
<b>Figure 3.3</b>	TEM image of mesoporous silica nanoparticles images of a) MSNs, b1) MSNs-SH (zoom out) and b2) MSNs-SH (zoom in) .....	64
<b>Figure 3.4</b>	XRD patterns of MSNs.....	64
<b>Figure 3.5</b>	a) nitrogen adsorption/desorption isotherms and b) pore size distribution of MSNs .....	65

<b>Figure 3.6</b>	Standard addition curve of 2-thiolpyridone for the investigation of accessible thiol group on MSNs-SH in Tris buffer solution, pH 5, $\lambda_{ab} = 340$ nm.....	66
<b>Figure 3.7</b>	The $^1\text{H-NMR}$ spectrum of sensor <b>CB</b> in $\text{DMSO-}d_6$ at 400 MHz.....	68
<b>Figure 3.8</b>	The $^1\text{H-NMR}$ spectrum of sensor <b>B3</b> in $\text{CDCl}_3$ at 400 MHz.....	69
<b>Figure 3.9</b>	The $^1\text{H-NMR}$ spectrum of sensor <b>C2</b> in $\text{CDCl}_3$ at 400 MHz.....	71
<b>Figure 3.10</b>	The $^1\text{H-NMR}$ spectrum of sensor <b>ZnC2</b> in $\text{CDCl}_3$ at 400 MHz.....	71
<b>Figure 3.11</b>	a) The ESI-High Resolution Mass spectrum of <b>ZnC2</b> complex, b) isotope peak of Zn (II) in <b>ZnC2</b> .....	72
<b>Figure 3.12</b>	The $^1\text{H-NMR}$ spectrum of sensor <b>D2</b> in $\text{CDCl}_3$ at 400 MHz.....	74
<b>Figure 3.13</b>	The $^1\text{H-NMR}$ spectrum of sensor <b>E2</b> in $\text{CDCl}_3$ at 400 MHz.....	75
<b>Figure 3.14</b>	a) Reaction between <i>o</i> -phthalaldehyde ( <b>OPA</b> ), 3-mercaptopropyl trimethoxysilane ( <b>SH</b> ) and amino acids to form isoindole product b) fluorescence responses with various biogenic amines in homogeneous solution of 25 mM <b>SH</b> and <b>OPA</b> in 0.01 M PBS, pH 7.4, $\lambda_{ex} = 345$ nm.....	76
<b>Figure 3.15</b>	a) Fluorescence spectra and b) relative intensity at $\lambda_{em} = 450$ nm of the isoindole product of 1.5 mg/mL SNPs-OPTA with various biogenic amines (125 $\mu\text{M}$ ) in phosphate buffer solution, pH 7.4, $\lambda_{ex} = 345$ nm.....	77
<b>Figure 3.16</b>	Emission spectra at excitation wavelength at 350 nm and 450 nm in 10 $\mu\text{M}$ <b>CB</b> in 0.01 M PBS pH 7.4.....	79
<b>Figure 3.17</b>	a) Fluorescence spectra and b) relative intensity (at emission wavelength = 550 nm) of emission band of <b>CB</b> in the presence of 1.5 mg/mL SNPs-OPTA and 250 $\mu\text{M}$ <b>CB</b> with various biogenic amines (125 $\mu\text{M}$ ) in phosphate buffer solution, pH 7.4, $\lambda_{ex} = 345$ nm.....	80
<b>Figure 3.18</b>	The proposed Photoinduced Electron Transfer (PET) of <b>CB</b> .....	81
<b>Figure 3.19</b>	Emission bands of various amount of <b>ZnC2</b> a) in SNPs-OPTA and b) in SNPs-OPTA_CTAB with 125 $\mu\text{M}$ histidine in 10 mM phosphate buffer solution, pH 7.4, $\lambda_{ex} = 345$ nm.....	82
<b>Figure 3.20</b>	Fluorescence emission responses of 1.5 mg/mL SNPs-OPTA_CTAB a) in the absence and b) in the presence of 0.2 M <b>ZnC2</b> toward various biogenic amines at the concentration of 125 $\mu\text{M}$ , in 10 mM phosphate buffer solution, pH 7.4, $\lambda_{ex} = 345$ nm c) Naked-eye studies under UV light of (a) and (b).....	84

- Figure 3.21** a) Fluorescence responses and b) images under UV light of the solution consisting of 0.75 mg/mL MSNs-OPTA toward various amino acids (125  $\mu$ M) namely alanine (Ala), glutamic acid (Glu), glycine (Gly), histidine (His), leucine (Leu), lysine (Lys) and phenylalanine (Phe) in 10 mM phosphate buffer solution, pH 7.4,  $\lambda_{\text{ex}} = 345$  nm stirred for 20 minutes .....86
- Figure 3.22** a) Fluorescence titration of MSNs-OPTA with histidine concentration (5-150  $\mu$ M), b) calibration curve plotted between fluorescence intensity and histidine concentration and c) plotted on a semi-log scale at emission intensity changing at 450 nm in 1.0 mg/mL MSNs-OPTA diluted in 10 mM phosphate buffer solution pH 7.4 stirred for 40 minutes,  $\lambda_{\text{ex}} = 345$  nm .....87
- Figure 3.23** Kinetic measurements of the fluorescence detection of OPTA-derivatized mesoporous silica (MSNs-OPTA) toward 150  $\mu$ M of various amino acid in 0.01 M phosphate buffer solution, excited wavelength of 345 nm .....88
- Figure 3.24** Effects of pH on fluorescence intensity of isoindole products .....90
- Figure 3.25** Naked-eye fluorescence studies of MSNs-OPTA-E2-CTAB at various concentration of CTAB (0, 0.25, 0.5, 1 and 2 mM, respectively) in the presence of 0.1 mM E2, 0.01 M phosphate buffer solution at pH 7.4 under UV light .....91
- Figure 3.26** a) Zeta potential of the MSNs-OPTA 0.45 mg/mL at different concentrations of CTAB (0–1 mM) b) size distributions of MSNs-OPTA and MSNs-OPTA-CTAB at 1.0 mM CTAB analyzed by laser diffraction .....93
- Figure 3.27** Fluorescence responses of D2 toward different metal ions namely Cu (II), Ni (II), Zn (II), Co (II), Cr (II) and Mn (II) in 1% DMSO:HEPES buffer (0.01M, pH7.4) with excitation at 450 nm.....94
- Figure 3.28** Fluorescence responses of isoindole product in the presence of D2 at various concentrations in MSNs-OPTA (0.45 mg/mL), 1 mM CTAB dispersed in phosphate buffer solution, pH 7.4,  $\lambda_{\text{ex}} = 345$  nm .....96
- Figure 3.29** Fluorescence responses of sensor MSNs-OPTA (0.45 mg/mL), 1 mM CTAB and 75  $\mu$ M D2 in 1% DMSO:phosphate buffer solution (0.01 M, pH 7.4) in the presence of 150  $\mu$ M of various amino acids,  $\lambda_{\text{ex}} = 345$  nm .....97



<b>Figure 3.30</b>	Fluorescence responses of sensor MSNs-OPTA (0.45 mg/mL), 1 mM CTAB and 75 $\mu$ M <b>D2</b> in 1% DMSO: phosphate buffer solution (0.01 M, pH 7.4) in the presence of 150 $\mu$ M histidine .....	97
<b>Figure A1</b>	The $^1\text{H}$ -NMR spectrum of sensor <b>CB</b> in DMSO- <i>d</i> 6 at 400 MHz .....	110
<b>Figure A2</b>	The $^{13}\text{C}$ -NMR spectrum of sensor <b>CB</b> in DMSO- <i>d</i> 6 at 400 MHz.....	110
<b>Figure A3</b>	MALDI-TOF mass spectrum of sensor <b>CB</b> shown at 380.373 m/z ....	111
<b>Figure A4</b>	The $^1\text{H}$ -NMR spectrum of <b>B1</b> in $\text{CDCl}_3$ at 400 MHz.....	111
<b>Figure A5</b>	The $^1\text{H}$ -NMR spectrum of <b>B2</b> in $\text{CDCl}_3$ at 400 MHz.....	112
<b>Figure A6</b>	The $^1\text{H}$ -NMR spectrum of <b>B3</b> in $\text{CDCl}_3$ at 400 MHz.....	112
<b>Figure A7</b>	The $^1\text{H}$ -NMR spectrum of <b>C1</b> in $\text{CDCl}_3$ at 400 MHz.....	113
<b>Figure A8</b>	The $^1\text{H}$ -NMR spectrum of <b>C2</b> in $\text{CDCl}_3$ at 400 MHz.....	113
<b>Figure A9</b>	The ESI-High Resolution Mass spectrum of sensor <b>C2</b> shown at 521.781 m/z .....	114
<b>Figure A10</b>	The $^1\text{H}$ -NMR spectrum of <b>ZnC2</b> in $\text{CDCl}_3$ at 400 MHz.....	114
<b>Figure A11</b>	The ESI-High Resolution Mass spectrum of sensor <b>ZnC2</b> shown at 620.1749 m/z .....	115
<b>Figure A12</b>	The ESI-High Resolution Mass spectrum of isotope peak of Zn (II) in sensor <b>ZnC2</b> .....	115
<b>Figure A13</b>	The $^1\text{H}$ -NMR spectrum of <b>D1</b> in $\text{CDCl}_3$ at 400 MHz.....	115
<b>Figure A14</b>	The $^1\text{H}$ -NMR spectrum of <b>D2</b> in $\text{CDCl}_3$ at 400 MHz.....	116
<b>Figure A15</b>	The ESI-High Resolution Mass spectrum of isotope peak of Zn (II) in sensor <b>D2</b> .....	116
<b>Figure A16</b>	The $^1\text{H}$ -NMR spectrum of <b>E2</b> in $\text{CDCl}_3$ at 400 MHz.....	116
<b>Figure A17</b>	Proposed mechanism for a self-catalyst of histidine to form isoindole product in physiological solution. ....	117

## LIST OF SCHEMES

<b>Scheme 2.1</b>	Schematic representation of reaction between thiol (-SH) group on silica surface of SNPs-SH and excess 2,2'-dithiodipyridine and byproduct (2-thiopyridone) in Tris buffer solution, pH 5, $\lambda_{ab} = 345$ nm.....	30
<b>Scheme 3.1</b>	Concept for detection of biogenic amines .....	59
<b>Scheme 3.2</b>	Synthesis pathway of SNPs-OPTA and SNPs-OPTA_CTAB .....	60
<b>Scheme 3.3</b>	Schematic representation of reaction between thiol (-SH) group on silica surface of SNPs-SH and excess 2,2'-dithiodipyridine and byproduct (2-thiopyridone) in Tris buffer solution, pH 5, $\lambda_{ab} = 340$ nm [51] .....	62
<b>Scheme 3.4</b>	Synthesis pathway of MSNs-OPTA .....	63
<b>Scheme 3.5</b>	Schematic representation of reaction between thiol (-SH) group on mesoporous silica surface (MSNs-SH) and excess 2,2'-dithiodipyridine and byproduct (2-thiopyridone) in Tris buffer solution, pH 5, $\lambda_{ab} = 345$ nm [51] .....	65
<b>Scheme 3.6</b>	Synthesis pathway of sensor <b>CB</b> .....	67
<b>Scheme 3.7</b>	Synthesis pathway of <b>B3</b> .....	68
<b>Scheme 3.8</b>	Synthesis pathway of sensor <b>ZnC2</b> .....	70
<b>Scheme 3.9</b>	Synthesis pathway of sensor <b>ZnD2</b> .....	73
<b>Scheme 3.10</b>	Synthesis pathway of <b>E2</b> .....	74
<b>Scheme 3.11</b>	Conceptual design for detection of catecholamine .....	78
<b>Scheme 3.12</b>	Binding event between fluorescent sensor <b>CB</b> and dopamine in the presence of piperidine under physiological condition.....	79
<b>Scheme 3.13</b>	Proposed mechanism for a self-catalyst of histidine to form isoindole product .....	89
<b>Scheme 3.14</b>	Proposed structures of histidine at different pH [60].....	89
<b>Scheme 3.15</b>	Possible scheme of CTAB mono- and bilayers on SiO <sub>2</sub> /water interface, when the CTAB concentration was increased [61].....	91
<b>Scheme 3.16</b>	Binding event between MSNs-OPTA-CTAB and acceptor fluorophores ( <b>D2</b> or <b>E2</b> ).....	98

## LIST OF TABLES

<b>Table 1.1</b>	Association constants obtained for complexation of sensor <b>1</b> with analytes (biogenic amine and monosaccharide) in 100 mM Na <sub>2</sub> S <sub>2</sub> O <sub>3</sub> , 50 mM HEPES, 20 mM NaCl, pH 7.0, 37 °C.....	10
<b>Table 2.1</b>	Amounts of chemical for accessible thiol density investigation on SNPs-SH .....	31
<b>Table 2.2</b>	Amounts of chemical for investigation of accessible thiol density on MSNs-SH .....	33
<b>Table 2.3</b>	Preparing stock solution of biogenic amines ( $1 \times 10^{-2}$ M).....	45
<b>Table 2.4</b>	The amounts of compounds in energy transfer studies of <b>ZnC2</b> in both SNPs-OPTA systems .....	46
<b>Table 2.5</b>	The amount of compounds in energy transfer studies of <b>ZnC2</b> in SNPs-OPTA_CTAB systems.....	46
<b>Table 2.6</b>	The amounts of guest and SNPs-OPTA_CTAB used for study on the naked-eye responses of isiondole product.....	48
<b>Table 2.7</b>	The amounts of guest, SNPs-OPTA_CTAB and <b>ZnC2</b> used for study on naked-eye responses of <b>ZnC2</b> in detection of various guest .....	48
<b>Table 2.8</b>	Preparation of stock solution of biogenic amines ( $1 \times 10^{-2}$ M).....	49
<b>Table 2.9</b>	The amounts of guest and SNPs-OPTA_CTAB used for study on the naked-eye responses of isiondole product in various biogenic amines .	50
<b>Table 2.10</b>	The concentration of histidine used for compexation study of MSNs-OPTA by fluorecence spectrophotometric titration technique .....	51
<b>Table 2.11</b>	Different kinds of buffer solution at various pHs .....	52
<b>Table 2.12</b>	The amounts of CTAB used for study on the physical properties of MSNs-OPTA-CTAB system.....	53
<b>Table 2.13</b>	The amounts of CTAB used for study on zeta potential and size distribution of MSNs-OPTA-CTAB system.....	54
<b>Table 2.14</b>	The amounts of metal ion, <b>D2</b> and buffer solution for complexation study of metal ion (II) .....	54
<b>Table 2.15</b>	The amounts of compounds for energy transfer studies of <b>D2</b> in MSNs-OPTA-CTAB systems .....	56

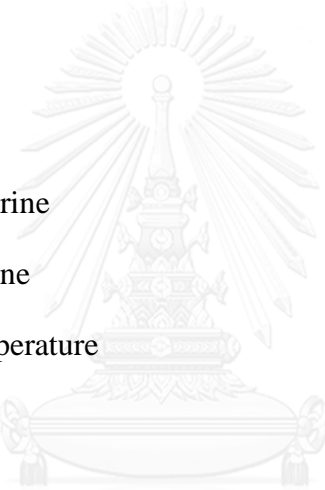
<b>Table 2.16</b>	The amounts of guest and MSNs-OPTA-CTAB used for study on visual changes of isiondole product in various biogenic amines .....57
-------------------	--



## LIST OF ABBREVIATIONS AND SYMBOLS

Ala	Alanine
Anal. Calcd.	Analysis calculated
$\delta$	Chemical shift
$^{13}\text{C-NMR}$	Carbon-13 nuclear magnetic resonance
$^{\circ}\text{C}$	Degree Celsius (centigrade)
$\text{CH}_2\text{Cl}_2$	Dichloromethane
DA	Dopamine
DMSO	Dimethyl sulfoxide
EPI	Epinephrine
ESI-HRMS	Electrospray Ionization High Resolution Mass Spectroscopy
EtOH	Ethanol
equiv	Equivalent
g	Gram
Glu	Glutamic acid
Gly	Glycine
$\text{g}\cdot\text{mol}^{-1}$	Gram per mole
$^1\text{H-NMR}$	Proton nuclear magnetic resonance
H	Hour
His	Histidine
Hist	Histamine
Hz	Hertz
$J$	Coupling constant
Leu	Leucine

Lys	L-lysine
m/z	Mass per charge ratio
$\mu\text{L}$	Microliter
$\mu\text{M}$	Micromolar
M	Molar
MeOH	Methanol
mg	Milligram
min	Minute
mL	Milliliter
mmol	Millimole
NE	Norepinephrine
Phe	Phenylalanine
rt	Room Temperature
Thre	Threonine
Tyr	Tyramine
s, d, t, m	Splitting patterns of $^1\text{H-NMR}$ (singlet, doublet, triplet, multiplet)
%	Percentage



จุฬาลงกรณ์มหาวิทยาลัย  
CHULALONGKORN UNIVERSITY

## CHAPTER I

### INTRODUCTION

Biogenic amine recognitions and sensing using artificial receptors have been current interest in supramolecular chemistry as biogenic amine plays important roles in many areas such as biology, medicine, and neuroscience [1-3]. A biogenic amine is a biogenic substance consisting of one or more amine groups involving in signaling. One of the high interesting biogenic amine is monoamine including neurotransmitters such as catecholamines, indolamines and histamine. Catecholamines are the phenylethylamine derivatives containing the phenolic *ortho*-hydroxy groups. The measurement of catecholamines, namely, dopamine, norepinephrine and epinephrine, is widely used in biological and diagnostic fields [4-6]. Patients suffering from phaeochromocytoma display a critically elevated concentration of the epinephrine in their blood which unavoidably leads to heart failure and death [7, 8]. Malfunction of the catecholamine dopamine-responsive neurons is a key feature for Parkinson's disease [9, 10]. Furthermore, the detection of histidine in body fluids, such as blood or urine, is an essential indicator in medical diagnostics, especially for patients suffering from histidinemia [11]. From this point of view, the development of catecholamines and histidine sensors that can selectively recognize the specific molecules is continually being developed. Usually, catecholamines analysis has been carried out by using high-resolution chromatography methods [12, 13] and electrochemical techniques due to the favorable redox properties of the catechol [14-16]. Moreover, NMR and mass spectroscopy have been used for determination of catecholamine by detection of complexes between catecholamine and creating receptors which bind specifically with catecholamines [17, 18]. Catecholamine chemosensors detected by fluorescence spectroscopy are one of highly selective and effective techniques. However, there is a minority of receptors that function in aqueous solution [19-22]. Aqueous recognitions of biogenic amines have been accomplished by using membrane-associated receptors [23, 24], sol gel films [25], RNA aptamers [26], and certain solid-state sensors [3, 27, 28].

Herein, we would like to develop chemosensors for detection of biogenic amine in an aqueous solution. To enhance water solubility, silica materials were applied as solid support. Mesoporous silica and silica nanosphere are attractive materials because of their interesting properties such as water solubility, chemically inert, thermally stable, harmless, and inexpensive. Therefore, the designs of fluorescent sensor by modification of the synthetic receptors on silica surface have been a great interest in developing biogenic amine sensors [27, 29].

### 1.1 Mesoporous silica

Mesoporous silica is a mesoporous form of silica and the most common types of mesoporous nanoparticles are MCM-41. These particles have a hexagonal array of pores achieved by building up hexagonal liquid-crystalline phase from rod micelles as a template to form the mesoporous framework in the synthesis solution. Cetyltrimethylammonium bromide (CTAB) is mostly used as surfactant in the synthesis of MCM-41. Adding silica species after forming the template, condensation reaction of silanol group occurs around the rod micelles to cover these. The template can be removed by calcination or under acidic conditions [30]. The mechanism involved in formation of mesoporous silica is depicted in Fig. 1.1. The MCM-41 has been applied in many fields such as catalysis, drug delivery and sensors [31-33].

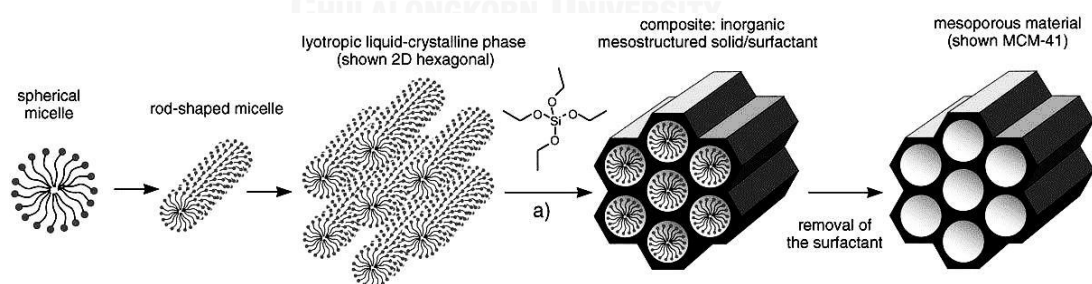


**Figure 1.1** Formation of mesoporous silica through liquid-crystal template mechanism

### 1.2 Organically Functionalized Mesoporous Silica Phases [34]

There are three ways to modify functionalities on silica surface namely by grafting, co-condensation, and periodic mesoporous organosilicas (PMOs).



### 1.2.1 Grafting (Post synthetic Functionalization of Silica)

Grafting process is achieved generally by reaction of organosilanes  $(R'O)_3SiR$ , or less frequently chlorosilanes  $ClSiR_3$  or silazanes  $HN(SiR_3)_3$  with the free silanol groups of the pore surfaces as shown in Fig. 1.2. Variation of the organic residue  $R$  produces functionalization with a variety of organic groups. Grafting refers to the modification of organic groups on pore surface of the inner surfaces of mesoporous silica. Pore blocking is a problem in the grafting method. Because of exclusive reaction of the organosilanes in the initial stages of the synthetic process, the diffusion of further molecules into the center of the pores can be decreased. Thus, a nonhomogeneous distribution and lower occupation of the organic groups within the pores can occur.

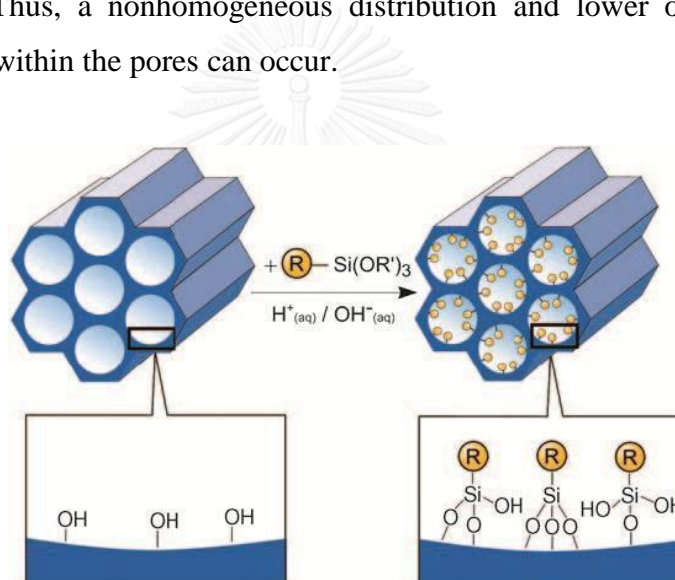


**Figure 1.2** Grafting (post synthetic functionalization) for organic modification of mesoporous pure silica phases with terminal organosilanes of the type  $(R'O)_3SiR$ ,  $R =$  organic functional group

### 1.2.2 Co-condensation (Direct Synthesis)

Co-condensation method or one-pot synthesis is an alternative method to synthesize organically functionalized mesoporous silica surface and avoid pore blocking. The particles are prepared by the co-condensation of tetraalkoxysilanes  $[(RO)_4Si(TEOS \text{ or } TMOS)]$  with terminal trialkoxyorganosilanes of the type  $(R'O)_3SiR$ . The method is depicted in Fig. 1.3. In co-condensation process, the organic functionalities are direct components of the silica matrix, so pore blocking is

not problem in incorporation. As a result, the organic groups are generally more homogeneous distribution than in materials synthesized with the grafting process.

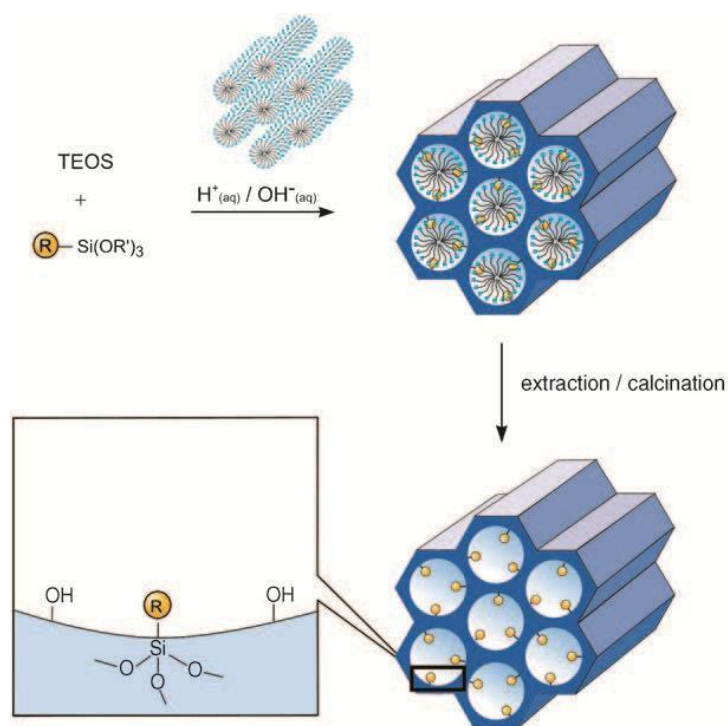


**Figure 1.3** Co-condensation method (direct synthesis) for the organic modification of mesoporous pure silica phases, R = organic functional group

### 1.2.3 Preparation of Periodic Mesoporous Organosilicas (PMOs)

Bridged organosilica precursors of the type  $(\text{R}'\text{O})_3\text{Si-R-Si(OR')}_3$  has been used for preparation of organic hybrid materials. Two covalent bonds of the bridged organosilica precursors in the silica matrix provide incorporated organic groups in three-dimensional network structure and totally homogeneous distribution in the pore walls. However, there are generally disordered pore systems of pore radii distribution. The method constructs a new class of structured organic hybrid materials called periodic mesoporous organosilicas (PMOs) in which the organic bridges are integral components of the silica network as shown in Fig. 1.4.

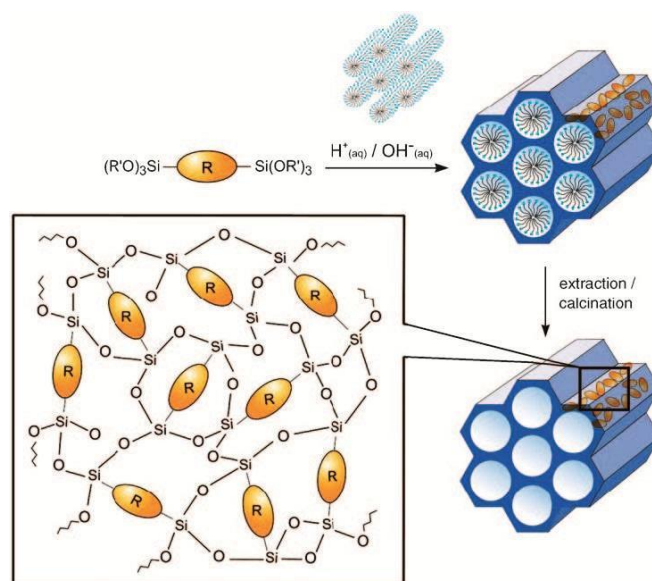


**Figure 1.4** Preparation of Periodic Mesoporous that are constructed from bisilylated organic bridging units,  $R = \text{bridge}$

### 1.3 Functionalized silica materials applied for detection of biogenic amines

In 2002, Raymo and Cejas [29] designed and synthesized fluorescent sensor by modification of 2,7-diazapyrenium dication as fluorescent probe on surface of silica particles for detection of dopamine. The dication showing the electron-deficient character encouraged the supramolecular association of dopamine displaying the electron-rich feature. The detection model is shown in Fig. 1.5.

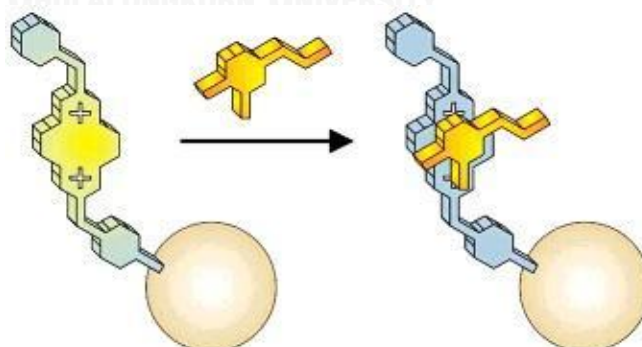


**Figure 1.5** The binding event of the fluorescent particles to dopamine in aqueous environment at neutral pH

The binding between the dications and dopamine produced a significant decrease in the fluorescence intensity. Model binding studies of catechol and propylamine revealed that no significant changes in the emission intensity was observed even at a relatively large propylamine concentration (ca. 0.01 M) but a pronounced fluorescence decay was observed for catechol. This result concluded that the interaction with the surface-confined electron-deficient dications involves the aromatic portion of dopamine. The result was demonstrated in Fig. 1.6.

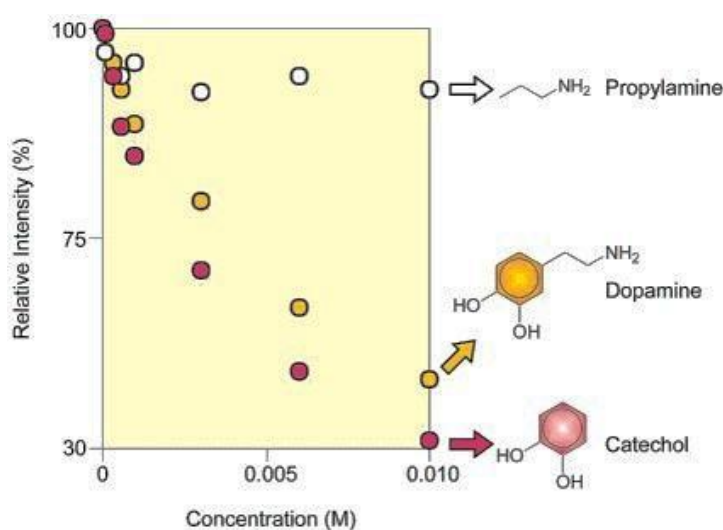


**Figure 1.6** Relative emission intensity of the fluorescent particles (0.3 mg/mL, sodium phosphate buffer, pH = 7.0, 32 °C,  $\lambda_{em} = 432$  nm,  $\lambda_{ex} = 342$  nm) in the presence of various concentrations of catechol, dopamine, or propylamine

Lin and co-workers [27] designed and synthesized fluorescence sensory particles to study the molecular recognition of biogenic molecules namely dopamine and glucosamine. Mesoporous silica was used as supporting matrix incorporated with a primary amine- sensitive *o*-phthalic hemithioacetal (OPTA) group on the pore-surface. The materials give advantage of the size-sieving ability that only small molecules can diffuse into the pores. And only amine compounds react with the OPTA group to provide high fluorescent intensity of isoindole products as shown in Fig. 1.7. Moreover, they prepared different type of multifunctionalized mesoporous silica to not only detect the target molecules with covalent interaction but also provide different secondary noncovalent interactions (hydrophobic and  $\pi$ - $\pi$  interactions) to

enhance the substrate selectivity by changing substrate accessibility and pore hydrophobicity. OPTA-mesoporous silica (OPTA-M1) and multifunctionalized mesoporous silica consisting of further functionalized groups of propyl, phenyl, and pentafluorophenyl to yield three other materials namely, OPTA-M2, OPTA-M3, and OPTA-M4, respectively. The reaction rate of dopamine and glucosamine complexation studied by fluorescence intensity at the emission of 440 nm belonging to isoindole was found that the selectivity depended on the pore environment in the mesoporous as shown in Fig. 1.8.

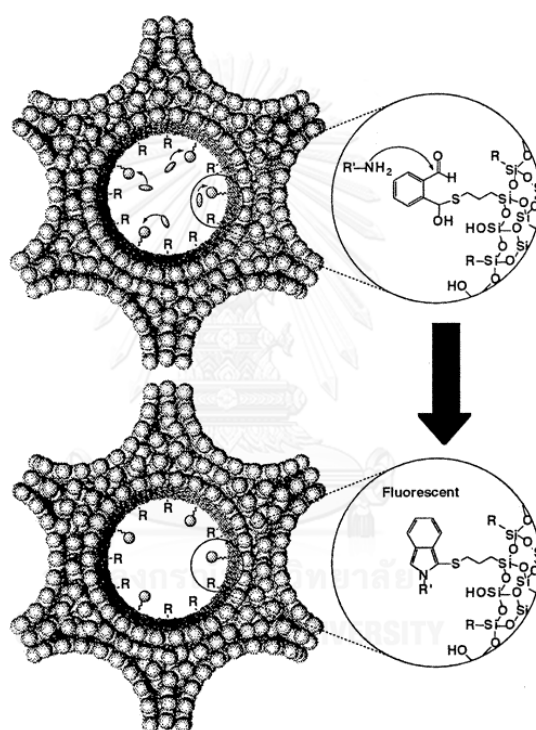


**Figure 1.7** Representation of the *o*-phthalic hemithioacetal (OPTA) functionalized mesoporous silica material and their fluorescent detection of amines. (R = siloxy, propyl, phenyl, or pentafluorophenyl groups), R'-NH<sub>2</sub> = dopamine or glucosamine

OPTA-M1 was the best materials in inducing both dopamine and glucosamine to react with the unit sensor. Reaction rates of glucosamine were considerably slower than dopamine because of a strong interaction between the abundant hydroxyl groups of glucosamine with silanol on the pore surface. The complexation of dopamine in OPTA-M4 gave a significantly higher increase of fluorescence intensities compared

to the propyl- and phenyl-functionalized pores of the OPTA-M2 and OPTA-M3 materials because of the better  $\pi$ - $\pi$  donor and acceptor type of stacking effect between the catechol rings of dopamine molecules and the pentafluorophenyl moieties of the OPTA-M4. The hydrophobic propyl-functionalized OPTA-M2 material discouraged the intercalation of dopamine. The same fluorescence study for glucosamine binding to OPTA-M2, 3 and 4 showed only small increases of fluorescence intensities with increasing glucosamine concentrations. These data further supported the possibility that the nonaromatic glucosamine molecules could not easily diffuse into the propyl-, phenyl-, or pentafluorophenyl-functionalized particles due to the hydrophobic environment inside the pores.

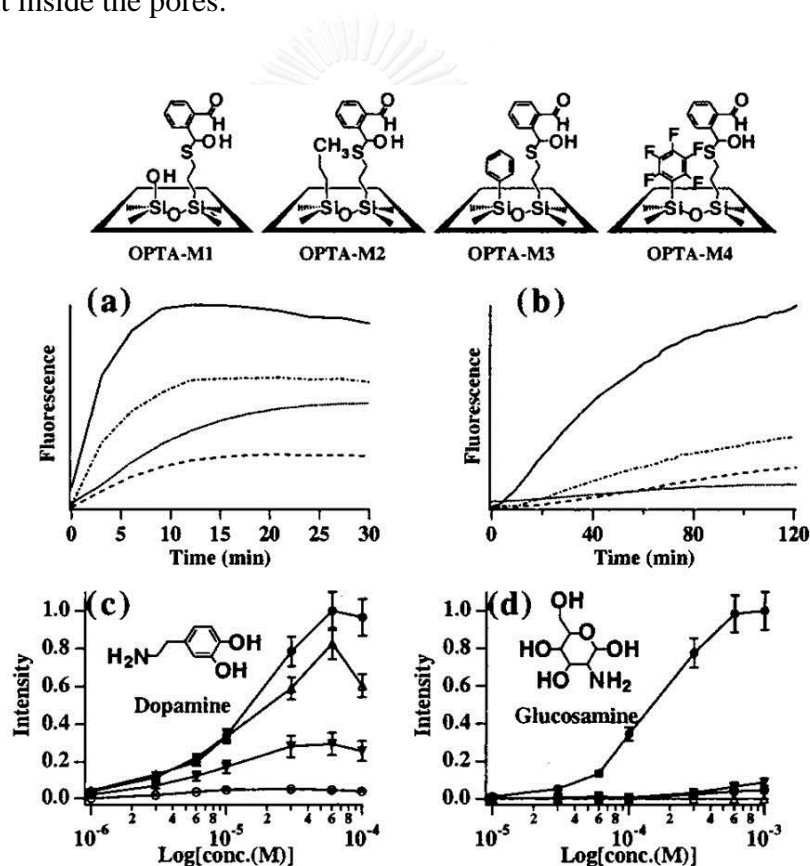
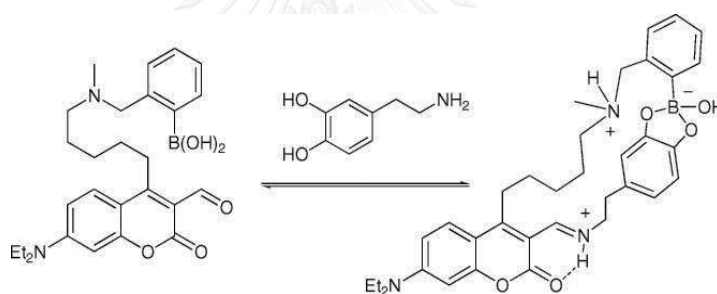


**Figure 1.8** Kinetic measurements of the fluorescence detection of dopamine (a) and glucosamine (b) with OPTA-derivatized mesoporous silica grafted with secondary functional groups, such as silanol (M1: solid line), propyl (M2: dotted line), phenyl (M3: dashed line), and pentafluorophenyl (M4: dash-dotted line) groups. Fluorescence increase of OPTA-MX (X = 1 (●); 2 (○); 3 (▽); 4 (△) as a function of dopamine (c) and glucosamine (d) concentrations

#### 1.4 Determination of catecholamine by fluorescence spectrophotometry

Catecholamine is a type of biogenic amines consisting of catechol groups interacting strongly with boronic acid. The formation of boronic acid esters with catechol by condensation reaction was early investigated by Smith and co-workers [17]. Then, the detection of biomolecules containing catechol by boronic acid-based fluorescent probes has been developed.

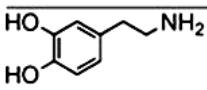
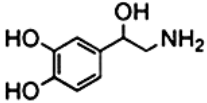
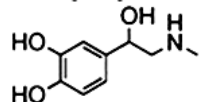
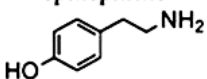
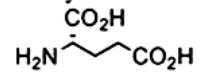
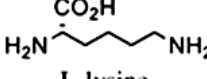
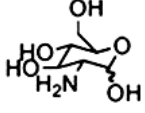
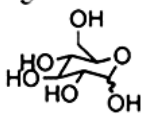
For first example, Secor and Glass [35] prepared a boronic acid containing coumarin aldehyde sensor **1** to detect dopamine and norepinephrine under physiological conditions. The probe binds to dopamine and norepinephrine by forming an iminium linkage with the amine moiety, as well as a boronate ester with the catechol group as shown in Fig. 1.9. For the detection, the electron rich property of catechol likely acts as a PET quencher of the coumarin fluorophore.



**Figure 1.9** Binding event between fluorescent sensor **1** and catecholamines under physiological conditions

The fluorescence of the sensor was quenched upon binding dopamine, norepinephrine and epinephrine, giving an overall decrease in emission. The fluorescence quenching effect was found to be directly related to the catechol group. Binding constants determined by fluorescence titration gave the binding constants as shown in Table 1.1. The sensor binds to primary catecholamines with good affinity and acts as an effective colorimetric sensor for dopamine, epinephrine and norepinephrine with excellent selectivity showing high binding constants over amino acids, and glucose.

**Table 1.1** Association constants obtained for complexation of sensor **1** with analytes (biogenic amine and monosaccharide) in 100 mM Na<sub>2</sub>S<sub>2</sub>O<sub>3</sub>, 50 mM HEPES, 20 mM NaCl, pH 7.0, 37 °C

guest	K <sub>a</sub> (M <sup>-1</sup> ) <sup>a</sup>
 dopamine	3400
 norepinephrine	6500
 epinephrine	5000
 tyramine	250
 L-glutamic acid	6.8
 L-lysine	4.0
 D-glucosamine	5.0
 D-glucose	-

In 2004, Coskun and Akkaya designed fluorescent chemosensor **2** based on a water-soluble naphthalimide (Lucifer yellow dyes) linked by a phenylboronic acid group for detection of L- DOPA [36]. Increasing the concentrations of L-DOPA, the fluorescence intensity at 535 nm was decreased. The emission data was estimated by Benesi-Hildebrand analysis to yield a dissociation constant of  $6.1 \times 10^{-4}$  M for 1:1 interaction. The effect of three-point recognition namely, reversible boronic ester



formation,  $\pi$ - $\pi$  interactions, and charge complementarity was examined. A set of structurally related the compounds including catechol, L- phenylalanine, L-tyrosine, and L- DOPA was studied.

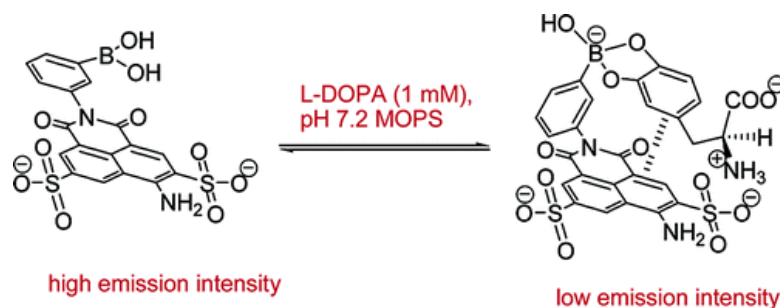


**Figure 1.10** Fluorescent sensor **2** recognizes L-DOPA through a combination of reversible interactions

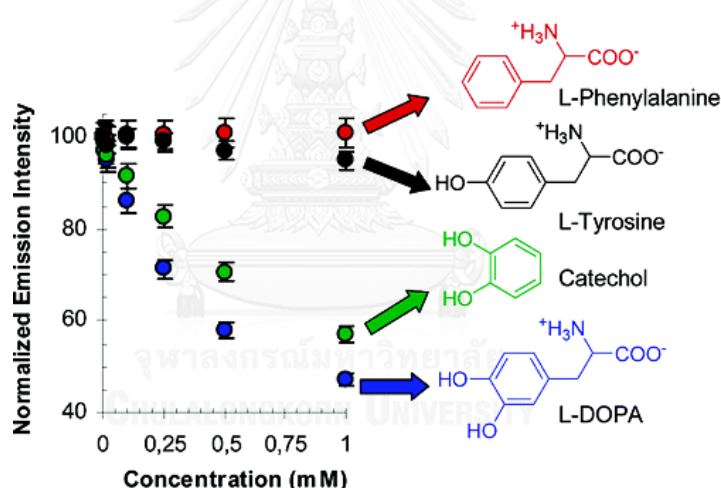


**Figure 1.11** Normalized peak emission intensity of **2** in the presence of catechol, L-DOPA, and its natural precursors in buffered aqueous solutions (0.1 M MOPS, pH 7.2) with excitation wavelength of 430 nm

The maximum change in signal intensity was observed in the presence of L-DOPA followed by catechol, while L-Phenylalanine and L-tyrosine did not cause any obviously change in the emission intensity as depicted in Fig. 1.11. The trend of the emission changes strongly suggested the change involving in the participation of multiple interactions such as a strong interaction of boronic ester formation and electrostatic interaction of sulfonate-ammonium group. Moreover, they also studied

binding mode of the complex by  $^1\text{H-NMR}$  titration in buffer solution found that an aromatic proton signal of phenyl boronic acid part shifted to up-field after the increasing concentration of L-DOPA.

In 2005, Jang and co-workers [37] synthesized and studied two new anthracene-based fluorescent probes **3** and **4** for detection of dopamine in MeOH and 50% MeOH in 0.05 M HEPES buffer at pH 7.4 as shown in Fig. 1.12. The results of titration studies on the two receptors showed that increasing concentration of epinephrine, dopamine, and catechol effects on fluorescence quenching. These results can be explained the electron rich on catechol which plays as a quencher of the anthracene upon the formation of complex. This phenomenon is called photoinduced electron transfer (PET) mechanism.

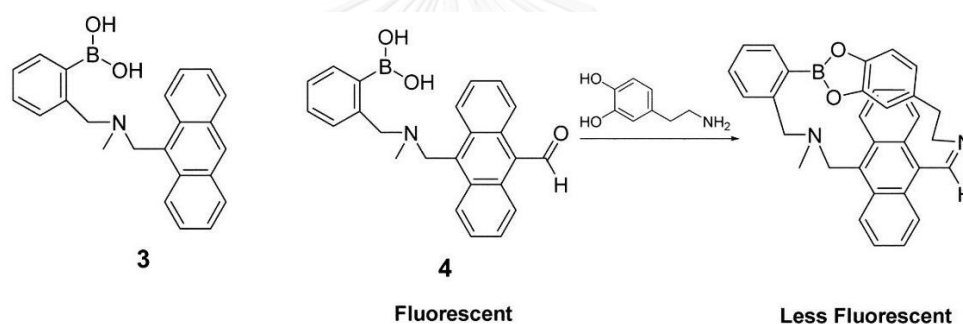


**Figure 1.12** Structure of sensor **3** and propose binding mode of sensor **4** with dopamine

The association constants of sensor **3** with dopamine, epinephrine and catechol in 50% MeOH in 0.05 M HEPES buffer at pH 7.4 were calculated from fluorescence titration as 5720, 5050 and 2010  $\text{M}^{-1}$ , respectively. Under the same conditions, the association constants of sensor **4** with dopamine, epinephrine and catechol were calculated as 7300, 5750 and 2030  $\text{M}^{-1}$ , respectively. Noticeably, sensor **4** containing aldehyde group binds dopamine about two better fold than sensor **3** in methanol. The result showed that only in methanol, aldehyde group of sensor **4** can bind with amino group of dopamine to produce the imine bond. Moreover, the complex was confirmed by the electrospray ionization (ESI) mass spectrum in methanol showing a peak at  $m/z$  483.3 which corresponds to  $[\mathbf{4} + \text{dopamine} + 3\text{H}_2\text{O}]^+$ .

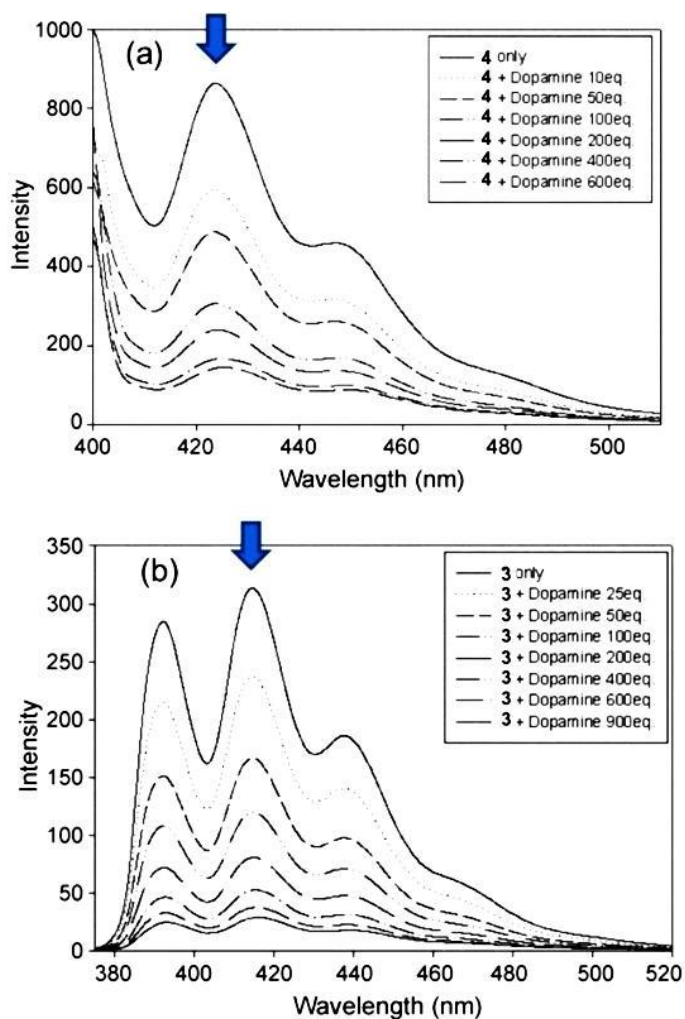


**Figure 1.13** Fluorescence spectra of a) sensor **4** ( $3 \mu\text{M}$ ) upon the addition of dopamine in MeOH (excitation at  $397 \text{ nm}$ ) b) sensor **3** ( $3 \mu\text{M}$ ) upon the addition of dopamine in 50% MeOH in 0.05 M HEPES buffer at pH 7.4 (excitation at  $367 \text{ nm}$ )

### 1.5 Histidine fluorescent sensor by metal complexes

Zinc ion shows ability in forming stable complexations with amino acids, in particular of histidine. Harding and Cole studied the crystal structure of di(histidino)zinc pentahydrate synthesized by slowly cooling in aqueous solution of zinc sulphate and D,L-histidine [38].

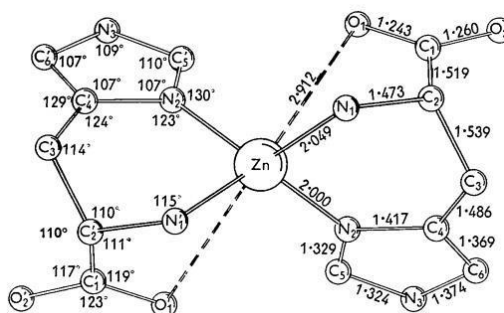


**Figure 1.14** Bond lengths and angles in one molecule of di(histidino)zinc

The crystal structure was determined by Fourier analysis showing a distorted tetrahedron which amino nitrogen and imidazole nitrogen of the each histidine coordinate to Zn (II) atom, while one oxygen atom from each histidine is weakly connected as shown in Fig. 1.14.

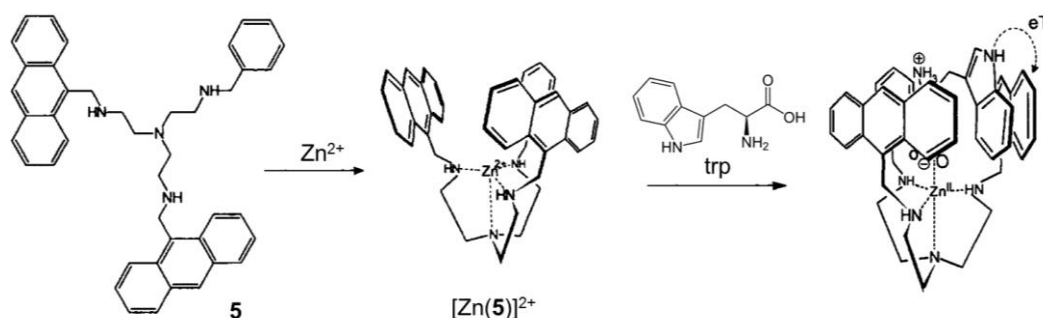


**Figure 1.15** Multipoint molecular recognition of tryptophane (trp) by the  $[Zn(\mathbf{5})]^{2+}$  system

Moreover, Zn (II) complexes display ability to bind with carboxylate and imidazole group. For example, Fabbrizzi and co-workers studied recognition of amino acids by an  $[Zn(\mathbf{5})]^{2+}$  complex consisting of tren framework armed with two anthracenyl and one benzyl substituents through fluorescence quenching [39]. For the detection, the metal center is coordinated with the  $COO^-$  group of the amino acid, whereas the anthracene substituents are involved in a  $\pi$ - $\pi$  stacking interaction with its aromatic moiety of the amino acid.  $\log K$  values associated to the formation of the  $[Zn(\mathbf{5})(phe)]^{2+}$  and  $[Zn(\mathbf{5})(trp)]^{2+}$  adducts estimated by spectrophotometric titration in 4:1 ethanol:water mixture, are 4.48 and 4.21, respectively. Those observed for

glycine showed lower values ( $\log K = 3.06$ ). The establishing of  $\pi$ - $\pi$  stacking interactions between the aromatic part of amino acid and poly aromatic substituents of the tren framework ascribed the high stability of  $[\text{Zn}(\mathbf{5})(\text{phe})]^{2+}$  and  $[\text{Zn}(\mathbf{5})(\text{trp})]^{2+}$  adducts. The binding situation in  $[\text{Zn}(\mathbf{5})(\text{trp})]^{2+}$  is tentatively illustrated in Fig. 1.15.

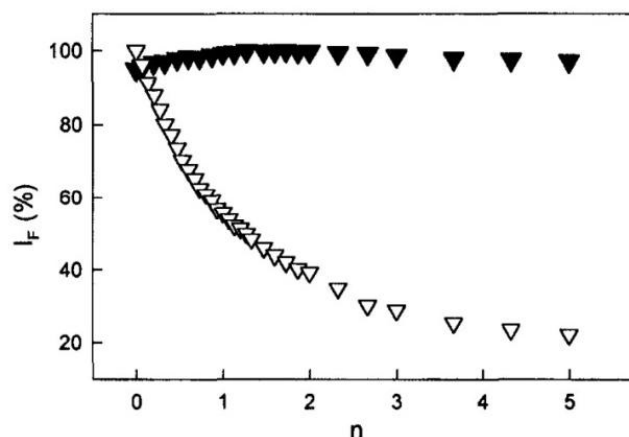


**Figure 1.16** Titration of the  $[\text{Zn}(\mathbf{5})]^{2+}$  receptor with tryptophane (trp,  $\nabla$ ) and phenylalanine (phe,  $\blacktriangledown$ ) in methanolic solution

Obviously, fluorometric titration of an aqueous ethanolic solution of  $[\text{Zn}(\mathbf{5})]^{2+}$  with trp induced fluorescence quenching as shown in Fig. 1.16. The fluorescence quenching was due to an electron transfer process from the donor indole moiety of trp to a nearby photo excited anthracene fragment that the indole substituent of trp possesses electron donor tendencies. The mechanism was not observed in the case of phe, because substituent (a phenyl group) does not exhibit electron donor properties. The titration indicated the formation of a 1:1 adduct between  $[\text{Zn}(\mathbf{5})]^{2+}$  and the amino acids.

In 1997, Fabbrizzi and co-workers studied recognition of imidazole anion and the imidazolate moiety of L-histidine by the dizinc (II) complex of an octamine containing the anthracene subunit [40]. At pH 9.6, imidazole was deprotonated and performed the bridges of two Zn (II) centres. The binding showed the fluorescence quenching because of electron tranfering from the electron rich imidazolate fragment to the nearby anthracene fragment. The binding situation in  $[\text{Zn}_2(\mathbf{6})(\text{im})]^{3+}$  is tentatively illustrated in Fig. 1.17.

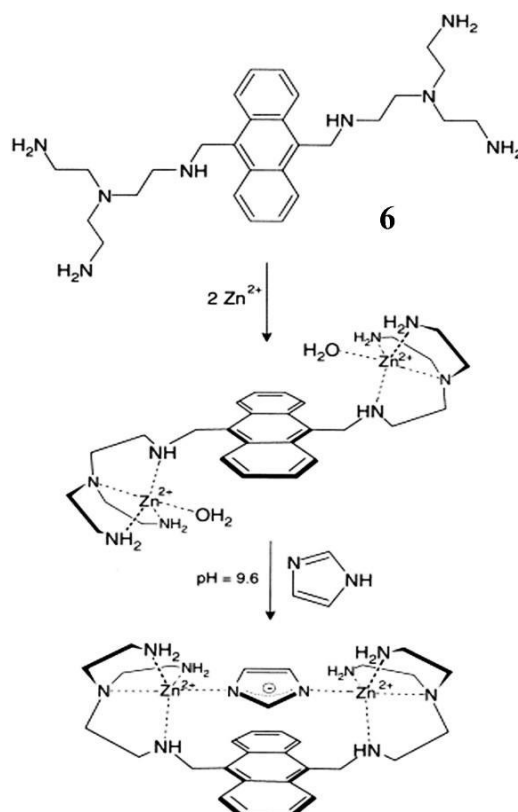


**Figure 1.17** Multipoint molecular recognition of tryptophane (trp) by the  $[\text{Zn}_2(\mathbf{6})]^{2+}$  system

Spectrofluorimetric titration of the  $[\text{Zn}_2(\mathbf{6})]^{4+}$  complex with L-histidine indicated a lower value for the binding constant than imidazole anion because of the possible existence of some steric repulsions between the imidazole supplemented amino acid fragment and the receptor framework. Interestingly, the titration event was not changed when the solution contains even a large excess of any other amino acid. Therefore,  $[\text{Zn}_2(\mathbf{6})]^{4+}$  showed high sensitivity for detection of L-histidine in the presence of any other natural amino acid (Fig. 1.18).

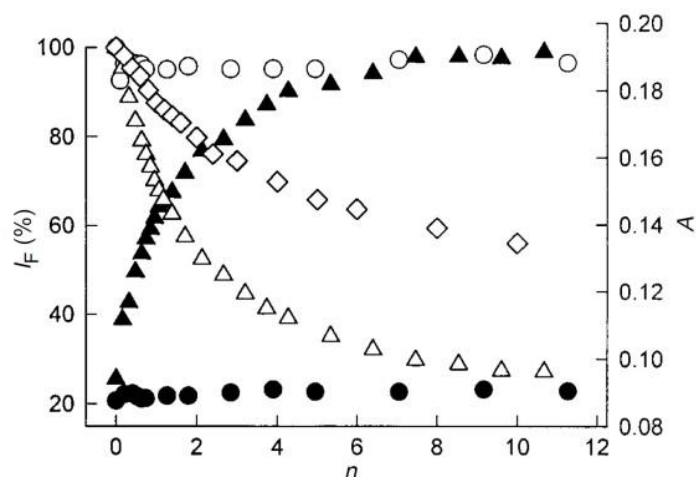


**Figure 1.18** Variation of the relative fluorescence intensity ( $I_F$ , left vertical axis) and of the absorbance at 300 nm ( $A$ , right vertical axis) during the titration of  $9 \times 10^{-6}$  M  $[\text{Zn}_2(\mathbf{6})]^{2+}$ , buffered at pH 9.6, with imidazole, histidine and acetate: ( $\Delta$ )  $I_F$  (imidazole); ( $\blacktriangle$ )  $A$  (imidazole); ( $\circ$ )  $I_F$  (acetate); ( $\bullet$ )  $A$  (acetate); ( $\diamond$ )  $I_F$  (L-histidine).  $n$  = number of equivalents of the added substrate

### 1.6 Ratio metric sensor under FRET mechanism

Fluorescence sensing has been expanded as a powerful tool for monitoring the recognized compound in biological system and bio-imaging. A large number of synthetic intensity-based fluorescent probes for those have been constructed [41-43]. However, intensity-based fluorescent probes have some limitations such as variations in probe concentration, environment condition, and excitation intensity may influence the fluorescence intensity measurements. As a result, researches have focused on the use of ratiometric fluorescent probes to alleviate this foible. Fluorescence resonance energy transfer (FRET) is one of the most widely used sensing mechanisms for ratiometric fluorescent probes.

Jisha and co-workers [45] synthesized the molecular sensor **8a** and **8b** consisting of dansyl and naphthalimide moiety for investigation of various metal ions in different conditions. The **8b** with longer spacer length (octamethylene unit) showed FRET-efficiency more than the **8a** consisting of a shorter spacer group (hexamethylene unit). Thus, the interactions between **8b** and various metal ions were observed. It was found that a solvent system of a mixture (4:1) of water and

acetonitrile containing neutral micelles triton X-100 (TX, 2mM) showed very effective with the stability of the sensor as well as the selectivity and sensitivity of the metal ion binding event. The sensor showed dual emission under FRET mechanism centered at around 375 and 525nm due to the locally excited state of the naphthalimide chromophore and energy transfer-mediated emission from the dansyl moiety, respectively.

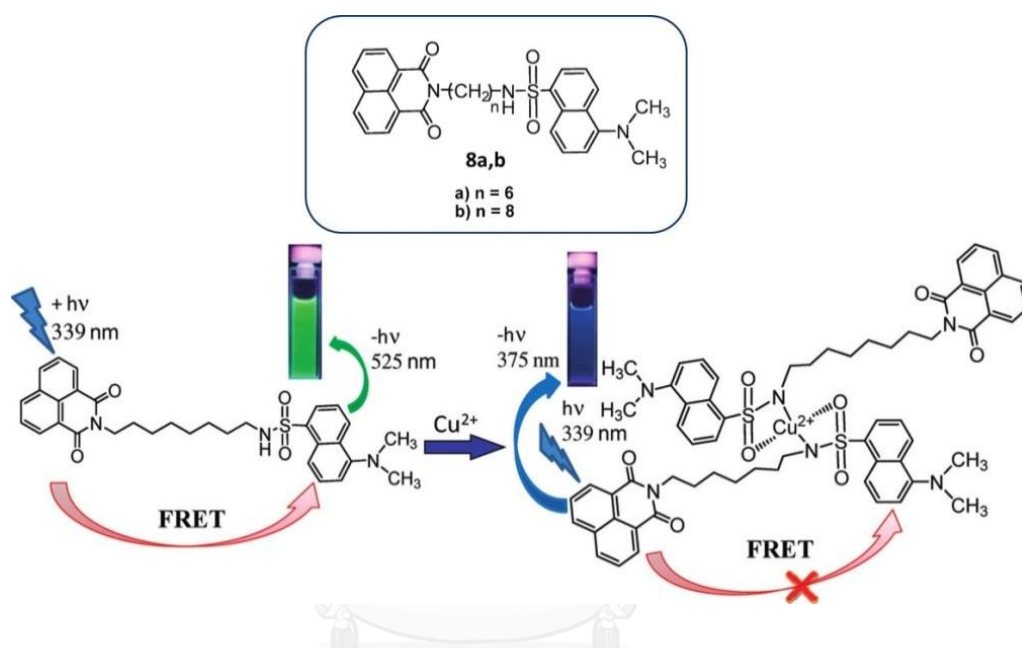


**Figure 1.19** Structure of **8a** and **8b**, and schematic representation of the complexation between sensor **8b** and  $\text{Cu}^{2+}$  ions

Titration **8b** with various metal ions exhibited selectivity for  $\text{Cu}^{2+}$  ions as shown in Fig. 1.20. The binding event occurred through inhibition of FRET mediated emission at 525 nm with enhancement in the emission intensity of the naphthalimide chromophore at 375 nm. The sensor formed stable 2:1 stoichiometric complexes of **8b**: $\text{Cu}^{2+}$  involving sulfonamide functionality as shown in Fig. 1.19.



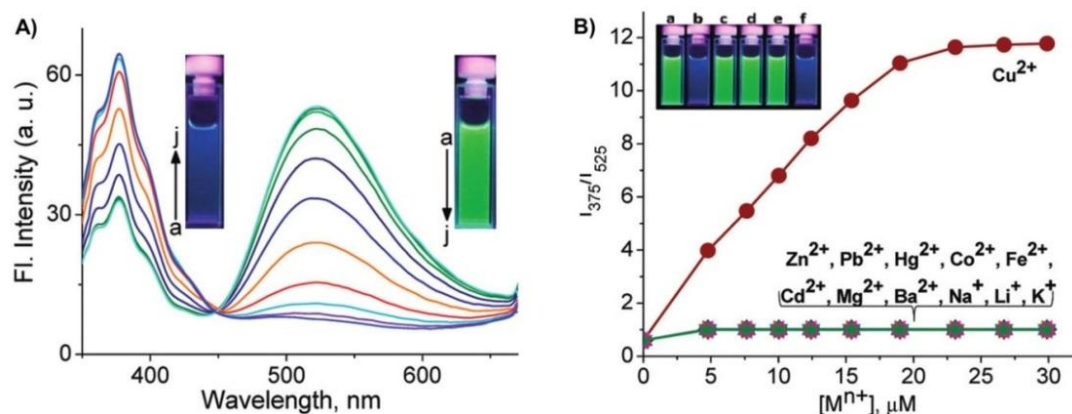


**Figure 1.20** A) Changes in the fluorescence spectrum of the **8b** (3  $\mu\text{M}$ ) in 20% acetonitrile containing neutralmicelles TX-100 (2mM) with increase in addition of  $\text{Cu}^{2+}$  ions,  $[\text{Cu}^{2+}]$  (a) 0 and (j) 20  $\mu\text{M}$  (excitation wavelength = 339 nm) B) Relative changes in the fluorescence intensity of the **8b** (3  $\mu\text{M}$ ) in the presence of various metal ions. Inset shows visual observation of fluorescence changes: (a) **8b** alone; (b-d) **8b** in the presence of  $\text{Cu}^{2+}$ ,  $\text{Li}^+$ ,  $\text{Hg}^{2+}$ , respectively; (e) equivalent mixture of various metal ions without  $\text{Cu}^{2+}$  ions; (f) equivalent mixture of various metal ions with  $\text{Cu}^{2+}$  ions

Yuan and co-workers [44] designed and synthesized **NRFTP** consisting of rhodamine acceptor, a thioester group, a piperazyl moiety, and a Bodipy dye, as a novel FRET-based ratiometric probe for detection of thiols such as cysteine taking advantage the unique ring opened/closed photophysical properties of rhodamine dyes. The Bodipy emission has strong overlap with the rhodamine absorption when the free probe was excited at the Bodipy absorption, the red emission of the rhodamine dye was observed. Incubation of **NRFTP** with cysteine resulted in a blue shift from 590 to 510 nm in the emission due to the cleavage of thiophenylester bond of **NRFTP** and formation of Bodipy (Fig. 1.19A). The new probe has also been successfully applied for ratiometric imaging of cysteine in living cells (Fig. 1.19C).

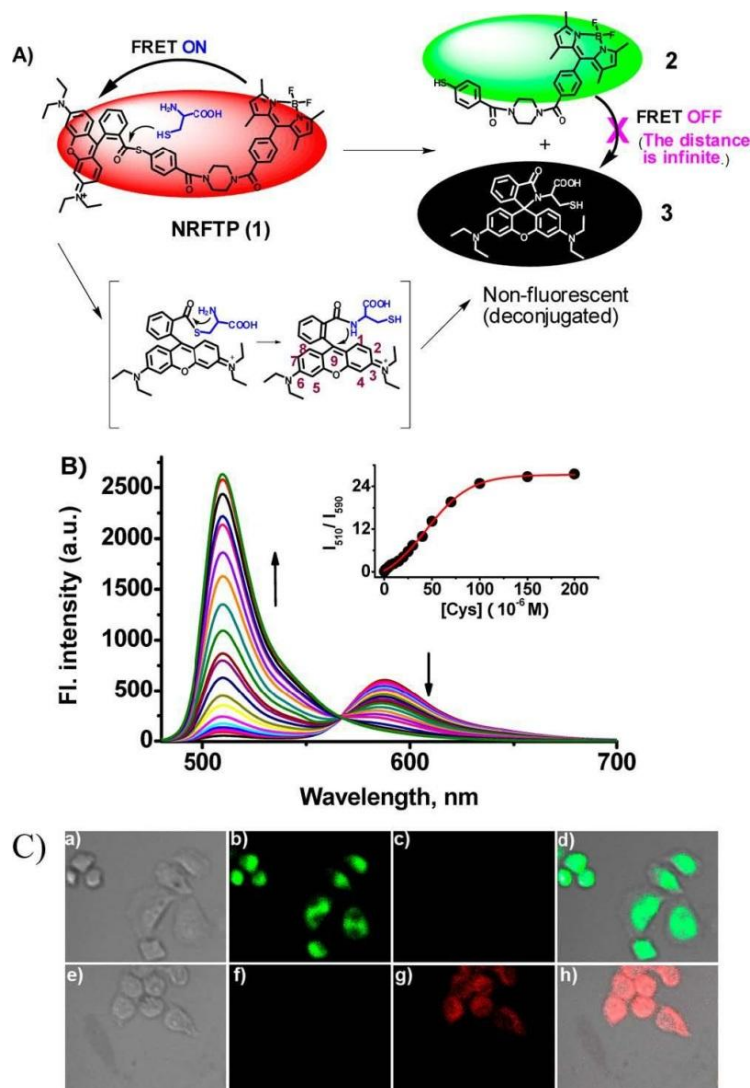


**Figure 1.21** A) The sensing mechanism of NRFTP for detection of cysteine. B) The emission spectra of NRFTP incubated with varying concentrations of cysteine. C) Confocal images of HeLa cells: (a-c) bright-field and fluorescence images of HeLa cells incubated with NRFTP; (d) overlay the images of panels a-c; (e-g) bright-field and fluorescence images of HeLa cells incubated with *N*-ethylmaleimide and then with NRFTP; (h) overlay the images of panels e-g

Moreover, our group have studied FRET-on process to categorize biogenic amines especially catecholamine namely dopamine, norepinephrine and epinephrine. In 2013, a FRET-on process induced by catecholamine as a guest linker between coumarin aldehyde (CA) and pyrene boronic acid (PBA) through an intermolecular assembly has been studied [46].

Sensor **PBA** as a donor fluorescence sensor reacting with the catechol group based on catecholamine could transfer energy to sensor **CA** as an acceptor fluorescence sensor which formed an iminium ion with primary amines. Because of overlapping of emission band of **PBA** with the absorption band of sensor **CA**, the energy transfer between the donor and acceptor fluorophore could occur. The proposed binding event was shown in Fig. 1.22.

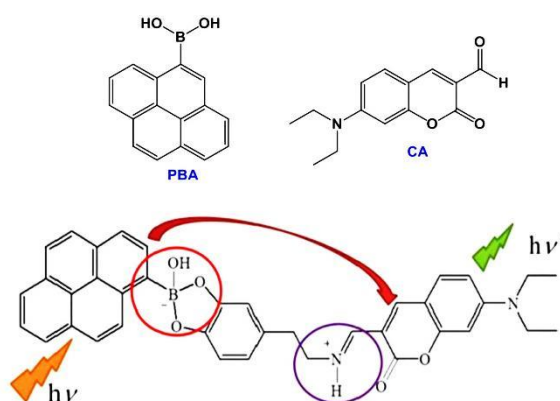


**Figure 1.22** The proposed structure of the **PBA–DA–CA** complex inducing the FRET process

It was found that the sensor **PBA** exhibited a strong emission band (monomeric band) in the region of 375–425 nm corresponding to monomeric pyrene species. Upon the addition of DA, NE or EPI, the fluorescence response exhibited a significant red shift assigned to the excimer band centered at 451 nm (Fig. 1.23). **PBA** is a promisingly selective fluorescence probe for catecholamines over other biogenic amines. The reaction of catechol based catecholamine and pyrene boronic acid induced the excimer fluorescence spectrum. The fluorescence response of sensor **CA** and **PBA** upon adding Lys, Tyr, or Glu showed similar fluorescence response which did not exhibit the fluorescence changing as shown in Fig. 1.24. In contrast, fluorescence response in the case of DA or NE showed a large quenching in the monomeric band of sensor **PBA** and a large enhancement of the emission band at 487 nm of sensor **CA** (Fig. 1.24). The addition of EPI, the excimer band at 451 nm was observed, while the emission band at 487 nm for sensor **CA** was decreased.

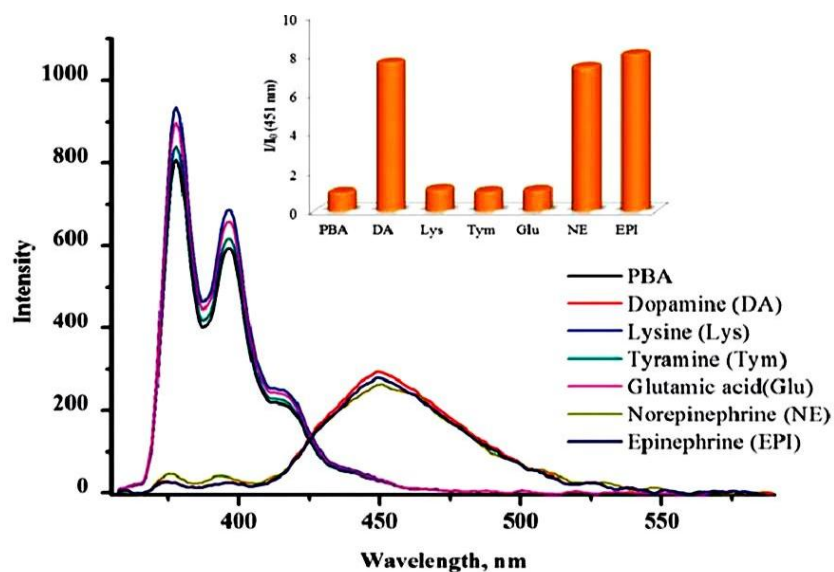


**Figure 1.23** Fluorescence spectra of sensor **PBA** (1 mM) in buffer solution (100 mM Na<sub>2</sub>S<sub>2</sub>O<sub>3</sub>, 50 mM HEPES, 20 mM NaCl, pH 7.4) with various biogenic amines and inset: the relative fluorescence intensity of sensor **PBA** ( $\lambda_{\text{ex}} = 340$  nm) in the presence of various biogenic amines

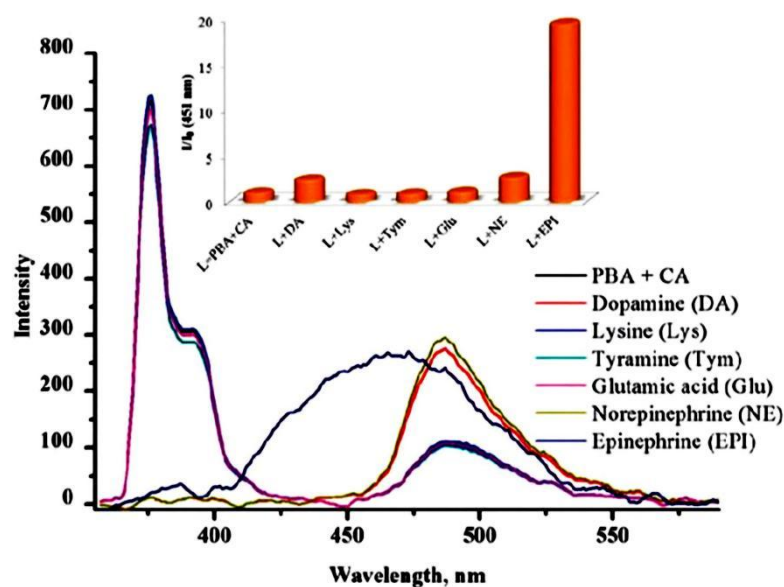


**Figure 1.24** Fluorescence spectra of the mixed sensors of **PBA** (1 mM) and **CA** (30 mM) in buffer solution (100 mM Na<sub>2</sub>S<sub>2</sub>O<sub>3</sub>, 50 mM HEPES, 20 mM NaCl, pH 7.4) with various biogenic amines and inset: relative fluorescence intensity of the mixed sensors of **PBA** and **CA** ( $\lambda_{\text{ex}} = 340$  nm) in the presence of various biogenic amines

This supported non-FRET process because of non-binding of EPI and sensor **CA**. Therefore, this system was used as a specific identification of EPI from other catecholamine derivatives since EPI containing secondary amine could not react with the aldehyde moiety of sensor **CA**, while primary amines of DA and NE able to react with the aldehyde moiety resulting in FRET-on process.

In 2015, Sanguansap and co-worker [47] reported two sensing components based on fluorescence probes for discrimination of catecholamines namely dopamine (DA) and norepinephrine (NE), acting as a proper guest linker between two self-recognition sensing elements. The two fluorescence chemosensors namely (i) **NB** containing boronic acid connected to a naphthalimide unit for covalent binding with catechol and giving the emission band at 381 nm and (ii) **CC** consisting of a crown-ether unit connected to coumarin for a non-covalent interaction with the ammonium ion based catecholamine providing an emission band at 475 nm. The structure of **NB** and **CC** as well as the conceptual hypothesis of the dual fluorescence response mechanism was shown in Fig. 1.25.

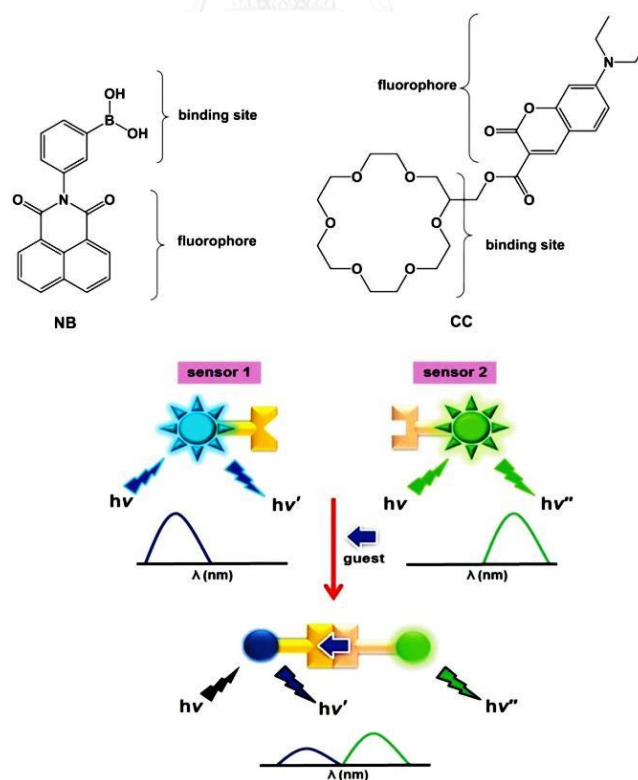


**Figure 1.25** Structure of **NB** and **CC**, and conceptual hypothesis of the dual fluorescence response mechanism

Surprisingly, in the presence of epinephrine (EPI) in sensor **NB** solution showed a very strong fluorescence enhancement, while a large fluorescence quenching was observed in the case of DA and NE as shown in Fig. 1.26. It can be reasonably explained that the ammonium ion on DA and NE preferred to promote the condensation reaction of the boronic acid and catechol group producing a negative boronate ester. It is reliably rationalized that the log  $K_s$  values of sensor **NB** with DA and NE are slightly higher than those for the sensor **NB** with EPI with the log  $K_s$  values for complex **NB** with DA, NE and EPI of 4.13, 4.17 and 4.01, respectively. To categorize DA and NE, the combination of **NB** and **CC** was applied to differentiate DA and NE with dual emission bands under a PET mechanism. Since the structures of DA and NE are different in the side chain, the different ratio of dual fluorescence response which was the different ratiometric fluorescence intensities of coumarin and naphthalimide ( $I_{\text{coumarin}}/I_{\text{naphthalimide}}$ ) was expected. The dual emission ratio ( $I_{475}/I_{384}$ ) of the **NB**–**DA**–**CC** complex showed different values from the **NB**–**NE**–**CC** complex with emission ratio 4.84 and 4.28, respectively. And the ratiometric fluorescence changes of each complex still allowed a constant ratio with different concentrations of sensors and guests as well as different conditions in the presence of excess amounts of guests.

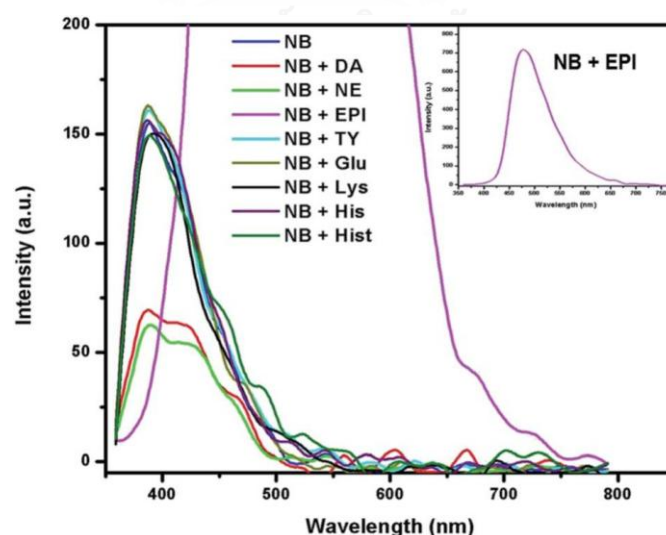


**Figure 1.26** Fluorescence spectra of sensor **NB** ( $1 \times 10^{-5}$  M) in 1:9 v/v of DMSO: phosphate buffer at 0.01 M, pH 7.4 in the presence of 100 equivalents of various guests and the inset shows the fluorescence spectrum of sensor **NB** and EPI

Additionally, the PCA analysis using mixed sensors of **NB** and **CC** obviously separated DA and NE was better than a single sensing element. This systematic approach is the first report showing a high potential for the identification of DA and NE using ratiometric fluorescence sensors with dual emission by two sensing elements.

### 1.7 Concept of this study

Design and synthesis of fluorescent receptors that can differentiate between various biogenic amines have been a research challenge. Recently, many efforts have been focused on the design of receptors that function in aqueous solution because of the benefit application in biological system such as blood and urine. Decoration molecular sensor on solid support is widely used to enhance water solubility. Mesoporous silica is one of the most interesting materials because of their properties namely high water solubility, modifiable surface, large surface area and biocompatibility. Furthermore, modification with different organic group on the surface allows for exact regulation of the penetration of selective molecules with certain sizes and chemical properties. Therefore, in this research we have designed molecules sensor decorated on silica nanoparticles and mesoporous silica to enhance solubility in water under idea of Lin et al [27]. The *o*-phthalic hemithioacetal (OPTA) unit modified on silica surface as a unit sensor react primary amine. Furthermore, we have designed the fluorescent receptor to bind with side chain groups of biogenic amine, namely catechol and imidazole group of catecholamine and histidine, respectively to highly differentiate each group of biogenic amines. Catecholamine such as dopamine, epinephrine and norepinephrine consisting of catechol group can react with boronic acid [35-37]. Imidazole group being side chain group of histidine enables to bind with zinc ion and zinc complexes [38-40].

Ideally, biogenic amines consisting of the part of primary amine would react with OPTA on surface of mesoporous silica nanoparticles to form isoindole product that enhance fluorescence signal at 450 nm under an excited wavelength at 345 nm. To classify catecholamine and histidine, another portion of them, namely catechol and imidazole groups enable to react with boronic acid and Zn (II), respectively. Therefore, **CB**, **ZnC2** and **ZnD2** were designed as acceptor fluorophore. The proper

biogenic amine as a guest linker links between donor isoindole and acceptor fluorophore resulting in the energy transfer. Concepts for the detections of catecholamine and histidine were shown in Fig. 1.27 and 1.28, respectively.

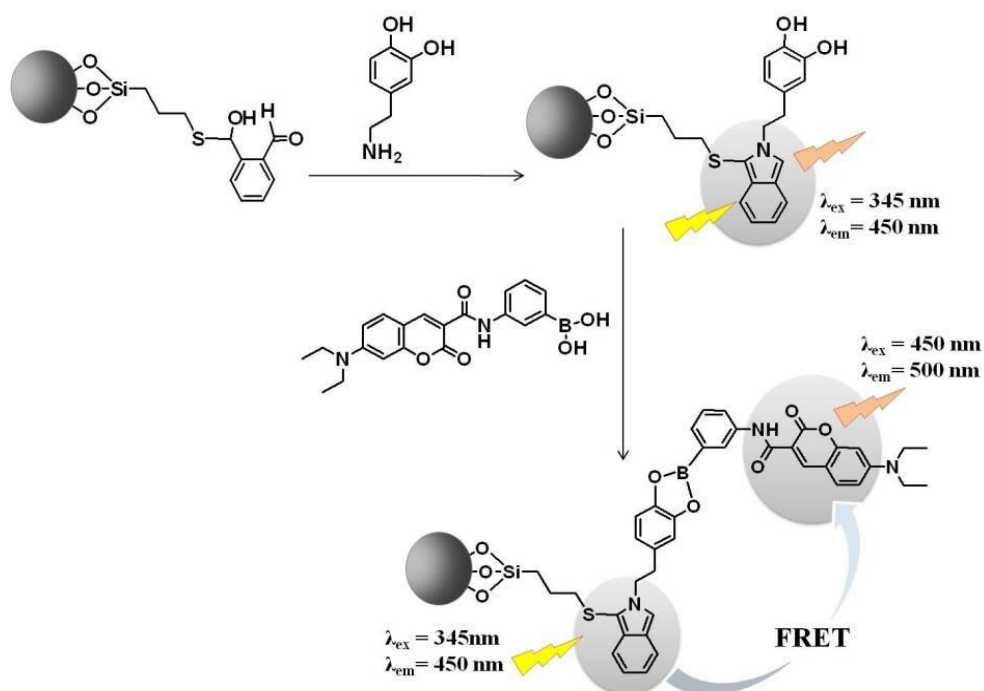


**Figure 1.27** Concept for detection of catecholamine

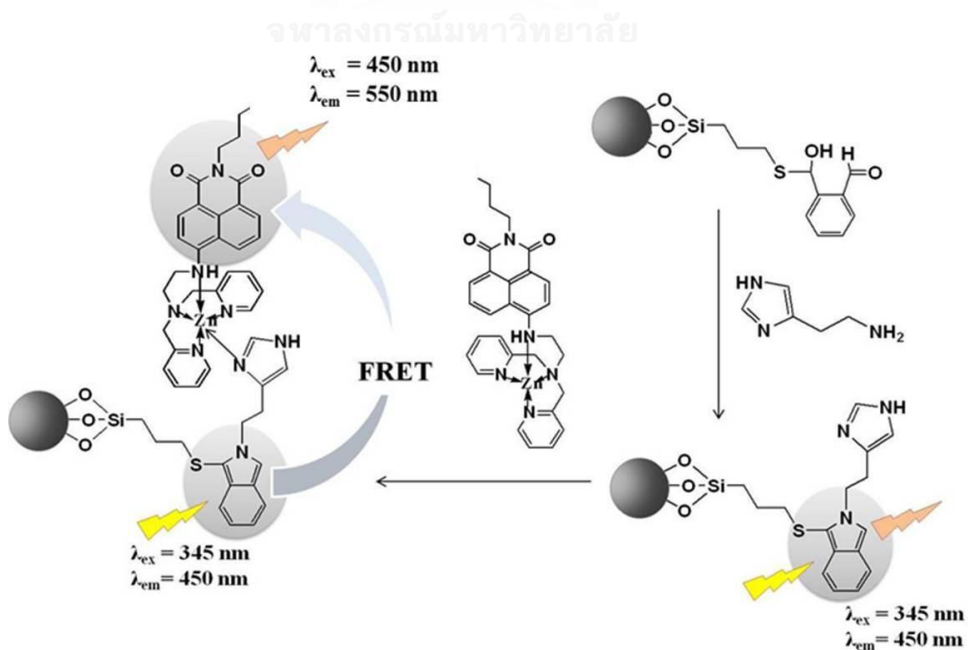


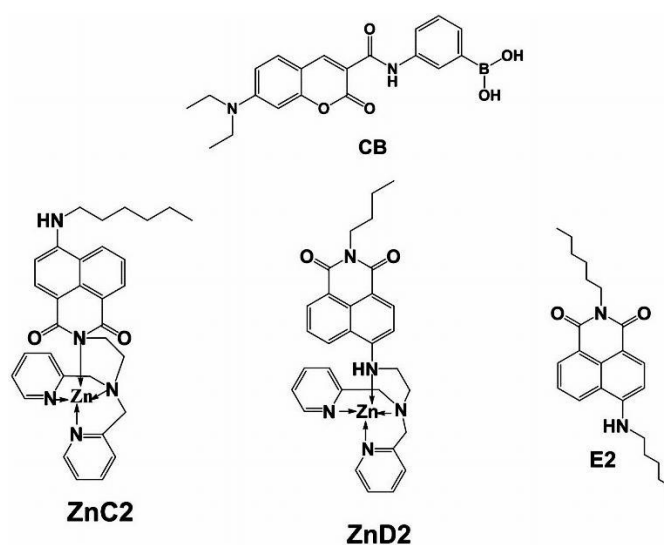
**Figure 1.28** Concept for detection of histidine



## 1.8 Objective and scope of the research

To synthesize

- Silica nanoparticles and mesoporous silica nanoparticles and modify the surface of the particles with OPTA group.
- CB, ZnD2, ZnC2 and E2 as receptor molecules to categorize guest molecules.



To study the sensing abilities via photophysical properties under fluorescence spectroscopy.

## CHAPTER II

### EXPERIMENTAL

#### 2.1 General Procedure

##### 2.1.1 Analytical measurements

<sup>1</sup>H NMR spectra and <sup>13</sup>C NMR spectra were recorded on a Varian Mercury 400 NMR spectrometer and a Bruker DRX 400 MHz nuclear magnetic resonance spectrometer. All chemical shifts were reported in part per million (ppm) using the residual proton or carbon signal in deuterated solvent namely CDCl<sub>3</sub> and DMSO-*d*<sub>6</sub>. MALDI-TOF mass spectra were recorded on a Biflex Bruker Mass spectrometer using 2-cyano-4-hydroxycinnamic acid (CCA) as a matrix. High-resolution mass spectra were recorded on Electrospray Ionization High Resolution Mass Spectroscopy (ESI-HRMS). All fluorescence spectra were measured by a Varian Cary Eclipse Probe fluorescence spectrophotometer by personal computer data processing unit. The light source is Cary Eclipse a pulsed xenon lamp and a detector is a photomultiplier tube. All UV-Vis spectra were recorded with a Varian Cary 50 Probe UV-Visible spectrometer. IR spectrophotometric measurement of the dried particle samples was performed on Thermo, Nicolet 6700 FT-IR. Zeta potential and Dynamic Light Scattering were monitored under NanoPlus-3 (NanoPlus zeta/nano particle analyzer). TEM images were recorded on a transmission electron microscopy (JEOL, JEM-2100 electron microscope). X-ray diffraction pattern (XRD) was determined on D4 X-ray diffractometer using Cu K $\alpha$  radiation ( $\lambda = 0.1541$ ).

##### 2.1.2 Materials

Chemicals and the solvents being standard analytical grade were purchased from Fluka, Aldrich, Carlo erba, Merck, TCI or Lab scan and used without further purification. Dichloromethane were distilled using calcium hydride as drying agent under nitrogen prior to use. Column chromatography was carried out using silica gel (Kieselgel 60, 0.063 0.200 mm, Merck). Thin layer chromatography (TLC) was performed on silica gel plates (Kieselgel 60, F<sub>254</sub>, 1mm). Dimethyl sulfoxide as AR grade used in fluorescence measurement was used without drying.

In this research, the 4 sensors including sensors **CB**, **ZnC2**, **D2** and **E2** were synthesized. Moreover, 2 types of silica nanoparticles namely silica nanospheres (SNPs) and mesoporous silica nanoparticles (MSNs), and the modified particles with *o*-phthalic hemithioacetal (OPTA) group on silica surface were prepared. Moreover, SNPs-OPTA and MSNs-OPTA were coated with CTAB to prepare SNPs-OPTA\_CTAB and MSNs-OPTA-CTAB, respectively. These sensors and silica materials were applied for complexation study toward biogenic amine.

## 2.2 Synthesis

### 2.2.1 Synthesis of SNPs-OPTA and SNPs-OPTA\_CTAB

#### 2.2.1.1 Preparation of silica nanospheres (SNPs)

Mixture solution containing quantities of absolute ethanol (25 mL) and 25% ammonia (1.5 mL) was stirred for 10 min to ensure complete mixing. Then, 1.5 mL tetraethyl orthosilicate (TEOS) dissolved in 5 mL ethanol was gradually added to the solution and the reaction was kept stirring at ambient temperature for 24 h. The particles were centrifuged and washed thoroughly with ethanol, and dried under vacuum for 10 h.

#### 2.2.1.2 Synthesis of SNPs-SH nanoparticles

A 90 mg of white powder of SNPs was suspended in 20 mL absolute ethanol by sonication and then 1.8 mL of 3-mercaptopropyl trimethoxysilane was added to the solution. The mixture was refluxed at 50 °C for 24 h under nitrogen atmosphere and washed five times with ethanol to remove the remaining free thiol compound in the reaction. The particles were dried under vacuum for 10 h.

#### 2.2.1.3 Synthesis of SNPs-OPTA nanoparticles

Mixture solution including 115 mg SNPs-SH dispersed in 20 mL ethanol and 230 mg *o*-phthalic aldehyde was stirred at room temperature for 6 h. The particles were separated by centrifugation, washed with methanol and dried under vacuum for 10 h.

#### 2.2.1.4 Synthesis of SNPs-OPTA\_CTAB nanoparticles.

A 120 mg of SNPs-OPTA was dispersed in 5 mL of methanol and then 3 mg of CTAB was added to the solution. After stirred for 3 h, the mixture was left to equilibrate for 24 h. And then, the mixture was centrifuged and washed with ethanol to completely remove the unreacted reagents. Finally, the particles were dried under vacuum for 10 h.

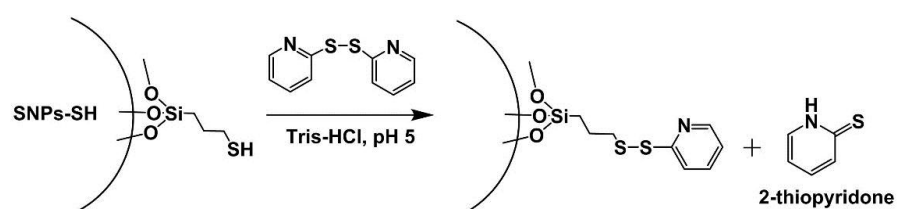
### 2.2.2 Characterization of SNPs and the modified SNPs

#### 2.2.2.1 Size and morphology of silica nanoparticles

The morphologies and the particle size of the silica nanoparticles (SNPs) and functionalized nanoparticles, namely, SNPs-SH and SNPs-OPTA have been measured by transmission electron microscopy (TEM). TEM specimens of these particles were prepared by dispersion particles in Milli Q water by ultrasonication for 10 minute. A drop of the solution was placed on carbon-coated copper grid. After 2 minute, the droplet was removed by adsorbing to a piece of filter paper. The specimen was dried in vacuum and monitored by TEM measurements.

#### 2.2.2.2 Study on accessible thiol density

To observe amount of thiol group (-SH) on surface of SNPs-SH, 2,2'-dithiodipyridine were used as a reagent to produce 2-thiopyridone as a detectable molecule which was monitored under UV-Vis spectroscopy as shown in Scheme 2.1.



**Scheme 2.1** Schematic representation of reaction between thiol (-SH) group on silica surface of SNPs-SH and excess 2,2'-dithiodipyridine and byproduct (2-thiopyridone) in Tris buffer solution, pH 5,  $\lambda_{ab} = 345$  nm

Firstly, stock solutions of 0.01 M 2,2'-dithiodipyridine and 2-thiopyridone in ethanol, and 5 mg/mL SNPs-SH in Tris buffer solution, pH 5, were prepared. Under UV-Vis spectroscopy, mixture solution consisting of SNPs-SH (100  $\mu$ L) and Tris buffer solution (1900  $\mu$ L) was treated with 2,2'-dithiodipyridine until an absorbance intensity at 340 nm was constant. It was found that 12  $\mu$ L of 2,2'-dithiodipyridine showed the constant absorbance intensity. The mixture solution consisting of SNPs-SH, 2,2'-dithiodipyridine and 2-thiopyridone in Tris buffer solution was monitored under UV-Vis spectroscopy by varying amount of 2-thiopyridone as listed in Table 2.1.

**Table 2.1** Amounts of chemical for accessible thiol density investigation on SNPs-SH

Entry	SNPs-SH (uL)	Tris-BS (uL)	DP <sup>a</sup> (uL)	TD <sup>b</sup> (uL)	[TD] ( $\times 10^{-5}$ M)	V <sub>total</sub> (uL)
1	100	1900	12	0	0.00	2012
2	100	1900	12	5	2.48	2017
3	100	1900	12	10	4.95	2022
4	100	1900	12	15	7.40	2027
5	100	1900	12	20	9.84	2032
6	100	1900	12	25	12.3	2037
7	100	1900	12	30	14.7	2042
8	100	1900	12	35	17.1	2047

<sup>a</sup>DP = 2,2'-dithiodipyridine, <sup>b</sup>TD = 2-thiopyridone

Standard addition curve was constructed by the plot of concentration of 2-thiopyridone and absorbent intensity at 345 nm.

## 2.2.3 Synthesis of MSNs-OPTA

### 2.2.3.1 Preparation of mesoporous silica nanoparticles (MSNs)

Aqueous solution of cetyltrimethylammonium bromide (CTAB, 0.1 g) and sodium hydroxide solution (2 M, 0.35 mL) was refluxed at 80 °C for 20 minutes. After that, tetraethyl orthosilicate (TEOS, 0.5 mL) was gradually added to the solution. The reaction mixture was vigorously refluxed at 80 °C for 2 h. After that, the particles in the mixture was centrifuged, washed thoroughly with solution of ethanol

and H<sub>2</sub>O (ethanol:water, 2:1) and dried under a vacuum for 1 day. The product was calcined at 550 °C for 6 h to remove CTAB template.

#### *2.2.3.2 Synthesis of MSNs-SH nanoparticles*

Mixture solution of MSNs (90 mg) suspended in 20 mL methanol and 3-mercaptopropyltrimethoxysilane (1.8 mL) was stirred at 50 °C for 24 h under nitrogen atmosphere. Then, the particles were separated by centrifugation and washed thoroughly with methanol and then the particles were dried under vacuum for 10 h.

#### *2.2.3.3 Synthesis of MSNs-OPTA nanoparticles*

Combination of 115 mg MSNs-SH dispersed in 20 mL methanol and 400 mg *o*-phthalic aldehyde was stirred at room temperature for 6 hours. The particles were washed with methanol and dried under vacuum for 10 hours.

### **2.2.4 Characterization of MSNs and the modified MSNs**

#### *2.2.4.1 Size and morphology of mesoporous silica nanoparticles*

The morphologies and the particle sizes of the mesoporous silica nanoparticles (MSNs) and MSNs-SH have been measured by transmission electron microscope (TEM). TEM specimens of these particles were prepared by dispersion particles in Milli Q water by ultrasonication for 10 minutes. A drop of the solution was placed on carbon-coated copper grid. After 2 minutes, the droplet was removed by adsorbing to a piece of filter paper. The specimen was dried in vacuum and monitored by TEM measurements.

#### *2.2.4.2 Surface area and accessible thiol density*

The amount of thiol group (-SH) on surface of MSNs-SH was investigated as the same method which was applied in SNPs-SH. Firstly, stock solutions of 0.01 M 2,2'-dithiodipyridine and 2-thiopyridone in ethanol, and 5 mg/mL SNPs-SH in Tris buffer solution, pH 5, were prepared. Under UV-Vis spectroscopy, mixture solution

consisting of MSNs-SH (40  $\mu\text{L}$ ) and Tris buffer solution (1,960  $\mu\text{L}$ ) was treated with 2,2'-dithiodipyridine until an absorbance intensity at 340 nm was constant. It was found that at 26  $\mu\text{L}$  of 2,2'-dithiodipyridine showed the constant absorbance intensity. The mixture solution consisting of MSNs-SH, 2,2'-dithiodipyridine and 2-thiopyridone in Tris buffer solution was monitored under UV-Vis spectroscopy by varying amount of 2-thiopyridone as listed in Table 2.2.

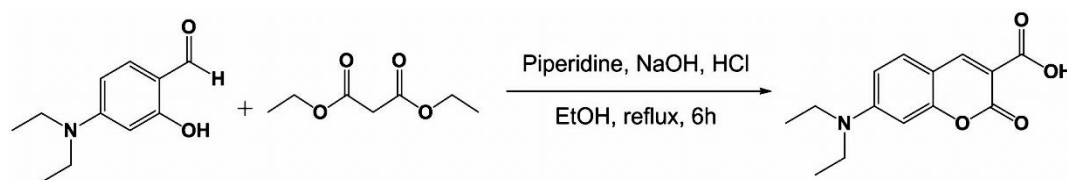
**Table 2.2** Amounts of chemical for investigation of accessible thiol density on MSNs-SH

Entry	MSNs-SH (uL)	Tris-BS (uL)	DP <sup>a</sup> (uL)	TD <sup>b</sup> (uL)	[TD <sup>b</sup> ] ( $\times 10^{-5}$ M)	V <sub>total</sub> (uL)
1	40	1960	26	0	0	2026
2	40	1960	26	5	2.46	2031
3	40	1960	26	10	4.91	2036
4	40	1960	26	15	7.35	2041
5	40	1960	26	20	9.78	2046
6	40	1960	26	25	12.20	2051
7	40	1960	26	30	14.60	2056

<sup>a</sup> DP = 2,2'-dithiodipyridine, <sup>b</sup> TD = 2-thiopyridone

## 2.2.5 Synthesis of CB

### 2.2.5.1 Synthesis of AI



Mixture of 4-(diethylamino)-2-hydroxybenzaldehyde (386 mg, 2 mmol), diethylmalonate (0.61 mL, 4 mmol) and piperidine (0.2 mL) in 6 mL absolute ethanol was stirred in two-neck round bottom flask under refluxing for 6 h. And then, 6 mL of 10% NaOH solution was added to the reaction. After further refluxed for 15 minutes, the mixture was cooled to room temperature. The mixture was acidified to pH 2 by

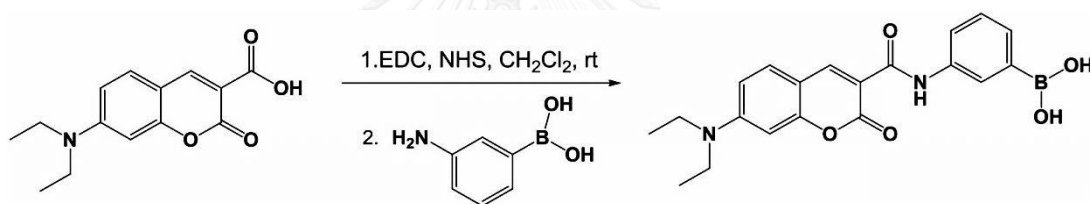
using the concentrated hydrochloric acid at 0 °C in ice bath. In this step, yellow sediment was obtained. The sediment was filtered, washed with water, dried and recrystallized with ethanol yielding yellow powder of **A1** (371 mg, 71% yield).

Characterization data for sensor **A1**

<sup>1</sup>H-NMR (400 MHz, CDCl<sub>3</sub>): δ (in ppm) = 12.37 (s, 1H, COOH), 8.67 (s, 1H, ArH), 7.46 (d, *J* = 9.2 Hz, 1H, ArH), 6.71 (dd, *J* = 4.27 Hz, 1H, ArH), 6.53 (d, *J* = 2.0 Hz, 1H, ArH), 3.49 (q, *J* = 7.07 Hz, 4H, CH<sub>2</sub>CH<sub>3</sub>), 1.26 (t, *J* = 7.2 Hz, 6H, CH<sub>2</sub>CH<sub>3</sub>)

<sup>13</sup>C-NMR (400 MHz, CDCl<sub>3</sub>): δ (in ppm) = 165.52, 164.42, 158.07, 153.78, 150.27, 131.94, 110.91, 108.59, 105.70, 96.89, 45.34, 12.39

#### 2.2.5.2 Synthesis of **CB**



Into a two-neck round bottom flask equipped with a magnetic bar, **A1** (0.26 g, 1 mmol) was dissolved in dichloromethane 20 mL, and then ethyl(dimethylaminopropyl) carbodiimide (EDC) (0.17 g, 1.1 mmol) and *N*-hydroxysuccinimide (NHS) (0.14 g, 1.1 mmol) were added to the solution and left for 1 h under a nitrogen atmosphere. And then, 3-aminophenylboronic acid hydrochloride (0.19 g, 1 mmol) and triethylamine (0.11 g, 1.1 mmol) dissolved in dichloromethane were added into the reaction and stirred at room temperature for 24 hours. The mixture was evaporated and recrystallized in ethanol. The yellow crystal of **CB** (289 mg, 76% yield) was obtained.

Characterization data for sensor **CB**

<sup>1</sup>H-NMR (400 MHz, CDCl<sub>3</sub>): δ (in ppm) = 10.75 (s, 1H, CONH), 8.76 (s, 1H, ArH), 8.11 (s, 2H, BOH), 7.97 (d, *J* = 7.2 Hz, 1H, ArH), 7.81 (s, 1H, ArH), 7.72 (d, *J* = 9.0 Hz, 1H, ArH), 7.51 (d, *J* = 7.2 Hz, 1H, ArH), 7.32 (t, *J* = 7.2 Hz, 1H, ArH), 6.83 (dd,



$J_1 = 8.6$  Hz,  $J_2 = 1.8$  Hz, 1H, ArH), 6.66 (s, 1H, ArH), 3.48 (q,  $J = 6.8$  Hz, 4H,  $-CH_2-$ ), 1.13 (t,  $J = 6.8$  Hz, 6H,  $-CH_3$ )

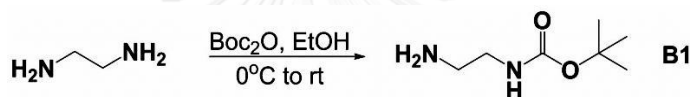
$^{13}\text{C-NMR}$  (400 MHz,  $\text{CDCl}_3$ ):  $\delta$  (in ppm) = 155.82, 137.45, 137.31, 132.42, 128.46, 127.82, 127.71, 127.45, 127.32, 121.74, 116.03, 115.58, 77.39, 77.07, 76.64, 71.52, 71.49, 35.71, 28.48

**MALDI-TOF mass:** Anal. Calcd.  $[\text{C}_{20}\text{H}_{21}\text{BN}_2\text{O}_5]^+$   $m/z = 380.15$

Found  $[\text{C}_{20}\text{H}_{21}\text{BN}_2\text{O}_5]^+$   $m/z = 380.37$

## 2.2.6 Synthesis of ZnC2

### 2.2.6.1 Synthesis of (2-Aminoethyl) carbamic acid tert-butyl ester, **B1**

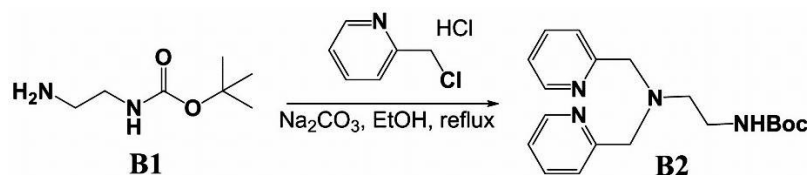


Ethylenediamine (1.35 mL, 20 mmol) dissolved in 10 mL ethanol was added with di-*t*-butyl dicarbonate (441 mg, 2 mmol) by dropwise at  $0^\circ\text{C}$ . The reaction mixture was warmed up to room temperature and stirred for 24 h under a nitrogen atmosphere. The solution mixture was then evaporated in *vacuo*. The residue was dissolved in 20 mL of dichloromethane and washed with aqueous solution of sodium hydroxide. The organic layer was dried with magnesium sulfate, filtered and evaporated in *vacuo* to give the crude product of **B1** as colorless oil (208 mg, 65 % yield).

Characterization data for **B1**

$^1\text{H-NMR}$  (400 MHz,  $\text{CDCl}_3$ ):  $\delta$  (in ppm) = 4.97 (s, 1H, CONH), 3.12 (d,  $J = 5.2$  Hz, 2H,  $-CH_2-$ ), 2.74 (t,  $J = 5.8$  Hz, 2H,  $-CH_2-$ ), 1.92 (s,  $\text{NH}_2$ ), 1.38 (s, 9H,  $-CH_3$ )

### 2.2.6.2 Synthesis of *tert*-Butyl 2-(bis(pyridin-2-ylmethyl)amino) ethylcarbamate, **B2**



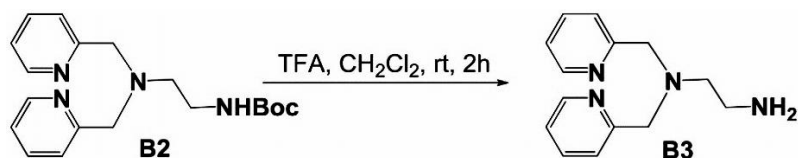
Mixture solution including **B1** (208 mg, 1.3 mmol), 2-pyridylmethyl chloride hydrochloride (426 mg, 2.6 mmol) and sodium carbonate (551 mg, 5.2 mmol) dissolved in 20 mL was refluxed for 12 h under a nitrogen atmosphere. Then the mixture was evaporated and the residue was dissolved in 20 mL of aqueous solution of sodium hydroxide and extracted with dichloromethane ( $3 \times 30$  mL). The combined organic layer was dried with magnesium sulfate, filtered and evaporated in *vacuo*. The crude product was purified by silica gel column chromatography using triethylamine/methanol/ dichloromethane (1:1:100) as the eluent to afford **B2** as brown oil (338 mg, 76% yield).

Characterization data for **B2**

$^1\text{H-NMR}$  (400 MHz,  $\text{CDCl}_3$ ):  $\delta$  (in ppm) = 8.49 (d,  $J = 4.7$  Hz, 2H, ArH), 7.59 (t,  $J = 7.2$  Hz, 2H, ArH), 7.37 (d,  $J = 6.8$  Hz, 2H, ArH), 7.11 (dd,  $J_1 = 5.6$  Hz,  $J_2 = 4.8$  Hz, 2H, ArH), 5.85 (s, 1H, NH), 3.82 (s, 4H,  $-\text{CH}_2-$ ), 3.17 (d,  $J = 4.8$  Hz, 2H,  $-\text{CH}_2-$ ), 2.66 (t,  $J = 5.0$  Hz, 2H,  $-\text{CH}_2-$ ), 1.38 (s, 9H,  $-\text{CH}_3$ )

$^{13}\text{C-NMR}$  (400 MHz,  $\text{CDCl}_3$ ):  $\delta$  (in ppm) = 159.42, 156.34, 149.26, 136.53, 123.24, 122.24, 78.72, 60.34, 53.61, 38.69, 28.60

### 2.2.6.3 Synthesis of *N*-Bis-pyridin-2-ylmethylethane-1,2-diamine, **B3**



A solution of **B2** (338 mg, 0.99 mmol) in 10 mL dichloromethane was treated with trifluoroacetic acid (TFA) through dropwise addition at  $0^\circ\text{C}$ . The reaction was

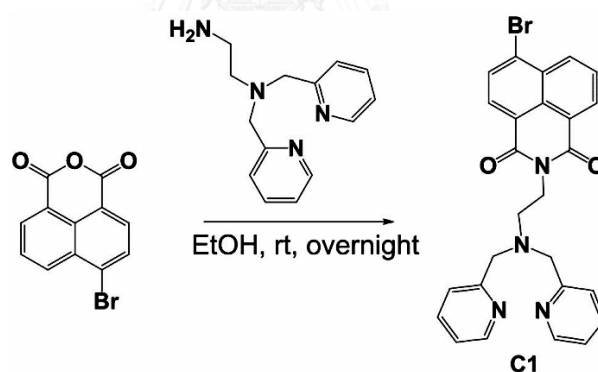
warmed up to room temperature and stirred for 2 h. under a nitrogen atmosphere, and then evaporated in *vacuo*. The residue was dissolved in an aqueous solution of sodium hydroxide and extracted with dichloromethane ( $3 \times 20$  mL). The combined organic layer was dried with magnesium sulfate, filtered and evaporated in *vacuo* to afford **B3** as brown oil (228 mg, 95% yield).

Characterization data for **B3**

$^1\text{H-NMR}$  (400 MHz,  $\text{CDCl}_3$ ):  $\delta$  (in ppm) = 8.52 (d,  $J = 4$  Hz, 2H, ArH), 7.62 (t,  $J = 7.6$  Hz, 2H, ArH), 7.43 (d,  $J = 7.6$  Hz, 2H, ArH), 7.13 (t,  $J = 6$  Hz, 2H, ArH), 3.82 (s, 4H,  $-\text{CH}_2-$ ), 2.80 (t,  $J = 5.5$  Hz, 2H,  $-\text{CH}_2-$ ), 2.67 (t,  $J = 5.6$  Hz, 2H,  $-\text{CH}_2-$ )

$^{13}\text{C-NMR}$  (400 MHz,  $\text{CDCl}_3$ ):  $\delta$  (in ppm) = 159.64, 149.23, 136.62, 123.41, 122.82, 60.87, 57.90, 39.25

#### 2.2.6.4 Synthesis of **C1**

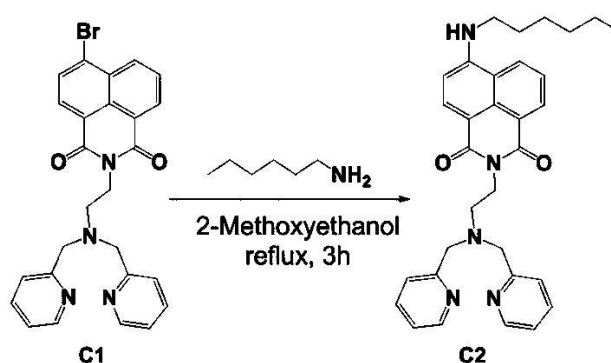


A mixture solution of **B3** (228 mg, 0.94 mmol) and 4-bromo-1,8-naphthalic anhydride (260 mg, 0.94 mmol) in 20 mL of ethanol was stirred at room temperature for overnight under a nitrogen atmosphere. Then, the mixture was evaporated and the crude product was purified by silica gel column chromatography using triethylamine/ethyl acetate / dichloromethane (1:70:30) as the eluent to afford **C1** as brown oil (401 mg, 85% yield).

### Characterization data for **C1**

**<sup>1</sup>H-NMR** (400 MHz, CDCl<sub>3</sub>): δ (in ppm) = 8.57 (t, *J* = 6.8 Hz, 2H, ArH), 8.37 (d, *J* = 4 Hz, 2H, ArH), 8.32 (d, *J* = 7.6 Hz, 1H, ArH), 8.04 (d, *J* = 8 Hz, 1H, ArH), 7.84 (t, *J* = 7.8 Hz, 1H, ArH), 7.32-7.27 (m, 4H, ArH), 6.98 (t, *J* = 5.2 Hz, 2H, ArH), 4.37 (t, *J* = 6.2 Hz, 2H, -CH<sub>2</sub>-), 3.88 (s, 4H, -CH<sub>2</sub>-), 2.91 (t, *J* = 6.2 Hz, 2H, -CH<sub>2</sub>-)

### 2.2.6.5 Synthesis of **C2**



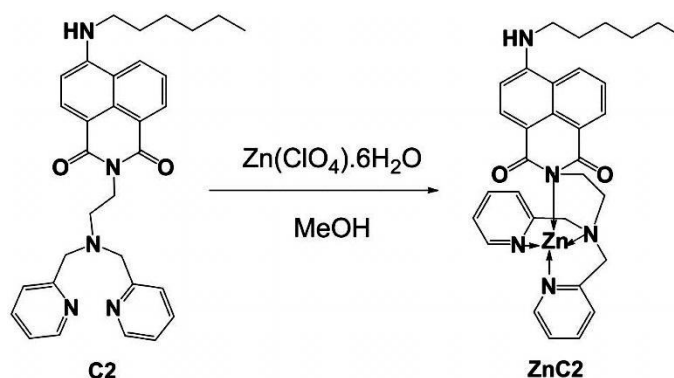
A mixture of **C1** (401 mg, 0.80 mmol) and hexylamine (81 mg, 0.80 mmol) in 10 mL of 2-methoxyethanol was refluxed for 3 h under a nitrogen atmosphere. Then, the mixture was evaporated and the crude product was purified by silica gel column chromatography using triethylamine/methanol/dichloromethane (1:1:100) as the eluent to afford **C2** as brown oil (188 mg, 45% yield).

### Characterization data for **C2**

**<sup>1</sup>H-NMR** (400 MHz, CDCl<sub>3</sub>): δ (in ppm) = 8.44 (d, *J* = 7.2 Hz, 1H, ArH), 8.38- 8.34 (m, 3H, ArH), 8.19 (d, *J* = 8.4 Hz, 1H, ArH), 7.57 (t, *J* = 7.8 Hz, 1H, ArH), 7.41 (d, *J* = 7.6 Hz, 2H, ArH), 7.35 (t, *J* = 7.4 Hz, 2H, ArH), 7.03 (t, *J* = 5.8 Hz, 2H, ArH), 6.68 (d, *J* = 8.4 Hz, 1H, ArH), 5.64 (s, 1H, NH), 4.39 (t, *J* = 6 Hz, 2H, -CH<sub>2</sub>-), 4.02 (s, 4H, -CH<sub>2</sub>-), 3.40 (q, *J* = 6.6 Hz, 2H, -CH<sub>2</sub>-), 2.99 (t, *J* = 5.8 Hz, 2H, -CH<sub>2</sub>-), 1.84-1.77 (m, 2H, -CH<sub>2</sub>-), 1.50-1.47 (m, 2H, -CH<sub>2</sub>-), 1.36 (m, 4H, -CH<sub>2</sub>-), 0.904 (t, *J* = 6.8 Hz, 3H, -CH<sub>3</sub>)

**ESI-HRMS**: Anal. Calcd. [C<sub>32</sub>H<sub>35</sub>N<sub>5</sub>O<sub>2</sub>]<sup>+</sup> *m/z* = 521.2791

Found [C<sub>32</sub>H<sub>35</sub>N<sub>5</sub>O<sub>2</sub>]<sup>+</sup> *m/z* = 521.781

2.2.6.6 Synthesis of **ZnC2**

A mixture of **C2** (260 mg, 0.5 mmol) and  $\text{Zn}(\text{ClO}_4)_2 \cdot 6\text{H}_2\text{O}$  (522 mg, 1.0 mmol) in 10 mL of methanol was stirred at room temperature for overnight. Then, the solvent was evaporated, and the mixture was dissolved in 20 mL of aqueous solution of sodium hydroxide and extracted with ethyl acetate ( $3 \times 30$  mL). The combined organic layer was dried with magnesium sulfate, filtered and evaporated in *vacuo* to give yellow powder of **ZnC2** (295 mg, 95% yield).

Characterization data for **ZnC2**

**$^1\text{H-NMR}$**  (400 MHz,  $\text{CDCl}_3$ ):  $\delta$  (in ppm) = 9.23 (s, 2H, ArH), 8.38 (t, 2H,  $J = 9.4$  Hz, ArH), 8.11 (d,  $J = 8.4$  Hz, 1H, ArH), 7.92 (t,  $J = 6.8$  Hz, 2H, ArH), 7.47-7.54 (m, 5H, ArH), 6.67 (d,  $J = 7.6$  Hz, 1H, ArH), 5.51 (s, 1H, NH), 4.38-4.0 (m, 6H,  $-\text{CH}_2-$ ), 3.40 (q,  $J = 6.2$  Hz, 2H,  $-\text{CH}_2-$ ), 2.98 (t,  $J = 6.2$  Hz, 2H,  $-\text{CH}_2-$ ), 1.82-1.78 (m, 2H,  $-\text{CH}_2-$ ), 1.52-1.45 (m, 2H,  $-\text{CH}_2-$ ), 1.36-1.37 (m, 4H,  $-\text{CH}_2-$ ), 0.91 (t,  $J = 6.8$  Hz, 3H,  $-\text{CH}_3$ )

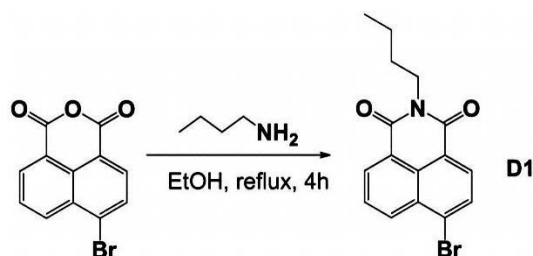
**$^{13}\text{C-NMR}$**  (400 MHz,  $\text{CDCl}_3$ ):  $\delta$  (in ppm) = 162.31, 159.86, 153.47, 145.69, 137.30, 136.82, 136.28, 130.21, 127.26, 126.94, 124.54, 124.26, 123.17, 120.90, 115.33, 110.41, 61.76, 53.52, 51.72, 50.23, 31.75, 30.13, 26.71, 20.74, 13.16

**ESI-HRMS**: Anal. Calcd.  $[\text{Zn}(\text{II})\text{C}_{32}\text{H}_{35}\text{N}_5\text{O}_2 + \text{Cl}]^+$   $m/z = 620.1776$

Found  $[\text{Zn}(\text{II})\text{C}_{32}\text{H}_{35}\text{N}_5\text{O}_2 + \text{Cl}]^+$   $m/z = 620.1749$

## 2.2.7 Synthesis of ZnD2

### 2.2.7.1 Synthesis of D1

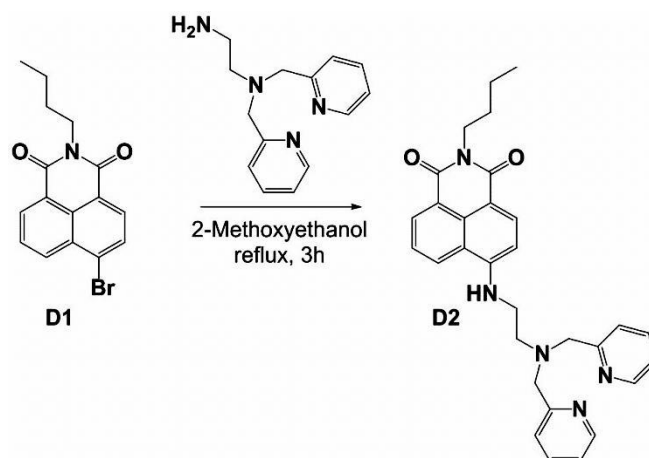


Into a two-neck round bottom flask equipped with a magnetic bar, 4-bromo-1,8-naphthalic anhydride (554 mg, 2 mmol) and *n*-butylamine (146 mg, 2 mmol) dissolved in ethanol 20 mL were refluxed for 4 h under a nitrogen atmosphere. The mixture was evaporated and recrystallized in ethanol which gave yellow powder of **D1** (1.236 g, 93% yield).

Characterization data for **D1**

<sup>1</sup>H-NMR (400 MHz, CDCl<sub>3</sub>): δ (in ppm) = 8.66 (dd, *J* = 7.6, 1.0 Hz, 1H, ArH), 8.57 (dd, *J* = 8.4, 0.8 Hz, 1H, ArH), 8.42 (d, *J* = 8.0 Hz, 1H, ArH), 8.04 (d, *J* = 7.6 Hz, 1H, ArH), 7.87-7.83 (m, 1H ArH), 4.18 (t, *J* = 7.6 Hz, 2H, -CH<sub>2</sub>-), 1.74-1.69 (m, 2H, -CH<sub>2</sub>-), 1.48-1.42 (m, 2H, -CH<sub>2</sub>-), 0.98 (t, *J* = 7.4 Hz, 3H, -CH<sub>3</sub>)

### 2.2.7.2 Synthesis of D2



A mixture of **D1** (221 mg, 0.80 mmol) and **B3** (194 mg, 0.80 mmol) in 10 mL of 2-methoxyethanol was refluxed for 3 h under a nitrogen atmosphere. Then the solvent was evaporated and the crude product was purified by silica gel column chromatography using triethylamine/methanol/dichloromethane (1:1:100) as the eluent to afford **D2** as yellow powder (246 mg, 78% yield).

Characterization data for **D2**

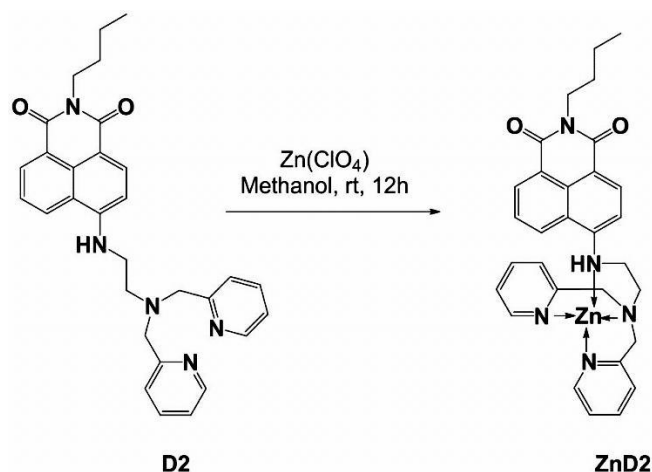
$^1\text{H-NMR}$  (400 MHz,  $\text{CDCl}_3$ ):  $\delta$  (in ppm) = 8.76 (d,  $J = 8.0$  Hz, 1H, ArH), 8.62 (d,  $J = 7.2$  Hz, 1H, ArH), 8.57 (d,  $J = 4.8$  Hz, 2H, ArH), 8.40 (d,  $J = 8.4$  Hz, 1H, ArH), 7.69 (t,  $J = 7.8$  Hz, 2H, ArH), 7.56 (t,  $J = 7.6$  Hz, 2H, ArH), 7.39 (d,  $J = 8.0$  Hz, 2H, ArH), 7.15 (t,  $J = 6.8$  Hz, 2H, ArH), 6.53 (d,  $J = 8.8$  Hz, 1H, NH), 4.17 (t,  $J = 7.4$  Hz, 2H,  $-\text{CH}_2-$ ), 4.00 (s, 4H,  $-\text{CH}_2-$ ), 3.40 (t,  $J = 5.0$  Hz, 2H,  $-\text{CH}_2-$ ), 3.05 (t,  $J = 5.4$  Hz, 2H,  $-\text{CH}_2-$ ), 1.76-1.68 (m, 2H,  $-\text{CH}_2-$ ), 1.50-1.40 (m, 2H,  $-\text{CH}_2-$ ), 0.97 (t,  $J = 7.4$  Hz, 3H,  $-\text{CH}_3$ )

$^{13}\text{C-NMR}$  (400 MHz,  $\text{CDCl}_3$ ):  $\delta$  (in ppm) = 164.93, 164.29, 158.62, 150.33, 149.02, 136.86, 134.77, 131.03, 130.05, 127.49, 124.32, 123.47, 122.98, 122.47, 120.81, 109.37, 103.99, 59.70, 51.30, 40.96, 39.97, 30.37, 20.47, 14.10

**ESI-HRMS**: Anal. Calcd.  $[\text{C}_{30}\text{H}_{31}\text{N}_5\text{O}_2 + \text{H}]^+$   $m/z = 494.2551$

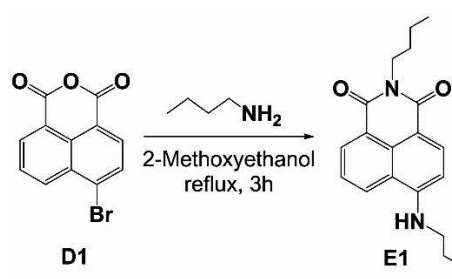
Found  $[\text{C}_{30}\text{H}_{31}\text{N}_5\text{O}_2 + \text{H}]^+$   $m/z = 494.2630$

### 2.2.7.3 Synthesis of **ZnD2**



A mixture of **D2** (247 mg, 0.5 mmol) and  $\text{Zn}(\text{ClO}_4)_2 \cdot 6\text{H}_2\text{O}$  (522 mg, 1.0 mmol) in 10 mL of methanol was stirred at room temperature for overnight. Then, the solvent was evaporated, and the mixture was dissolved in 20 mL of aqueous solution of sodium hydroxide and extracted with ethyl acetate ( $3 \times 30$  mL). The combined organic layer was dried with magnesium sulfate, filtered and evaporated in *vacuo*. Unfortunately, **ZnD2** was not obtained.

### 2.2.8 Synthesis of E1



A mixture solution including 4-bromo-1,8-naphthalic anhydride (554 mg, 2 mmol) and *n*-butylamine (292 mg, 4 mmol) in 20 mL 2-methoxyethanol was refluxed for 4 h under a nitrogen atmosphere. The mixture was evaporated and recrystallized in ethyl acetate affording yellow powder of **E1** (1.168 g, 90% yield).

Characterization data for **E1**

$^1\text{H-NMR}$  (400 MHz,  $\text{CDCl}_3$ ):  $\delta$  (in ppm) = 8.57 (dd,  $J = 7.6, 1.0$  Hz, 1H, ArH), 8.46 (d,  $J = 8.4$  Hz, 1H, ArH), 8.08 (dd,  $J = 8.4, 0.8$  Hz, 1H, ArH), 7.61 (t,  $J = 7.8$  Hz, 1H, ArH), 6.72 (d,  $J = 8.4$  Hz, 1H, ArH), 5.26 (s, 1H, NH), 4.16 (t,  $J = 7.6$  Hz, 2H,  $-\text{CH}_2-$ ), 3.41 (q,  $J = 6.4$  Hz, 2H,  $-\text{CH}_2-$ ), 1.84-1.77 (m, 2H,  $-\text{CH}_2-$ ), 1.75-1.67 (m, 2H,  $-\text{CH}_2-$ ), 1.60-1.40 (m, 4H,  $-\text{CH}_2-$ ), 1.03 (t,  $J = 7.4$  Hz, 3H,  $-\text{CH}_3$ ), 0.98 (t,  $J = 7.2$  Hz, 3H,  $-\text{CH}_3$ )



## 2.3 Complexation studies by fluorescence spectroscopy

### 2.3.1 Apparatus

All Emission spectra were recorded by a Varian Cary Eclipse fluorescence spectrophotometer.

### 2.3.2 Chemical

All materials were standard analytical grade. The solvents were spectrochemical grade. Biogenic amines used as guest molecules in this study are dopamine (DA), norepinephrine (NE), tyramine (Tyr), L-glutamic acid (Glu), L-lysine (Lys), histidine (His), histamine (Hist) glycine (Gly), alanine (Ala), threonine (Thre), phenylalanine (Phe) and leucine (Leu). Their structures were shown in Fig. 2.1.

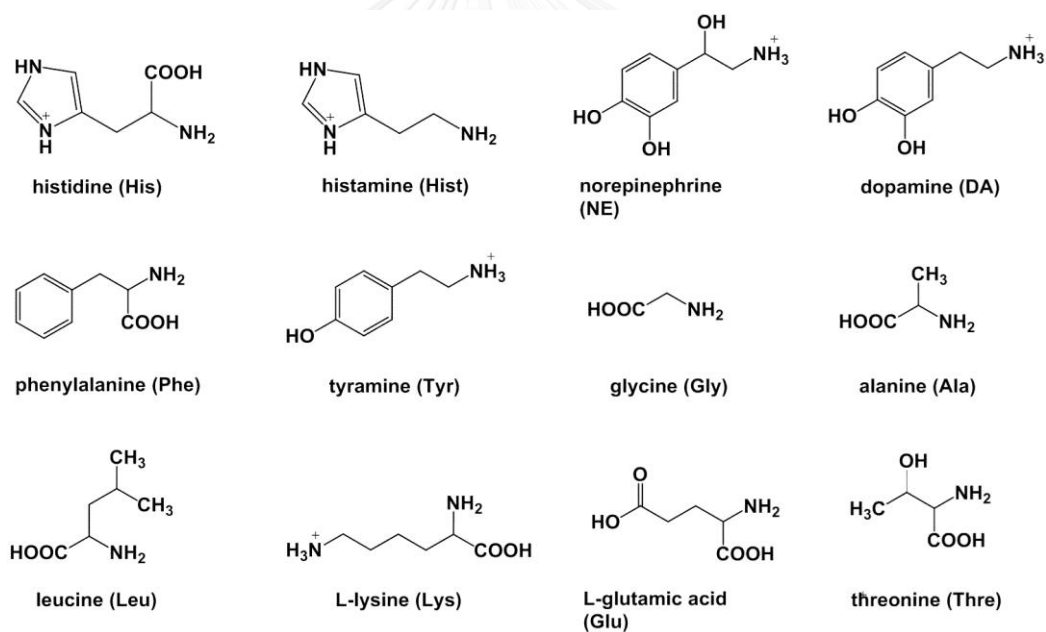


**Figure 2.1** The structures of various biogenic amines

### 2.3.3 Experimental procedure

The conditions set in each fluorescence experiment are illustrated below:

Excitation wavelength: 345 nm

Range of emission spectrum: 350-700 nm

Width of excitation and emission slit: 10 nm

Smoothing factor: 15

Scan rate: medium

PMT voltage: medium

### 2.3.4 Complexation studies

#### 2.3.4.1 Complexation studies in homogeneous solution of isoindole product with various biogenic amines

The fluorescence response of homogenous reaction including *o*-phthalaldehyde (**OPA**) with various amino acids in the presence of 2-mercaptoethyltrimethoxysilane (**SH**) to form isoindole product was studied. Initially, stock solution of 0.1 M **OPA** and **SH** in ethanol and 0.01 M biogenic amines in phosphate buffer (0.01 M, pH 7.4) was prepared. In a 1cm path length quartz cuvette, the solution of each biogenic amine (100  $\mu$ L) was added directly to the solution consisting of 1890  $\mu$ L phosphate buffer (0.01 M, pH 7.4) and 5  $\mu$ L **OPA** and 5  $\mu$ L **SH**. The mixture solution was stirred for 10 seconds before measurement of fluorescence spectrophotometer.

#### 2.3.4.2 Complexation studies of SNPs-OPTA and **CB** with various biogenic amines

Typically, a stock solution of 4.5 mg/mL SNPs-OPTA in 0.01 M phosphate buffer solution, pH 7.4 and a stock solution of  $1 \times 10^{-2}$  M **CB** consisting of piperidine (1:10, **CB**: piperidine) in DMSO were prepared. The stock solutions of  $1 \times 10^{-2}$  M of various biogenic amines namely dopamine (DA), norepinephrine (NE), tyramine (Tyr), L-glutamic acid (Glu), L-lysine (Lys), histidine (His), and histamine (Hist) were prepared in the buffer solution as shown in Table 2.3.

**Table 2.3** Preparing stock solution of biogenic amines ( $1 \times 10^{-2}$  M)

Guest	Molecular weight ( $\text{gmol}^{-1}$ )	Weight (mg)	Volume (mL)
DA	189.64	3.79	2
NE	205.64	4.11	2
Tyr	137.18	2.74	2
Glu	147.13	2.94	2
Lys	146.19	2.92	2
His	155.16	3.10	2
Hist	111.15	2.22	2

Under fluorescence spectroscopy, the solution consisting of 667  $\mu\text{L}$  stock solution of SNPs-OPTA and 1258  $\mu\text{L}$  phosphate buffer solution, which was treated with 25  $\mu\text{L}$  of each the guest stock solution, were monitored after stirring the mixture for 30 minutes. And then, each mixture was filled with 50  $\mu\text{L}$  of **CB** stock solution and stirred for 20 minutes before measurement.

#### 2.3.4.3 Complexation studies of SNPs-OPTA\_CTAB and **ZnC2**

##### 2.3.4.3A Energy transfer studies of **ZnC2** in both SNPs-OPTA and SNPs-OPTA\_CTAB systems

Energy transfer between isindole product of histidine and **ZnC2** in both modified siliaca namely SNPs-OPTA and SNPs-OPTA\_CTAB was investigated. Firstly, a 4.5 mg/mL stock solution of SNPs-OPTA and SNPs-OPTA\_CTAB in 0.01 M phosphate buffer solution (pH 7.4) and a stock solution of  $1 \times 10^{-2}$  M **ZnC2** in DMSO were prepared. A stock solution of histidine in phosphate buffer solution was  $1 \times 10^{-2}$  M.

In SNPs-OPTA system, the solution consisting of 667  $\mu\text{L}$  SNPs-OPTA stock solution and 1308  $\mu\text{L}$  phosphate buffer solution was treated with 25  $\mu\text{L}$  of histidine and stirred for 30 minutes to generate isindole product. And then **ZnC2** was added directly to the solution as following the condition listed in Table 2.4.

**Table 2.4** The amounts of compounds in energy transfer studies of **ZnC2** in both SNPs-OPTA systems

Entry	His/ <b>ZnC2</b>	[His] ( $\times 10^{-4}$ M)	[ <b>ZnC2</b> ] ( $\times 10^{-5}$ M)	V <sub>ZnC2</sub> ( $\mu$ L)	V <sub>total</sub> ( $\mu$ L)
1	1:0.00	1.250	0	0	2,000
2	1:0.20	1.247	2.494	5	2,005
3	1:0.60	1.241	7.444	15	2,015
4	1:1.00	1.235	12.35	25	2,025
5	1:1.40	1.229	17.20	35	2,035

In SNPs-OPTA\_CTAB system, the mixture between 667  $\mu$ L of SNPs-OPTA\_CTAB stock solution and 1308  $\mu$ L of phosphate buffer solution was treated with 25  $\mu$ L of histidine and stirred for 30 minutes to generate isoindole product. And then **ZnC2** was added to the solution as following the condition listed in Table 2.5.

**Table 2.5** The amount of compounds in energy transfer studies of **ZnC2** in SNPs-OPTA\_CTAB systems

Entry	His/ <b>ZnC2</b>	[His] ( $\times 10^{-4}$ M)	[ <b>ZnC2</b> ] ( $\times 10^{-5}$ M)	V <sub>ZnC2</sub> ( $\mu$ L)	V <sub>total</sub> ( $\mu$ L)
1	1:0.00	1.250	0	0	2,000.0
2	1:0.10	1.248	1.248	2.5	2,002.5
3	1:0.20	1.247	2.494	5	2,005.0
4	1:0.40	1.244	4.975	10	2,010.0
5	1:0.60	1.241	7.444	15	2,015.0
6	1:0.80	1.238	9.901	20	2,020.0
7	1:1.00	1.235	12.35	25	2,025.0
8	1:1.20	1.232	14.78	30	2,030.0
9	1:1.40	1.229	17.20	35	2,035.0

#### 2.3.4.3B Complexation studies of SNPs-OPTA\_CTAB and **ZnC2** with various biogenic amines

The system consisting of SNPs-OPTA\_CTAB with and without **ZnC2** was studied for specific detection toward various biogenic amines namely dopamine

(DA), norepinephrine (NE), tyramine (Tyr), L-glutamic acid (Glu), L-lysine (Lys), histidine (His), and histamine (Hist) in 0.01 M phosphate buffer solution, pH 7.4.

Firstly, 4.5 mg/mL stock solution of SNPs-OPTA\_CTAB in 0.01 M phosphate buffer solution (pH 7.4) and a stock solution of  $1 \times 10^{-2}$  M **ZnC2** in DMSO were prepared. A stock solution of biogenic amine in the phosphate buffer solution was  $1 \times 10^{-2}$  M. To study specific detection of SNPs-OPTA\_CTAB toward various biogenic amines, each biogenic amine (25  $\mu$ L) was added to the solution consisting of 667  $\mu$ L SNPs-OPTA\_CTAB and 1308  $\mu$ L phosphate buffer solution. The mixture was stirred for 30 minutes before measurement of fluorescence spectroscopy. Furthermore, to study specific detection through energy transfer in the system consisting of **ZnC2** and SNPs-OPTA\_CTAB, 25  $\mu$ L of each biogenic amine (concentration) was added to the solution consisting of 667  $\mu$ L SNPs-OPTA, 40  $\mu$ L **ZnC2** ( $1 \times 10^{-2}$  M) and 1,268  $\mu$ L phosphate buffer solution. The mixture was stirred for 30 minutes before measurement under fluorescence spectroscopy.

#### *2.3.4.3C Naked-eye studies of SNPs-OPTA\_CTAB and SNPs-OPTA\_CTAB consisting of ZnC2 with various biogenic amines*

To study naked-eye fluorescence responses under UV light, fluorescence emission image of the isoindole products in SNPs-OPTA\_CTAB system and fluorescence emission images of **ZnC2** in the system consisting of SNPs-OPTA\_CTAB and **ZnC2** was investigated toward various biogenic amines. Firstly, a 4.5 mg/mL stock solution of SNPs-OPTA\_CTAB in 0.01 M phosphate buffer solution (pH 7.4) and a stock solution of  $1 \times 10^{-2}$  M **ZnC2** in DMSO were prepared. The stock solution of biogenic amines in phosphate buffer solution was  $1 \times 10^{-2}$  M. To study naked-eye responses of isoindole product obtained from various biogenic amines, the stock solution of each biogenic amine (100  $\mu$ L) was added directly to the solution consisting of 1,334  $\mu$ L of SNPs-OPTA\_CTAB stock solution and 566  $\mu$ L of the phosphate buffer solution in vial. The amount of each compound was listed in Table 2.6. The mixture was stirred for 30 minutes before investigation under the black light or UV light.

**Table 2.6** The amounts of guest and SNPs-OPTA\_CTAB used for study on the naked-eye responses of isiondole product

Vial	Guest	V <sub>SNPs-OPTA_CTAB</sub> (μL)	V <sub>buffer</sub> (μL)	V <sub>Guest</sub> (μL)	V <sub>total</sub> (μL)
1	-	1,334	566	100	2,000
2	Hist	1,334	566	100	2,000
3	Tyr	1,334	566	100	2,000
4	His	1,334	566	100	2,000
5	DA	1,334	566	100	2,000
6	Glu	1,334	566	100	2,000
7	Lys	1,334	566	100	2,000
8	NE	1,334	556	100	2,000

To study the naked-eye responses of **ZnC2** in system consisting of SNPs-OPTA\_CTAB and **ZnC2** toward various biogenic amines, the solution of each biogenic amine (100 μL) was added directly to the solution consisting of 1,334 μL of SNPs-OPTA\_CTAB stock solution, 526 μL of the phosphate buffer solution and 40 μL of **ZnC2** ( $1 \times 10^{-2}$  M) in 2 cm<sup>3</sup> vials as amount of compounds listed in Table 2.7. The mixture was stirred for 30 minutes before investigation under the black light or UV light.

**Table 2.7** The amounts of guest, SNPs-OPTA\_CTAB and **ZnC2** used for study on naked-eye responses of **ZnC2** in detection of various guest

Vial	Guest	V <sub>SNPs-OPTA_CTAB</sub> (μL)	V <sub>buffer</sub> (μL)	V <sub>ZnC2</sub> (μL)	V <sub>Guest</sub> (μL)	V <sub>total</sub> (μL)
1	-	1,334	526	40	100	2,000
2	Hist	1,334	526	40	100	2,000
3	Tyr	1,334	526	40	100	2,000
4	His	1,334	526	40	100	2,000
5	DA	1,334	526	40	100	2,000
6	Glu	1,334	526	40	100	2,000
7	Lys	1,334	526	40	100	2,000
8	NE	1,334	526	40	100	2,000

#### 2.3.4.4 Complexation studies of MSNs-OPTA with various biogenic amines

##### 2.3.4.4A Fluorescence responses of MSNs-OPTA in various biogenic amines

Mesoporous silica nanoparticles were also utilized as the supporting matrix incorporated with amine-sensitive *o*-phthalic hemithioacetal (OPTA) group on the pore-surface. The materials was investigated by fluorescent technique in 0.01 M phosphate buffer solution, pH 7.4, toward various biogenic amines namely alanine (Ala), glutamic acid (Glu), glycine (Gly), histidine (His), leucine (Leu), lysine (Lys) and phenylalanine (Phe). Firstly, stock solution of MSNs-OPTA (4.5 mg/mL) and biogenic amine ( $1 \times 10^{-2}$  M) was prepared in 0.01 M phosphate buffer solution pH 7.4. In 1 cm path length cuvette, the solution consisting of 667  $\mu$ L stock solution of SNPs-OPTA and 1308  $\mu$ L phosphate buffer solution was treated with 25  $\mu$ L of each biogenic amine and stirred for 30 minutes before recording the fluorescence spectra.

##### 2.3.4.4B Naked-eye studies of MSNs-OPTA in various biogenic amines

Naked-eye responses of the isoindole products obtained by reaction of MSNs-OPTA and various guests namely alanine (Ala), glutamic acid (Glu), glycine (Gly), histidine (His), leucine (Leu), lysine (Lys) and phenylalanine (Phe) were studied through fluorescence response under UV light. Firstly, stock solution of MSNs-OPTA (4.5 mg/mL) was prepared in 0.01 M phosphate buffer solution pH 7.4. The guest stock solutions of various biogenic amines ( $1 \times 10^{-2}$  M) were prepared in the buffer solution as shown in Table 2.8.

**Table 2.8** Preparation of stock solution of biogenic amines ( $1 \times 10^{-2}$  M)

Guest	Molecular weight (gmol <sup>-1</sup> )	Weight (mg)	Volume (mL)
Ala	89.09	1.78	2
Glu	147.13	2.94	2
Gly	75.07	1.50	2
His	155.16	3.10	2
Leu	131.17	2.62	2
Lys	146.19	2.92	2
Phe	165.19	3.30	2

The stock solution of each biogenic amine (30  $\mu\text{L}$ ) was added directly to the solution consisting of 667  $\mu\text{L}$  of MSNs-OPTA and 1303  $\mu\text{L}$  of the phosphate buffer solution in vial. The detail was shown in Table 2.9. The mixture was stirred for 30 minutes before investigation under black light or UV light.

**Table 2.9** The amounts of guest and SNPs-OPTA\_CTAB used for study on the naked-eye responses of isiondole product in various biogenic amines

Vial	Guest	V <sub>SNPs-OPTA_CTAB</sub> ( $\mu\text{L}$ )	V <sub>buffer</sub> ( $\mu\text{L}$ )	V <sub>Guest</sub> ( $\mu\text{L}$ )	[SNPs-OPTA] (mg/mL)	[Guest] ( $\mu\text{M}$ )	V <sub>total</sub> ( $\mu\text{L}$ )
1	-	667	1,303	30	1.50	150	2,000
2	Ala	667	1,303	30	1.50	150	2,000
3	Glu	667	1,303	30	1.50	150	2,000
4	Gly	667	1,303	30	1.50	150	2,000
5	His	667	1,303	30	1.50	150	2,000
6	Lue	667	1,303	30	1.50	150	2,000
7	Lys	667	1,303	30	1.50	150	2,000
8	Phe	667	1,303	30	1.50	150	2,000

#### 2.3.4.4C Complexation study of sensor MSNs-OPTA with histidine by fluorescence spectrophotometric titration technique

Firstly, a stock solution of 4.5 mg/mL MSNs-OPTA and  $1 \times 10^{-3}$  M histidine in 0.01 M phosphate buffer solution was prepared. The titration was carried out through classical titration method. The different concentration of histidine was prepared and measured in each cuvette. Various amounts of histidine were added directly to the solution of MSNs-OPTA in a 1-cm quartz cuvette as shown in Table 2.10. The solution was stirred for 40 minutes before recording fluorescence spectrum.



**Table 2.10** The concentration of histidine used for complexation study of MSNs-OPTA by fluorescence spectrophotometric titration technique

Entry	V <sub>MSNs-OPTA</sub> ( $\mu$ L)	V <sub>buffer</sub> ( $\mu$ L)	V <sub>histidine</sub> ( $\mu$ L)	[histidine] ( $\mu$ M)	V <sub>total</sub> ( $\mu$ L)
1	667	1,333	0	0	2,000
2	667	1330	6	3	2,000
3	667	1328	10	5	2,000
4	667	1326.75	12.5	6.25	2,000
5	667	1325	16	8	2,000
6	667	1323	20	10	2,000
7	667	1320.5	25	12.5	2,000
8	667	1318	30	15	2,000
9	667	1313	40	20	2,000
10	667	1308	50	25	2,000
11	667	1303	60	30	2,000
12	667	1298	70	35	2,000
13	667	1283	100	50	2,000
14	667	1273	120	60	2,000
15	667	1253	160	80	2,000
16	667	1233	200	100	2,000
17	667	1213	240	120	2,000
18	667	1183	300	150	2,000

#### 2.3.4.4D Kinetic study of isoindole formation in MSNs-OPTA toward various biogenic amines

To study reaction rate of isoindole formation generated from the reaction of OPTA-derivatized mesoporous silica (MSNs-OPTA) and various biogenic amines including alanine (Ala), glutamic acid (Glu), glycine (Gly), histidine (His), leucine (Leu), lysine (Lys) and phenylalanine (Phe), the measurements of the fluorescent product per unit time of each biogenic amine were investigated. The change of fluorescence intensity at 450 nm, when the product was excited at 345 nm, was monitored and plotted per time unit.

Firstly, a stock solution of 4.5 mg/mL MSNs-OPTA and  $1 \times 10^{-2}$  M biogenic amines in 0.01 M phosphate buffer solution was prepared. In cuvette, the solution consisting of MSNs-OPTA stock solution (667  $\mu$ L) and phosphate buffer solution (1,303  $\mu$ L) was treated with biogenic amine (30  $\mu$ L). After stirring, the fluorescent

response was recorded every 2 minutes for 60 minutes. The relative intensity  $[(I-I_0)_{\text{biogenic amine}}/(I-I_0)_{\text{max}}]$  of emission band at 450 nm was calculated and plotted per unit time.

#### 2.3.4.4E Study of the proposed mechanism of histidine in forming isiondole product

A 0.1 M buffer solution at different pH was prepared by different kinds of buffer as shown in Table 2.11.

**Table 2.11** Different kinds of buffer solution at various pHs

Entry	pH	Buffer solution	[Buffer solution] M
1	4.0	KH	0.10
2	5.0	KH	0.10
3	6.0	PBS	0.10
4	7.4	PBS	0.10
5	8.0	PBS	0.10
6	8.5	Na <sub>2</sub> B <sub>4</sub> O <sub>7</sub>	0.10
7	9.0	Na <sub>2</sub> B <sub>4</sub> O <sub>7</sub>	0.10
8	10.0	Na <sub>2</sub> B <sub>4</sub> O <sub>7</sub>	0.10

A stock solution of 4.5 mg/mL MSNs-OPTA and  $1 \times 10^{-2}$  M histidine in 0.01 M milli Q water was prepared. The solution consisting of MSNs-OPTA stock solution (667  $\mu$ L) and buffer solution (1,303  $\mu$ L) was treated with histidine (30  $\mu$ L) and stirred for 45 minutes before recording fluorescent spectrum. And the fluorescent intensity at 450 nm of histidine detection in each pH buffer solution was plotted versus pH values in order to study the effect of pH value toward isoindole formation.

#### 2.3.4.5 Complexation studies of MSNs-OPTA-CTAB and receptor molecules (**ZnD2** and **E2**) with various biogenic amines

##### 2.3.4.5A Suspension ability

Self-quenching of fluorophore on the modified mesoporous silica nanoparticles (MSNs-OPTA) in histidine detection was reduced by CTAB modification. To verify the proper condition of MSNs-OPTA-CTAB system by varying the amount of CTAB, **E2** was employed as an optical probe. The solutions of

MSNs-OPTA and **E2** in various concentration of CTAB were prepared and the suspension ability of the particle through naked-eye responses was monitored under UV-light at various concentration of CTAB (0, 0.25, 0.5, 1 and 2 mM, respectively).

Firstly, the stock solutions of 4.5 mg/mL MSNs-OPTA and 0.1 M CTAB in phosphate buffer solution and  $1 \times 10^{-2}$  M **E2** in DMSO were prepared. MSNs-OPTA-CTAB systems at various concentrations of CTAB were prepared in vial. The various portions of the stock solutions of CTAB, MSNs-OPTA and **E2** were listed in Table 2.12.

**Table 2.12** The amounts of CTAB used for study on the physical properties of MSNs-OPTA-CTAB system

Entry	[CTAB] (mM)	V <sub>CTAB</sub> ( $\mu$ L)	V <sub>MSNs-OPTA</sub> ( $\mu$ L)	V <sub>E2</sub> ( $\mu$ L)	V <sub>PBS</sub> ( $\mu$ L)	V <sub>total</sub> ( $\mu$ L)
1	0.00	0	200	20	1780	2000
2	0.25	5	200	20	1775	2000
3	0.50	10	200	20	1770	2000
4	1.00	20	200	20	1760	2000
5	2.00	40	200	20	1720	2000

And then the solutions were stirred for 30 minutes and left for 5 minutes before investigation by naked-eye responses under UV-light.

#### 2.3.4.5B Zeta potential and size distribution

Zeta potential of MSNs-OPTA-CTAB dispersed in phosphate buffer solution at various concentrations of CTAB (0.125, 0.5, 0.75 and 1.00) was studied to elucidate the formation between silica nanoparticles and CTAB in each condition. The solutions were prepared as the condition listed in Table 2.13.

**Table 2.13** The amounts of CTAB used for study on zeta potential and size distribution of MSNs-OPTA-CTAB system

Entry	[CTAB] (mM)	V <sub>CTAB</sub> (μL)	V <sub>MSNs-OPTA</sub> (μL)	V <sub>E2</sub> (μL)	V <sub>PBS</sub> (μL)	V <sub>total</sub> (μL)
1	0.00	0	200	20	1780	2000
2	0.125	2.5	200	20	1777.5	2000
3	0.50	10	200	20	1770	2000
4	0.75	15	200	20	1765	2000
5	1.00	20	200	20	1760	2000

The solutions were measured under NanoPlus-3 with different mode namely Zeta Potential Analyzer and Particle size Analyzer.

#### 2.3.4.5C Complexation studies of **D2** toward various metal ions

**ZnD2** was designed as a receptor molecule to induce FRET process in MSNs-OPTA-CTAB system. **ZnD2** was not successfully synthesized. However, **D2** as a ligand was investigated in binding ability of **ZnD2** complex in buffer solution. The formation between **D2** and different metal ions in HEPES buffer solution, pH 7.4 was investigated. Firstly, 0.01 M HEPES buffer and 0.01 M phosphate buffer solution were prepared. A stock solution of 10 mM **D2** in DMSO and 1 mM metal ions in milli Q water were prepared. Under fluorescence spectroscopy, the solution of metal ions was added directly to solution of **D2** and the mixture solution was stirred for 5 minutes before measurement. The amounts of metal (II) ion, **D2** and buffer solution were listed in Table 2.14.

**Table 2.14** The amounts of metal ion, **D2** and buffer solution for complexation study of metal ion (II)

Entry	Metal ion	[Metal ion] (mM)	V <sub>metal ion</sub> (μL)	V <sub>D2</sub> (μL)	V <sub>buffer</sub> (μL)	V <sub>total</sub> (μL)
1	Cu(II)	0.01	20	10	1,970	2,000
2	Ni(II)	0.01	20	10	1,970	2,000
3	Zn(II)	0.01	20	10	1,970	2,000
4	Co(II)	0.01	20	10	1,970	2,000
5	Cr(II)	0.01	20	10	1,970	2,000
6	Mn(II)	0.01	20	10	1,970	2,000

#### *2.3.4.5D Complexation studies of MSNs-OPTA-CTAB and ZnD2 prepared in buffer solution*

**ZnD2** prepared in buffer solution (mixture between Zn (II) and **D2**) was applied to detect histidine in MSNs-OPTA-CTAB system. Firstly, stock solutions of 4.5 mg/mL MSNs-OPTA, 0.1 M CTAB and  $1 \times 10^{-2}$  M histidine in 0.01 M HEPES buffer solution were prepared. **D2** was dissolved in DMSO to prepare 10 mM stock solution. A stock solution of 1 mM  $\text{ZnClO}_4$  was prepared in milli Q water. To study suspension ability, the stock solution of 20  $\mu\text{L}$   $\text{ZnClO}_4$  and 10  $\mu\text{L}$  **D2** was mixed in 470  $\mu\text{L}$  HEPES buffer solution to form **ZnD2**. In MSNs-OPTA-CTAB system, 200  $\mu\text{L}$  of MSNs-OPTA stock solution and 1,280  $\mu\text{L}$  HEPES buffer solution were treated with 20  $\mu\text{L}$  of CTAB stock solution and stirred for 20 minutes. Finally, both solutions were mixed together. The mixture was studied under naked-eye observation.

#### *2.3.4.5E Energy transfer studies of isoindole product of histidine in MSNs-OPTA-CTAB by D2 as a receptor*

Firstly, a stock solution of 4.5 mg/mL MSNs-OPTA and 0.1 M CTAB in 0.01 M phosphate buffer solution (pH 7.4) and a stock solution of  $1 \times 10^{-2}$  M **D2** in DMSO were prepared. The stock solution of histidine was  $1 \times 10^{-2}$  M. Under fluorescence spectroscopy, the solution consisting of MSNs-OPTA (200  $\mu\text{L}$ ), CTAB stock solution (20  $\mu\text{L}$ ) and phosphate buffer solution (1,750  $\mu\text{L}$ ) was treated with 30  $\mu\text{L}$  of histidine and stirred for 60 minutes to generate isoindole product, and then  $1 \times 10^{-3}$  M **D2** was added directly to the solution as following the condition listed in Table 2.15.

**Table 2.15** The amounts of compounds for energy transfer studies of **D2** in MSNs-OPTA-CTAB systems

Entry	His/ <b>D2</b>	[His] ( $\mu\text{M}$ )	[ <b>D2</b> ] ( $\mu\text{M}$ )	$V_{\text{D2}}$ ( $\mu\text{L}$ )	$V_{\text{total}}$ ( $\mu\text{L}$ )
1	1:0.00	150	0	0	2000
2	1:0.033	149.2537	4.975124	10	2010
3	1:0.067	148.5149	9.90099	20	2020
4	1:0.100	147.7833	14.77833	30	2030
5	1:0.133	147.0588	19.60784	40	2040
6	1:0.167	146.3415	24.39024	50	2050
7	1:0.200	145.6311	29.12621	60	2060
8	1:0.233	144.9275	33.81643	70	2070
9	1:0.300	143.5407	43.0622	90	2090
10	1:0.367	142.1801	52.1327	110	2110
11	1:0.467	140.1869	65.42056	140	2140
12	1:0.533	138.8889	74.07407	160	2160

#### 2.3.4.5F Complexation studies of MSNs-OPTA and **D2** with various biogenic amines

The system consisting of MSNs-OPTA, CTAB and **D2** was applied to study specific detection of biogenic amines namely alanine (Ala), glutamic acid (Glu), glycine (Gly), histidine (His), leusine (Leu), lysine (Lys) and phenylalanine (Phe) in 0.01 M phosphate buffer solution. A stock solution of 4.5 mg/mL MSNs-OPTA, a stock solution  $1 \times 10^{-2}$  M of the guest molecules and a stock solution of 0.1 M CTAB were prepared in 0.01 M phosphate buffer solution, pH 7.4. A stock solution of  $1 \times 10^{-1}$  M **D2** in DMSO was prepared. Each guest molecule was investigated through the same condition. 30  $\mu\text{L}$  of biogenic amine was added to the solution consisting of MSNs-OPTA (200  $\mu\text{L}$ ), CTAB (20  $\mu\text{L}$ ), **D2** (15  $\mu\text{L}$ ) and phosphate buffer solution (1,268  $\mu\text{L}$ ). The mixture was stirred for 30 minutes before investigation of fluorescence response. The amounts of compounds were listed in Table 2.16.

**Table 2.16** The amounts of guest and MSNs-OPTA-CTAB used for study on visual changes of isiondole product in various biogenic amines

Entry	Guest	V <sub>MSNs-OPTA</sub> ( $\mu$ L)	V <sub>CTAB</sub> ( $\mu$ L)	V <sub>D2</sub> ( $\mu$ L)	V <sub>buffer</sub> ( $\mu$ L)	V <sub>Guest</sub> ( $\mu$ L)	V <sub>total</sub> ( $\mu$ L)
1	-	200	20	15	1,735	30	2,000
2	Ala	200	20	15	1,735	30	2,000
3	Glu	200	20	15	1,735	30	2,000
4	Gly	200	20	15	1,735	30	2,000
5	His	200	20	15	1,735	30	2,000
6	Lue	200	20	15	1,735	30	2,000
7	Lys	200	20	15	1,735	30	2,000
8	Phe	200	20	15	1,735	30	2,000

*2.3.4.5G Energy transfer studies of isoindole product of histidine in MSNs-OPTA-CTAB by E2 as a receptor*

To study energy transfer of **E2** in MSNs-CTAB system, firstly a stock solution of 4.5 mg/mL MSNs-OPTA, a stock solution of  $1 \times 10^{-2}$  M of the guest molecules and a stock solution of 0.1 M of CTAB were prepared in 0.01 M phosphate buffer solution (pH 7.4). A stock solution of  $1 \times 10^{-2}$  M **E2** in DMSO was prepared. 30  $\mu$ L of histidine was added directly to the solution consisting of 200  $\mu$ L MSNs-OPTA, 20  $\mu$ L CTAB, 15  $\mu$ L **E2** and 1,735  $\mu$ L phosphate buffer solution. The mixture was stirred for 30 minutes before measurement of fluorescence spectroscopy.

## CHAPTER III

### RESULTS AND DISCUSSIONS

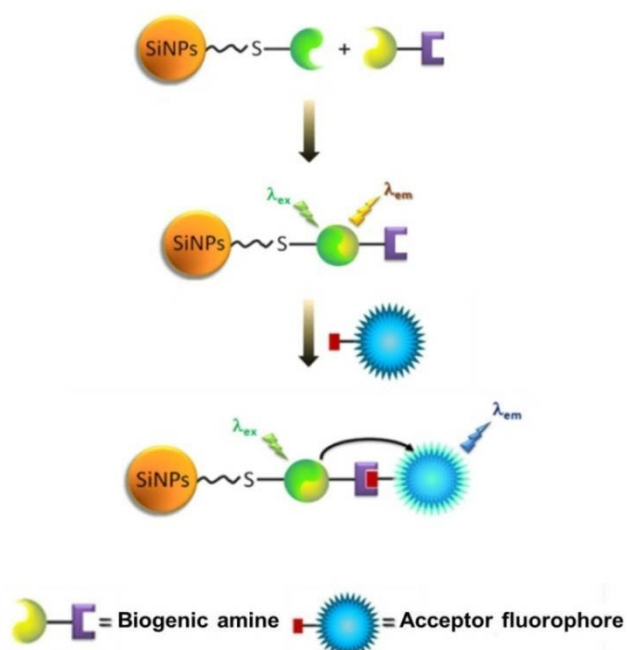
#### 3.1 Design and synthesis of biogenic amine base sensor

Design and synthesis of the sensors to categorize biogenic amines in biological system have been focused in this research. To enhance water solubility of sensor systems, both silica nanospheres and mesoporous silica were used as solid support. As basic knowledge, isoindole product was generated from the reaction of *o*-phthalaldehyde reacting with amino acids in the presence of 2-mercaptoethanol giving a strong fluorescent compounds (isoindole product) without selectivity in solution [48]. The reaction was applied and modified on mesoporous silica under idea of Lin et al [27] regarding to *o*-phthalic hemithioacetal (OPTA) unit modified on silica surface as a unit sensor of primary amine. However, this report demonstrated the selectivity of biogenic amine detection depending on interaction between pore environments of modified mesoporous silica and side chain group of biogenic amine which showed different rate to go inside the pore and to react with the unit sensor. As a result, the system could not classify different kinds of biogenic amines in mixture solution.

In this research, we have attempted to enhance the selectivity in detection of biogenic amines regarding the intermolecular FRET process of two fluorescence sensors consisting of the isoindole product generated from OPTA on silica surface as a donor fluorescence sensor and the designed organic molecules as acceptor fluorescence sensors. Therefore, the additional fluorescence acceptors that could bind specifically with side chain groups of biogenic amine namely catecholamine and imidazole group were designed and synthesized. Boronic acid compound (**CB**) was designed to specifically react with dopamine and norepinephrine under the reaction between catechol group and boronic acid. Moreover, zinc (II) complexes based naphthalamide chromophore (**ZnC2** and **ZnD2**) were designed for specific detection of histidine by coordination of imidazole group to the zinc (II) complex. **E2** was designed and synthesized as a control molecule being an acceptor molecule in histidine detection. Concepts for the detections and molecular detail were showed in Scheme 3.1 and



Table 3.1, respectively.



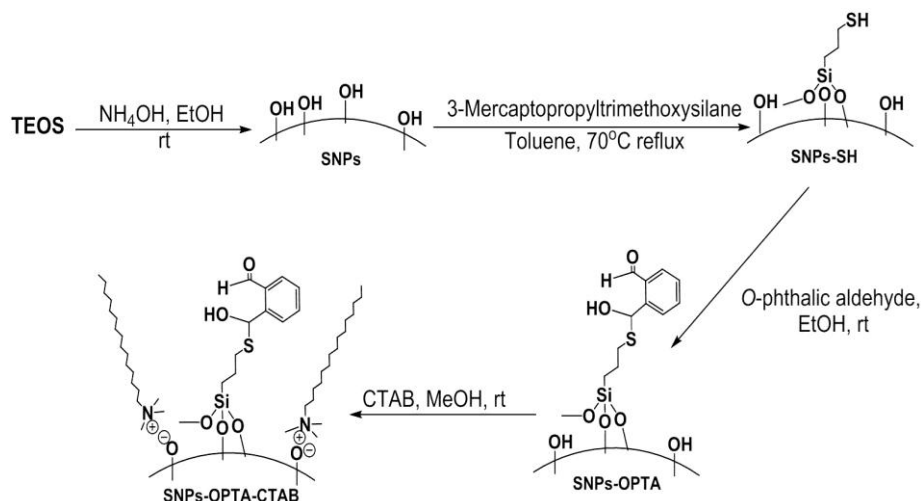
**Scheme 3.1** Concept for detection of biogenic amines

**Table 3.1** Molecular details of FRET donor and FRET acceptor in detection of catecholamine and histidine

FRET donors	Guest molecules	FRET acceptors
	catecholamine	<p style="text-align: center;"><b>CB</b></p>
<p style="text-align: center;"><b>FRET donor</b></p>	histidine	<p style="text-align: center;"><b>ZnC2      ZnD2      E2</b></p>

## 3.2 Synthesis and characterization

### 3.2.1 Synthesis of SNPs-OPTA and SNPs-OPTA\_CTAB



**Scheme 3.2** Synthesis pathway of SNPs-OPTA and SNPs-OPTA\_CTAB

Preparation of spherical silica nanoparticles (SNPs) was carried out by Stöber process [49] through hydrolysis and condensation reactions of tetraethyl orthosilicate (TEOS). Firstly, ethoxy groups of TEOS are substituted with hydroxyl groups by reacting with water molecule through the hydrolysis reaction, using ammonia as a basic catalyst, to form the intermediate  $[\text{Si}(\text{OC}_2\text{H}_5)_{4-X}(\text{OH})_X]$ . Secondly, the condensation reaction between hydroxyl groups of the intermediate and ethoxy group of TEOS called “alcohol condensation” and the condensation reaction between hydroxyl group of another hydrolysis intermediate called “water condensation” to form Si-O-Si bridges in forming of the silica nanoparticles were occurred immediately. In this step, the reaction was left for overnight to grow silica nanoparticles. To modify surface of the silica, the condensation reaction of hydroxyl groups on silica surface and ethoxy groups of 3-mercaptopropyl trimethoxysilane yielded SNPs-SH as white powder. Then, the particles react with *o*-phthalic aldehyde at room temperature to form SNPs-OPTA. Furthermore, the modification of CTAB on silica surface was carried out by adding CTAB to solution of SNPs-OPTA in methanol to form SNPs-OPTA\_CTAB through charge neutralization between negative charge on the silica surface and positive charge of head group of the

surfactant. The particle size and morphology of the particles were measured by TEM techniques. Moreover,  $-SH$  groups on SNPs-SH were determined by UV-Vis spectroscopy.

### 3.2.2 Characterization of SNPs-OPTA

#### 3.2.2.1 Size and morphology of the silica nanoparticles

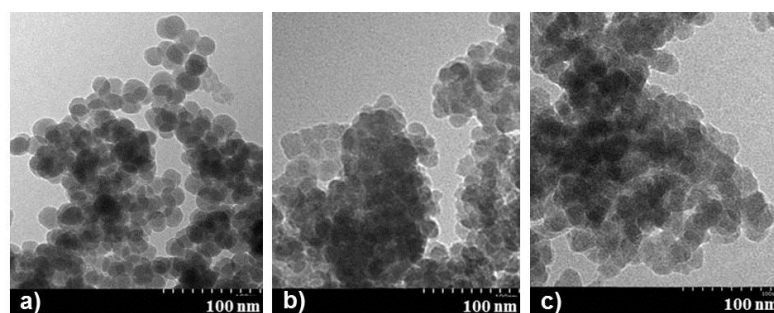


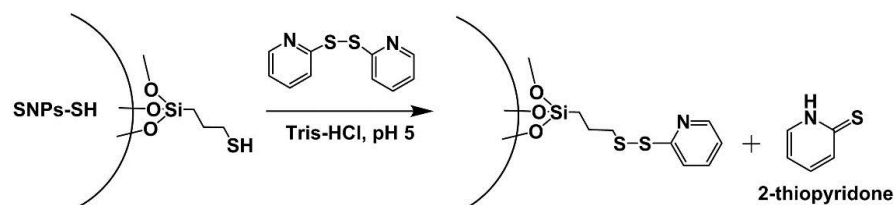
**Figure 3.1** TEM images of a) SNPs, b) SNPs-SH and c) SNPs-OPTA

The morphologies and the particle sizes of the silica nanoparticles (SNPs) and functionalized nanoparticles, namely, SNPs-SH and SNPs-OPTA, respectively, have been displayed by TEM images as shown in Fig. 3.1. The TEM images showed the spherical particles of SNPs, SNPs-SH and SNPs-OPTA with the particles size of  $25 \pm 02$ ,  $26 \pm 15$  and  $26 \pm 12$  nm, respectively. It was found that surface modification did not affect to the particle size, but it showed a slight distortion from the spherical particles. Moreover, higher aggregation of nanoparticles was observed in case of modification on silica surface.

#### 3.2.2.2 Surface area and accessible thiol density

From the nitrogen adsorption and desorption isotherm at 77 K, the specific surface area of SNPs nanoparticles calculated from the linear part of the Brunauer–Emmett–Teller (BET) plot [50] was  $215.95 \text{ m}^2\text{g}^{-1}$ . Moreover, to observe amount of thiol group on silica surface, 2,2'-dithiodipyridine was used as a reagent to produce 2-thiopyridone as a detectable molecule by UV-Vis spectroscopy. Under UV-Vis spectroscopy, 2-thiopyridone as side product generating from the reaction

between the surface thiol (-SH) and 2,2'-dithiodipyridine as shown in Scheme 3.3 was monitored.



**Scheme 3.3** Schematic representation of reaction between thiol (-SH) group on silica surface of SNPs-SH and excess 2,2'-dithiodipyridine and byproduct (2-thiopyridone) in Tris buffer solution, pH 5,  $\lambda_{ab} = 340 \text{ nm}$  [51]

Determination of the thiol group was carried out by standard addition method in 0.1 M Tris buffer solution, pH 5. Firstly, 2,2'-dithiodipyridine was added into the solution of SNPs-SH until the absorbance intensity at 345 nm of 2-thiopyridone was constant. This was assumed that all thiol group reacted with 2,2'-dithiodipyridine to form the detectable molecule (2-thiopyridone). Then, the exact amount of 2-thiopyridone was added to the solution and absorbance spectra were recorded at each concentration.

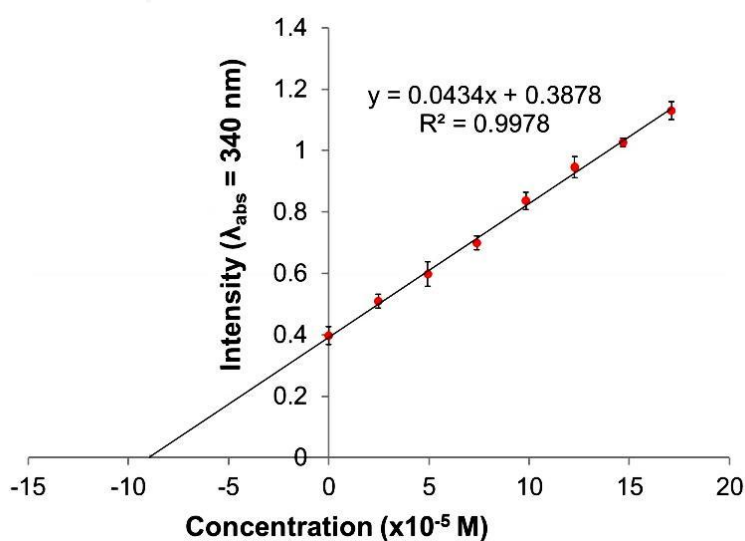
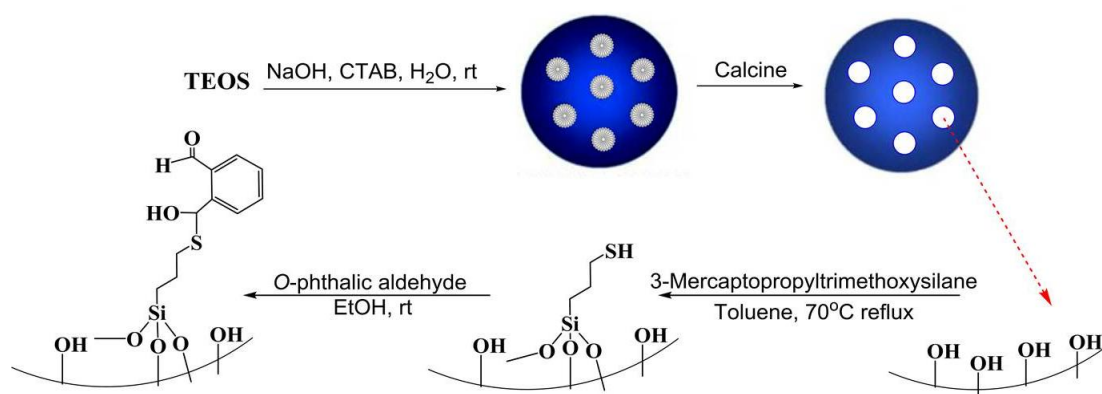


**Figure 3.2** Standard addition curve of 2-thiopyridone for the investigation of accessible thiol group on SNPs-SH, in Tris buffer solution, pH 5,  $\lambda_{ab} = 345 \text{ nm}$

To construct curve of standard addition, absorbance intensity at 345 nm was observed and plotted per unit concentration showing accessible thiol group at  $8.91 \times 10^{-5}$  M as shown in Fig. 3.2. The accessible thiol group on silica materials calculated per weight was  $0.36 \text{ mmol} \cdot \text{g}^{-1}$ .

### 3.2.3 Synthesis of MSNs-OPTA



**Scheme 3.4** Synthesis pathway of MSNs-OPTA

Mesoporous silica nanoparticles (MSNs) were prepared by Hyeheon Kim's method [52]. In preparation, hexagonal template was formed by combination of rod micelle of cetyltrimethylammonium bromide in the sodium hydroxide solution. And then, tetraethylorthosilicate (TEOS) as silica source was added to the solution and subsequent condensation reaction of silanol group occurred and covered around the template. After that, the CTAB template was removed by calcination. MSNs were functionalized with 3-mercaptopropyl trimethoxysilane through the condensation reactions and the redundant reagents were removed by centrifugation obtaining the white powder of MSNs-SH. Next, the particles reacted with *o*-phthalic aldehyde through nucleophilic addition reaction to yield the white powder of MSNs-OPTA nanoparticles. The particle size and morphology of the MSNs were investigated by TEM and XRD techniques. Moreover, -SH groups on MSNs-SH were determined by UV-Vis spectroscopy.

### 3.2.4 Characterization of MSNs-OPTA

#### 3.2.4.1 Size and morphology of the mesoporous silica nanoparticles

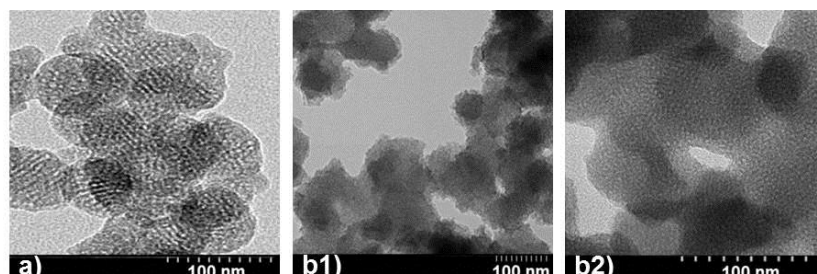


**Figure 3.3** TEM image of mesoporous silica nanoparticles images of a) MSNs, b1) MSNs-SH (zoom out) and b2) MSNs-SH (zoom in)

To observe morphology of MSNs and modified MSNs (MSNs-SH), the particles were investigated under transmission electron microscopy (TEM). The TEM images of mesoporous silica nanoparticles (MSNs) showed pore feature and circular shape of the particles with the particle size around  $75 \pm 02$  nm as depicted in Fig. 3.3 (a) and the modified MSNs (MSNs-SH) showed slightly distortion of the particles with particle size approximately  $76 \pm 14$  nm. These results indicated that surface modification did not affect to the particle size as showed in Fig. 3.3 (b1) and (b2).

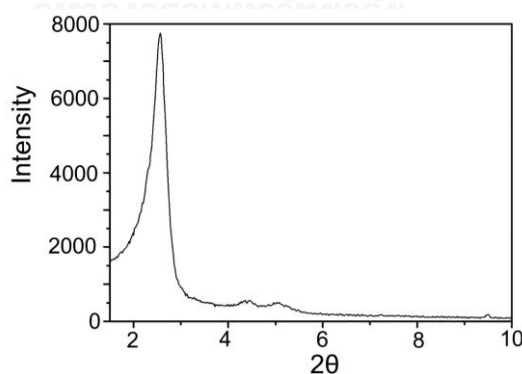


**Figure 3.4** XRD patterns of MSNs

X-ray Powder Diffraction (XRD) was applied to study phase identification of the nanoparticles. XRD pattern of MSNs (Fig. 3.4) exhibited a strong diffraction peak at the low  $2\theta$  region about  $2.2^\circ$  which is representative of short-range ordered mesoporous phase [53].

### 3.2.4.2 Surface area and accessible thiol density

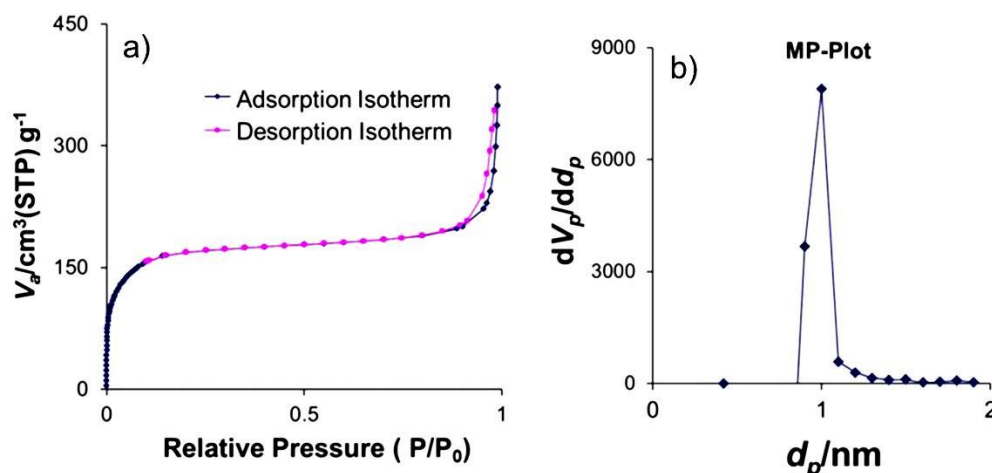
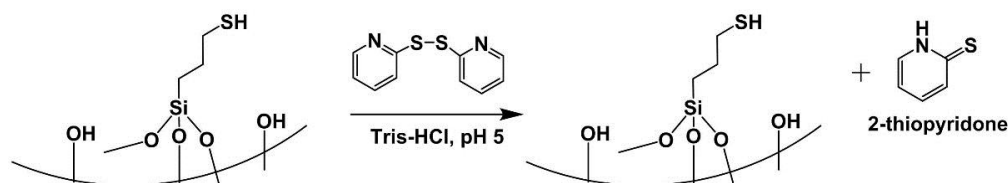


**Figure 3.5** a) nitrogen adsorption/desorption isotherms and b) pore size distribution of MSNs

The nitrogen adsorption and desorption isotherm at 77 K for MSNs (Fig. 3.5 (a)) showed type I isotherm which is characteristics of microporous solids [54]. The relatively high value of their specific surface area calculated from the linear part of the Brunauer–Emmett–Teller (BET) plot reached  $637.2 \text{ m}^2\text{g}^{-1}$  with the pore volume of  $0.249 \text{ cm}^3\text{g}^{-1}$ . The corresponding pore size distribution of MSNs calculated from the desorption branch of the nitrogen isotherms by using MP-Plot [53] had a narrow sharp peak at around 1 nm as shown in Fig. 3.5 (b).

Accessible thiol group on mesoporous silica (MSNs-SH) was investigated by motoring the amount of 2-thiopyridone generated by the reaction shown in Scheme 3.4. The method for detection of 2-thiopyridone is the same as calculating thiol group on the mentioned above mechanism.



**Scheme 3.5** Schematic representation of reaction between thiol (-SH) group on mesoporous silica surface (MSNs-SH) and excess 2,2'-dithiodipyridine and byproduct (2-thiopyridone) in Tris buffer solution, pH 5,  $\lambda_{\text{ab}} = 345 \text{ nm}$  [51]

The byproduct (2-thiolpyridone) and added 2-thiolpyridone were observed at the absorption band at 345 nm to construct standard addition curve of 2-thiolpyridone in Tris buffer solution, pH 5 as showed in Fig. 3.6.

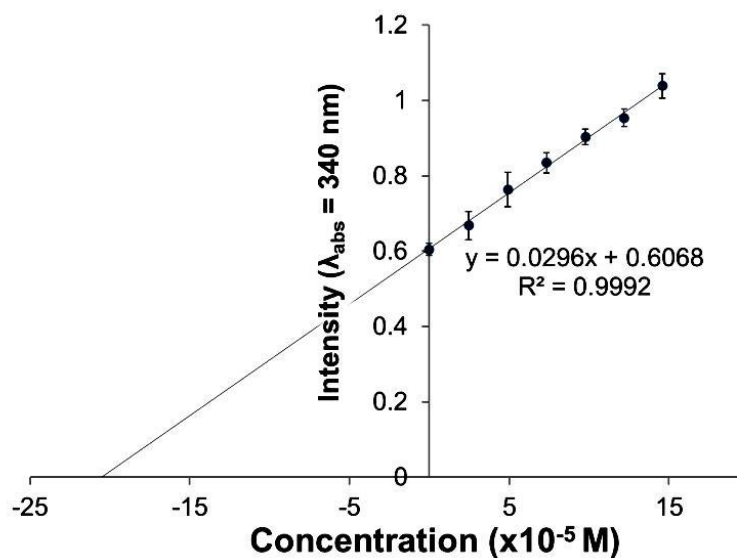
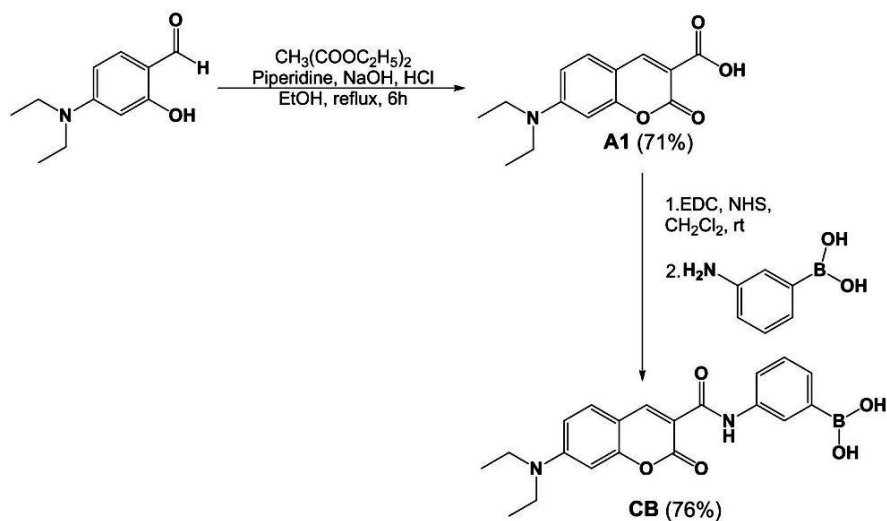


**Figure 3.6** Standard addition curve of 2-thiolpyridone for the investigation of accessible thiol group on MSNs-SH in Tris buffer solution, pH 5,  $\lambda_{ab} = 340$  nm

From standard addition curve, the accessible thiol group at  $20.5 \times 10^{-5}$  M was implied to the amount of thiol group attached on MSNs-SH to be  $0.82 \text{ mmol}\cdot\text{g}^{-1}$ . It obviously indicated that higher surface affected more amount of accessible thiol group on silica materials. Compared to the specific surface area of SNPs ( $215.95 \text{ m}^2\cdot\text{g}^{-1}$ ) and amount of thiol group ( $0.36 \text{ mmol}\cdot\text{g}^{-1}$ ) attached on the silica nanosphere surface, MSNs possessing more specific surface area of  $637.2 \text{ m}^2\cdot\text{g}^{-1}$  had more amount of accessible thiol group on the surface ( $0.82 \text{ mmol}\cdot\text{g}^{-1}$ ).



### 3.2.5 Synthesis and Characterization of CB



**Scheme 3.6** Synthesis pathway of sensor **CB**

Sensor **CB** was prepared in two steps as shown in **Scheme 3.6**. Nucleophilic substitution between 4-(diethylamino)-2-hydroxybenzaldehyde and diethyl malonate provided an orange crystal of **A1** in 71% yield. **A1** was characterized by  $^1\text{H-NMR}$  spectroscopy that showed the characteristic peak of acetic acid proton at 12.37 ppm and a singlet peak of the additional aromatic proton at 8.67 ppm. For next step, acetic acid group of **A1** reacted with ethyl(dimethylaminopropyl) carbodiimide (EDC) to form an active *o*-acylisourea intermediate which immediately reacted with *N*-hydroxysuccinimide (NHS) to form an NHS ester. The NHS ester group allowed efficient nucleophilic substitution with primary amine of 3-aminophenylboronic acid to form yellow powder of **CB** compound in 76% yield. The  $^1\text{H-NMR}$  data of **CB** showed the disappearance of the carboxylic proton at 12.37 ppm and showed the singlet peak of amide proton at 10.75 ppm. The  $^1\text{H-NMR}$  spectrum of sensor **CB** in  $\text{DMSO-}d_6$  was shown in Fig. 3.7. MALDI-TOF mass spectra also confirmed the molecular structure of **CB** with the intense peak at 380.37 m/z.

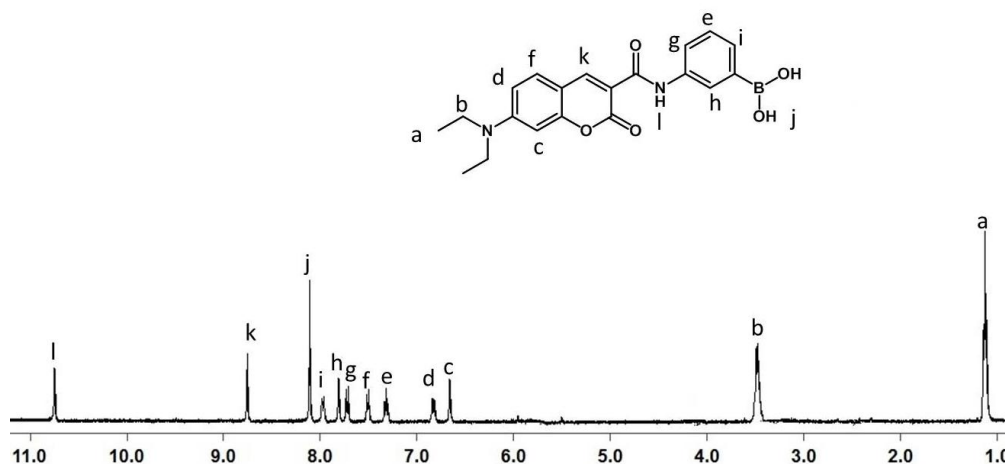
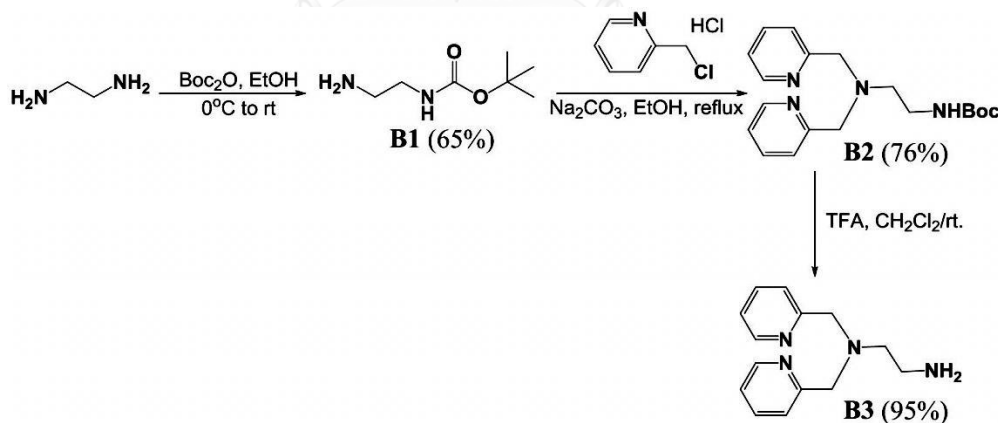


**Figure 3.7** The  $^1\text{H}$ -NMR spectrum of sensor **CB** in  $\text{DMSO-}d_6$  at 400 MHz

### 3.2.6 Synthesis and Characterization of ZnC2

To synthesis **ZnC2**, **B3** (*N*-bispyridin-2-ylmethylethane-1,2-diamine) as a binding part with Zn(II) was firstly prepared through 3 steps as shown in Scheme 3.7.



**Scheme 3.7** Synthesis pathway of **B3**

First of all, reaction between ethylenediamine and di-*t*-butyl dicarbonate occurred through nucleophilic substitution in ethanol solution at 0 °C providing colorless oil of **B1** compound in 65% yield. After that, the nucleophilic substitution reaction of **B1** and 2-pyridylmethyl chloride hydrochloride in the presence of  $\text{Na}_2\text{CO}_3$  as a basic reagent in ethanol solution produced the brown oil which was purified by

column chromatography to yield **B2** with 76% yield. Prior the coupling reaction with *N*-1,8-naphthalene dicarboxylic acid anhydride, *t*-butyl carbonate group of **B2** was removed by hydrolysis in acidic condition of trifluoroacetic acid (TFA) in dichloromethane solution, giving the free amino acid of **B3** in 95% yield. The  $^1\text{H}$ -NMR data of **B3** displayed aromatic protons at 7.13-8.51 ppm as shown in Fig. 3.8.

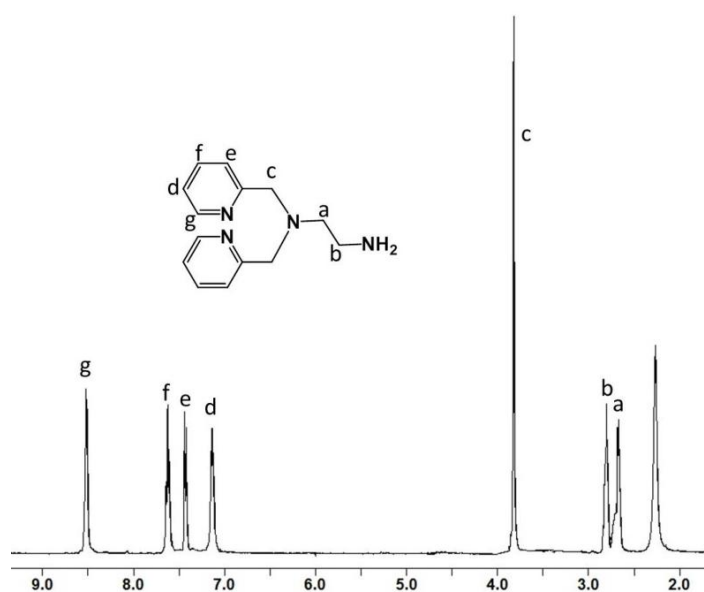
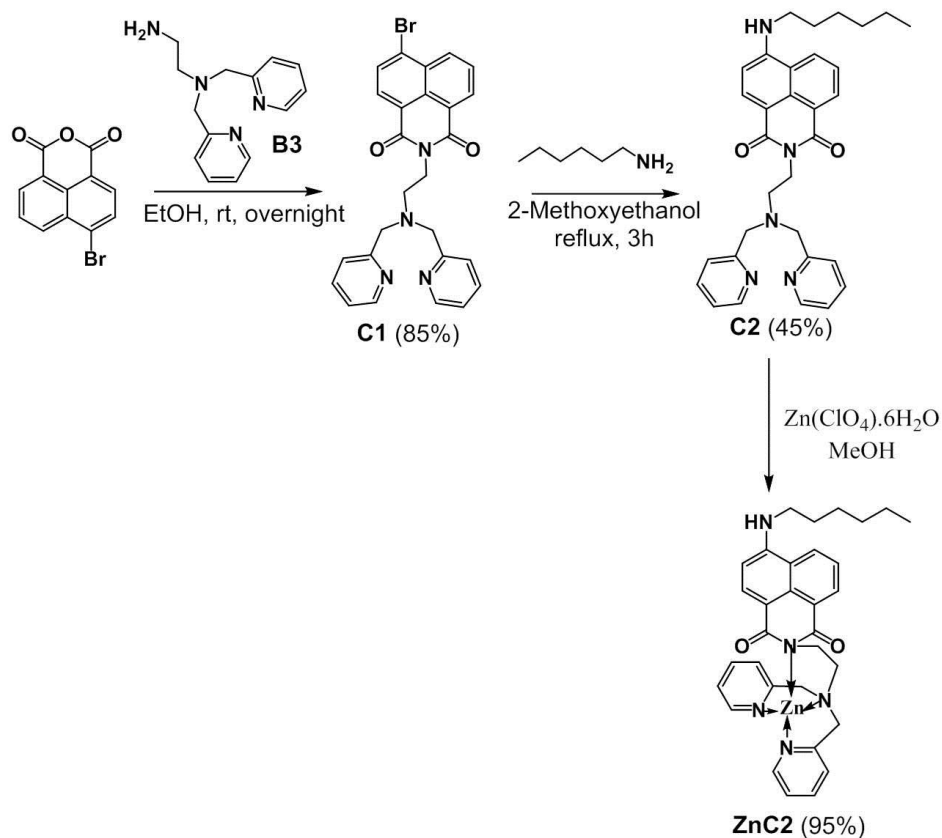


**Figure 3.8** The  $^1\text{H}$ -NMR spectrum of **B3** in  $\text{CDCl}_3$  at 400 MHz



**Scheme 3.8** Synthesis pathway of sensor **ZnC2**

For the synthesis of sensor **ZnC2**, 4-bromo-N-1,8-naphthalene dicarboxylic acid anhydride reacted with **B3** through nucleophilic substitution to form yellow powder of **C1** compound in 85% yield. After that, this compound reacted with hexylamine in 2-methoxyethanol to provide **C2** compound which interacted with  $\text{Zn}(\text{ClO}_4) \cdot 6\text{H}_2\text{O}$  in methanol providing **ZnC2** complex in 85% yield. It was found that  $^1\text{H-NMR}$  spectrum of **C2** showed singlet peak of NH proton at 5.64 ppm, while in the case of **ZnC2**, this signal displayed at 5.51 ppm. Moreover, aromatic peaks of **ZnC2** showed low field shift compared with the **C2** ligand as shown in Fig. 3.9 and 3.10.

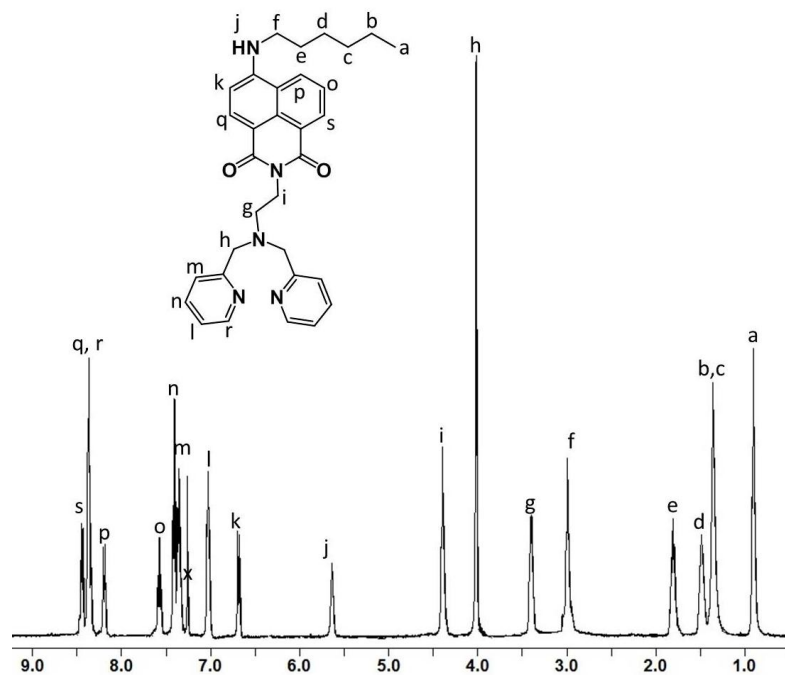


**Figure 3.9** The  $^1\text{H-NMR}$  spectrum of sensor **C2** in  $\text{CDCl}_3$  at 400 MHz

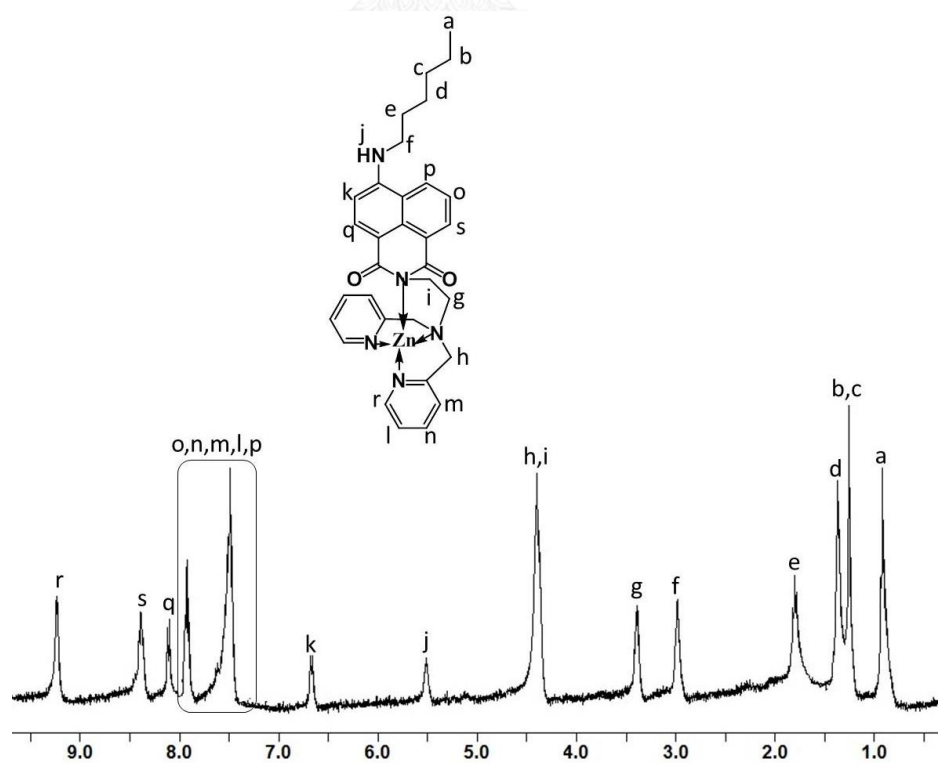


**Figure 3.10** The  $^1\text{H-NMR}$  spectrum of sensor **ZnC2** in  $\text{CDCl}_3$  at 400 MHz

ESI-High Resolution Mass spectrum confirmed the structures of **ZnC2** with the intense peak of  $m/z$  at 620.17 (Fig. 3.11 (a)) corresponding to  $[\text{ZnC}_2\text{Cl}]^+$  complex. The isotope peak of Zn(II) in **ZnC2** at 620.1749 showed the different mass peak around 1  $m/z$  indicating that the Zn(II) was coordinated with  $\text{Cl}^-$  in **ZnC2** complex as shown in Fig. 3.11 (b).

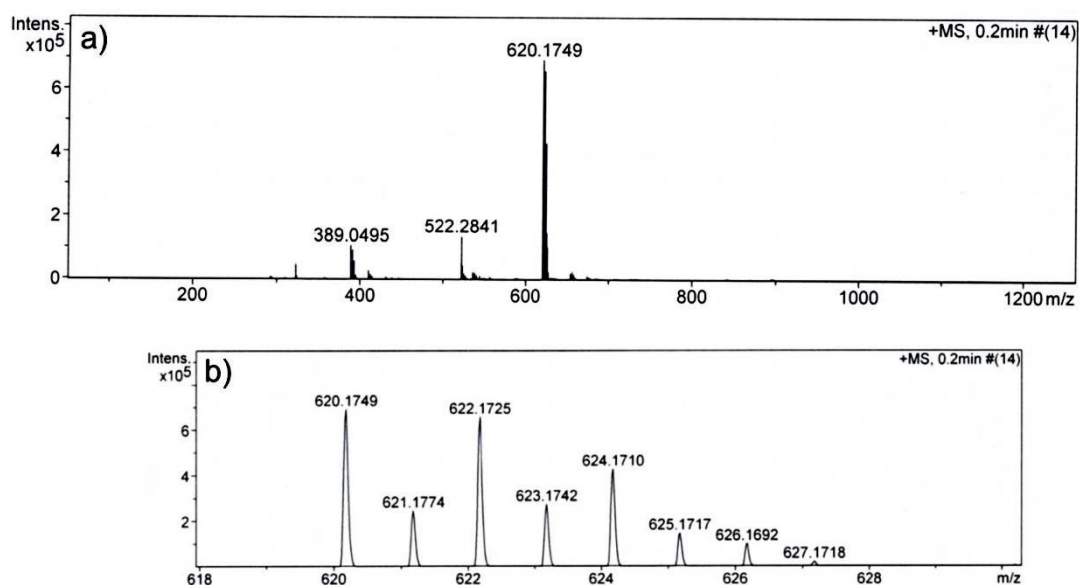
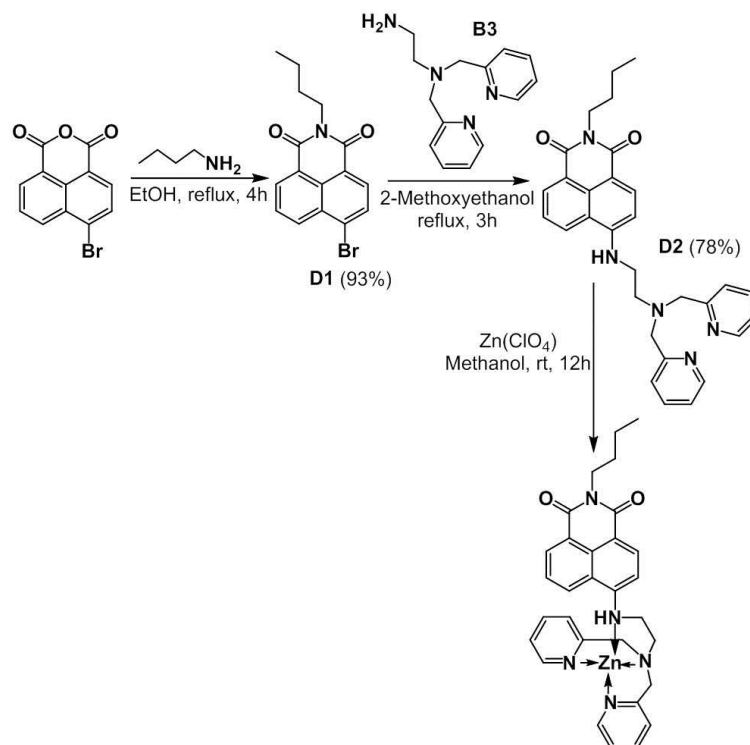


**Figure 3.11** a) The ESI-High Resolution Mass spectrum of **ZnC2** complex, b) isotope peak of Zn (II) in **ZnC2**

### 3.2.7 Synthesis and Characterization of ZnD2



**Scheme 3.9** Synthesis pathway of sensor **ZnD2**

Synthesis of **ZnD2** consists of 3 steps as shown in scheme 3.9. Firstly, ligand **D2** was prepared through nucleophilic substitution reaction of 4-bromo-*N*-1,8-naphthalene dicarboxylic acid anhydride and *n*-butylamine in ethanol solution providing light yellow solid of **D1** compound with 93% yield. Then, the **D1** compound reacted with **B3** through substitution reaction to form yellow solid of **D2** with 78% yield. Unfortunately, the preparation of **ZnD2** complex by stirring **D2** and  $\text{Zn}(\text{ClO}_4)_2 \cdot 6\text{H}_2\text{O}$  in methanol solution has not been achieved. **D1** and **D2** compounds were characterized by  $^1\text{H-NMR}$  spectroscopy. The  $^1\text{H-NMR}$  spectrum of **D2** showed aromatic peaks at 7.15-8.76 ppm and NH peak at 6.53 ppm as shown in Fig. 3.12, while **D1** showed aromatic peaks at 7.85-8.57 ppm. Moreover, **D2** were confirmed by ESI-High Resolution Mass spectrum showing the intent peak at 494.263 m/z corresponding to **D2** compound.

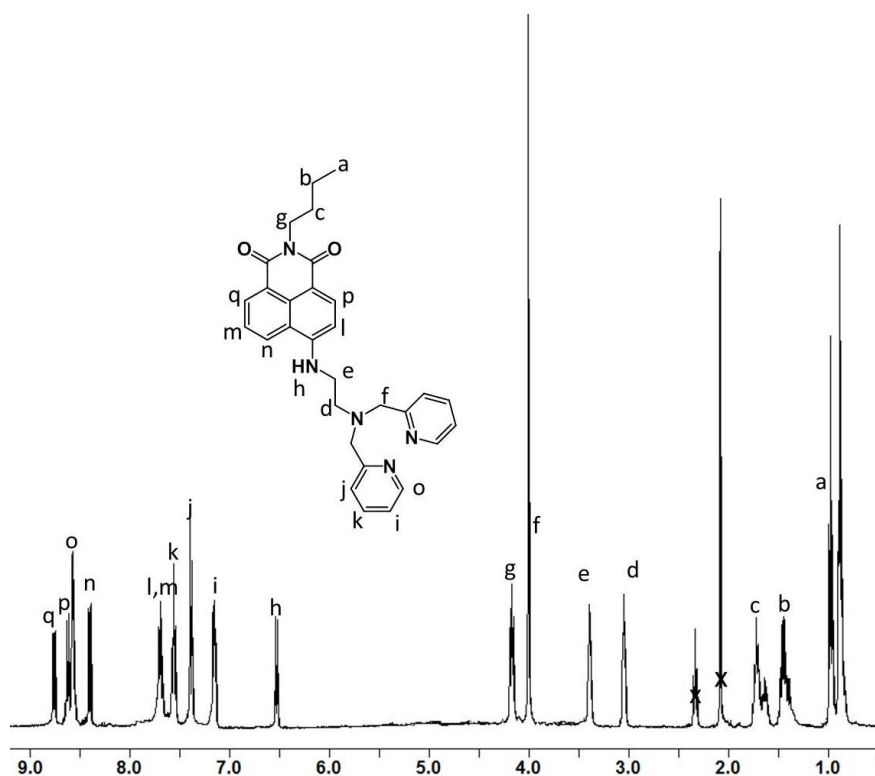
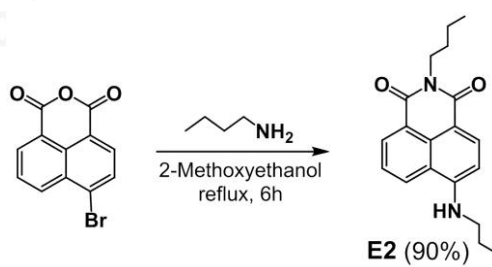


**Figure 3.12** The  $^1\text{H-NMR}$  spectrum of sensor **D2** in  $\text{CDCl}_3$  at 400 MHz

### 3.2.8 Synthesis and Characterization of **E2**



**Scheme 3.10** Synthesis pathway of **E2**

**E1** compound was prepared by nucleophilic substitution reaction of 4-bromo-*N*-1,8-naphthalene dicarboxylic acid anhydride and *n*-butylamine to form yellow solid of **E2** with 90% yield. The  $^1\text{H-NMR}$  spectrum of sensor **E2** was shown in Fig. 3.13.



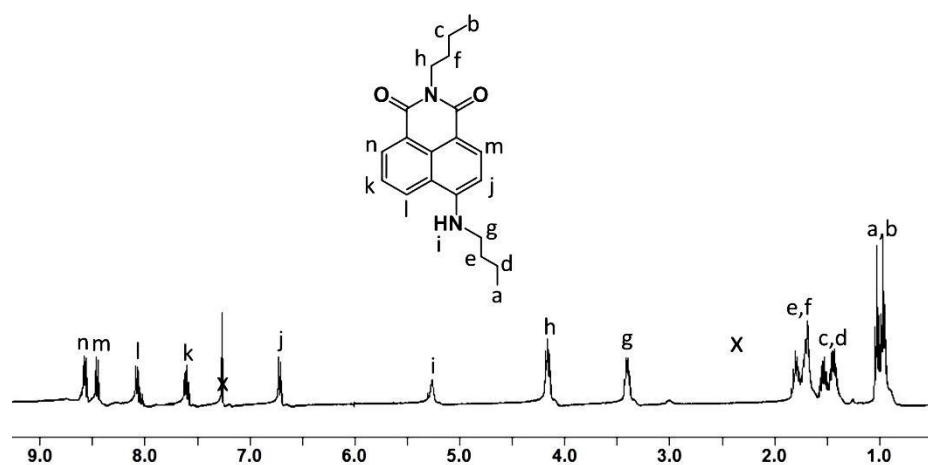


**Figure 3.13** The  $^1\text{H}$ -NMR spectrum of sensor **E2** in  $\text{CDCl}_3$  at 400 MHz

### 3.3 Complexation studies

#### 3.3.1 Complexation studies in homogeneous solution of isoindole product with various biogenic amines

*o*-Phthalaldehyde and amino acids in alkaline medium in the presence of 3-mercaptoethanol produced the strong fluorescent compound of isoindole product. This reaction is well-known assay to effectively determine an amino acid (primary amine compound) [48].

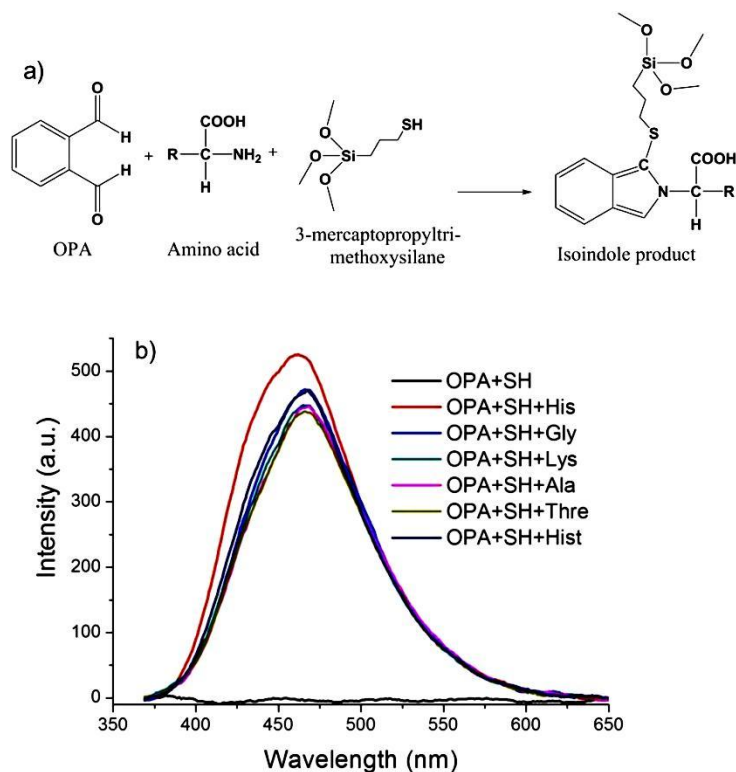


**Figure 3.14** a) Reaction between *o*-phthalaldehyde (OPA), 3-mercaptopropyl trimethoxysilane (SH) and amino acids to form isoindole product b) fluorescence responses with various biogenic amines in homogeneous solution of 25 mM SH and OPA in 0.01 M PBS, pH 7.4,  $\lambda_{\text{ex}} = 345 \text{ nm}$

In this research, the reaction of *o*-phthalaldehyde (OPA) with various amino acids in the presence of 3-mercaptopropyltrimethoxysilane (SH) to form isoindole product which gives strong fluorescence intensity was investigated as shown in Fig. 3.14 (a). The fluorescence detection in the system of all amino acids namely histidine (His), glycine (Gly), lysine (Lys), alanine (Ala), threonine (Thre) and histamine (Hist) investigated in 0.01 M phosphate buffer solution, pH 7.4, showed similarly strong fluorescence spectra (Fig. 3.14 (b)), since all amino acids are identical in their sizes and reactivity toward OPA in homogeneous solutions.

### 3.3.2 Complexation studies of SNPs-OPTA and CB with various biogenic amines

Homogeneous solution of isoindole product was applied in solid phase of silica materials through modification of primary amine sensitive *o*-phthalic hemithioacetal (OPTA) unit on silica surface under idea of Lin et al [27].

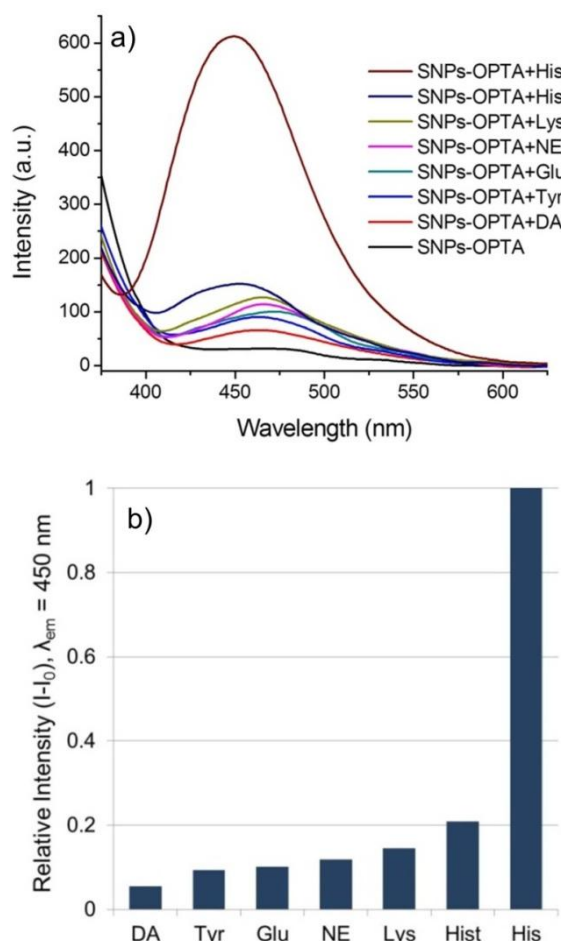
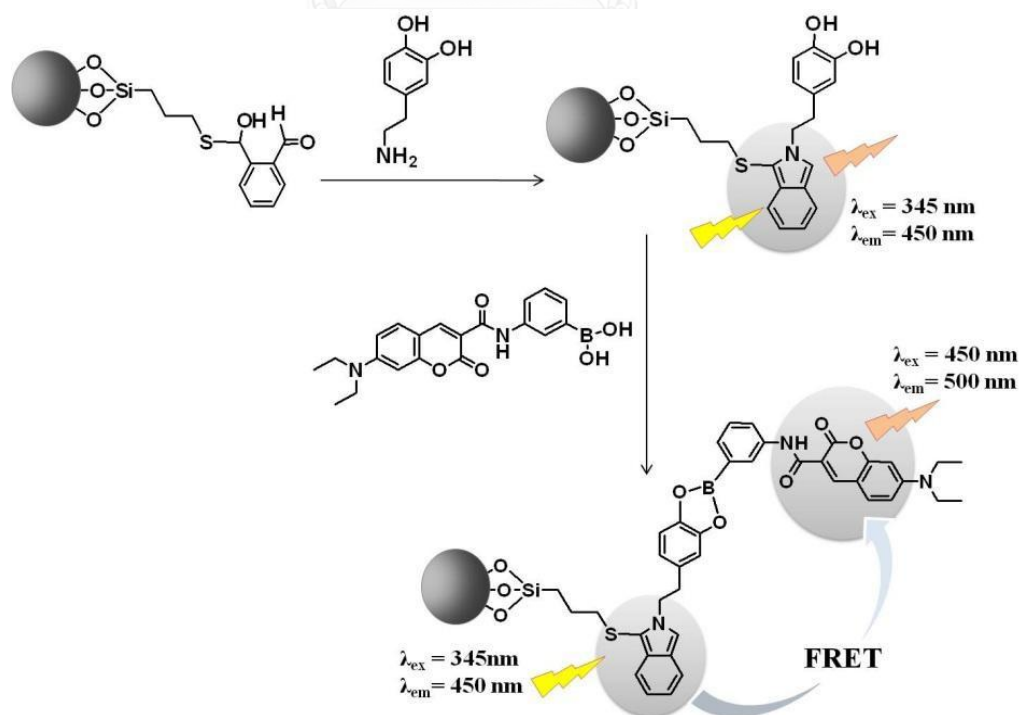


**Figure 3.15** a) Fluorescence spectra and b) relative intensity at  $\lambda_{em} = 450$  nm of the isoindole product of 1.5 mg/mL SNPs-OPTA with various biogenic amines (125  $\mu$ M) in phosphate buffer solution, pH 7.4,  $\lambda_{ex} = 345$  nm

Fluorescence responses of an amine-sensitive *o*-phthalic hemithioacetal (OPTA) group incorporated on the surface of silica nanosphere (SNPs-OPTA) toward the neurotransmitters and amino acids including dopamine (DA), norepinephrine (NE), tyramine (Tyr), L-glutamic acid (Glu), L-lysine (Lys), histidine (His), and histamine (Hist) were demonstrated. It was found that the entire guest molecules

enabled to form an isoindole product displaying the emission bands around 450-480 nm ( $\lambda_{\text{ex}} = 345$  nm). Interestingly, the case of histidine showed strong fluorescence intensity, while other biogenic amines showed weak fluorescent intensity possibly caused by substrate accessibility and the electron-rich aromatic amine. The fluorescence spectra and relative fluorescence intensity were shown in Fig. 3.15 (a) and (b).

Moreover, to discriminate the catecholamine namely dopamine and norepinephrine, the second sensing element of coumarin boronic acid (**CB**) was applied in the detection system. As anticipated, primary amine of the catecholamine compound would form isoindole product on the silica surface (SNPs-OPTA) and their catechol group would bind covalently with coumarin boronic acid to form boronate ester. Conceptually, the catecholamine as a guest linker could induce FRET process caused by the energy transfer between the isoindole products (donor) generated from reaction of *o*-phthalic hemithioacetal (OPTA) unit on the silica materials and coumarin fluorophore (acceptor) resulting in a consequent emission band at 550 nm of coumarin unit as a conceptual design in Scheme 3.10.



**Scheme 3.11** Conceptual design for detection of catecholamine

To study fluorescence response of **CB** in the system, emission spectra of the **CB** probe at 350 nm and 450 nm of excitation wavelength was firstly investigated.

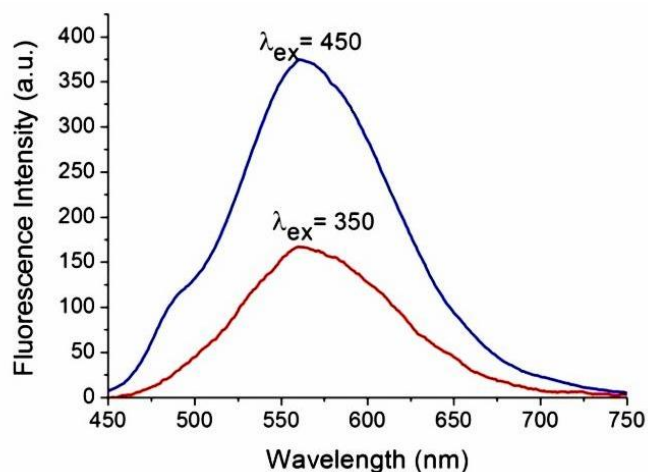
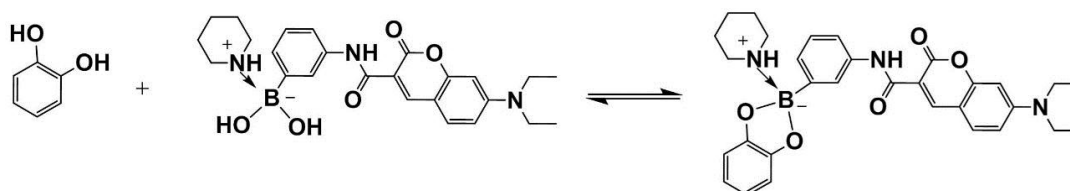


**Figure 3.16** Emission spectra at excitation wavelength at 350 nm and 450 nm in 10  $\mu$ M **CB** in 0.01 M PBS pH 7.4

Emission spectra at different excitations (350 nm and 450 nm) showed the same emission band at 555 nm with different intensity as shown in Fig. 3.16. This signified the excitation-dependent fluorescence intensity of **CB**.

Notably, boronic acid prefers to react with catechol group when the boronic acid groups are generated to be  $sp^3$  hybridization by lone pair electron of basic compound [55]. Therefore, in this study, boronic group of **CB** was evoked to form  $sp^3$  hybridization by adding piperidine. The proposed binding event was illustrated in Scheme 3.12.



**Scheme 3.12** Binding event between fluorescent sensor **CB** and dopamine in the presence of piperidine under physiological condition

Fluorescence responses of coumarin boronic acid (**CB**) in the presence of SNPs-OPTA toward various biogenic amines were studied in 0.01 M phosphate buffer solution, pH 7.4 as shown in Fig. 3.17.

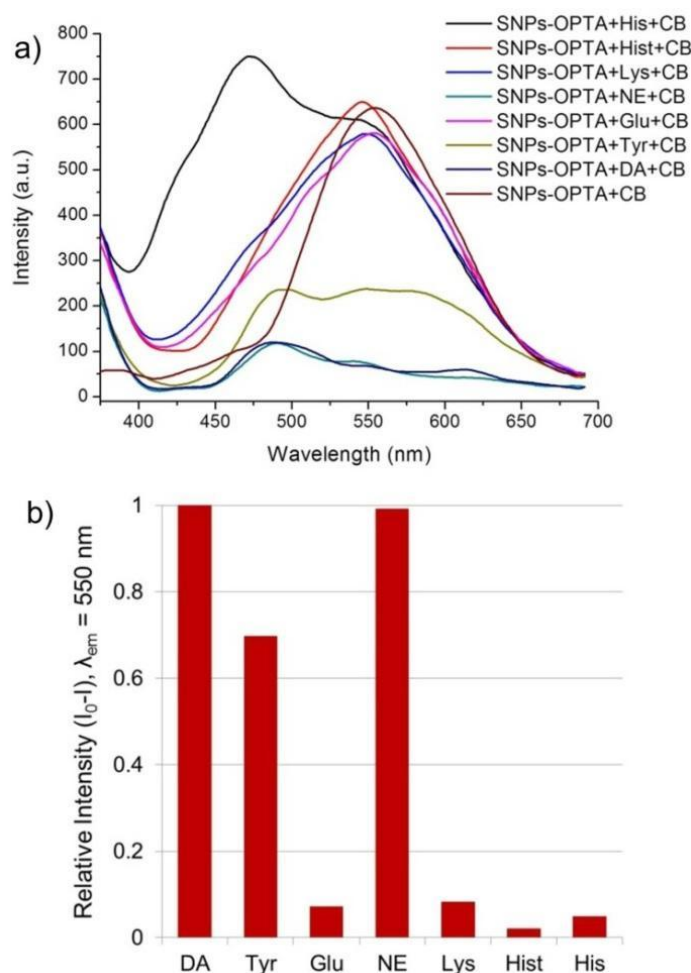


**Figure 3.17** a) Fluorescence spectra and b) relative intensity (at emission wavelength = 550 nm) of emission band of **CB** in the presence of 1.5 mg/mL SNPs-OPTA and 250  $\mu$ M **CB** with various biogenic amines (125  $\mu$ M) in phosphate buffer solution, pH 7.4,  $\lambda_{ex} = 345$  nm

The fluorescence responses did not exhibit as expected result. The energy transfer between isoindole products and coumarin fluorophore was not observed. However, the case of dopamine (DA) and norepinephrine (NE) exhibited significantly quenching of coumarin emission band at 550 nm suggesting that both catecholamines were interacted with **CB**. Moreover, tyramine (Tyr) demonstrated a small quenching

spectrum possibly caused by a weaker binding between hydroxyl group based on tyramine and boronic acid of **CB**. For the other biogenic amines, the fluorescence responses at 550 nm are similar to the fluorescence response of SNPs-OPTA in the presence of **CB** indicating non interaction of **CB** and these biogenic amines. It was proposed that the quenching event might occur through PET process due to electron rich on catechol group.

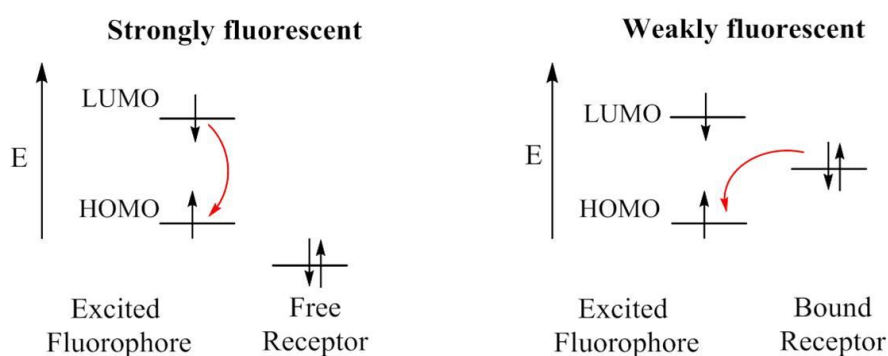


**Figure 3.18** The proposed Photoinduced Electron Transfer (PET) of **CB**

The fluorescence quenching of **CB** consisting of fluorophore (coumarin moiety) and receptor unit (boronic acid) was explained by energy level of molecular orbitals of the sensor. In the case of nonbinding (**CB** without binding with catecholamine), molecular orbital of receptor unit (catecholamine) would be lower than HOMO of the fluorophore (**CB**) resulting in the appearance of fluorescence emission band after an excited electron returns to ground state. In contrast, binding between the **CB** and catecholamine would affect to the energy level of receptor orbital which moves to be higher than HOMO and lower than LUMO of the fluorophore and consequently, the electron of the bound receptor easily transfers to HOMO of the fluorophore resulting that an excited electron on LUMO of fluorophore is inhibited to return to ground state of fluorophore. This aspect induces the fluorescence quenching of the fluorophore. The overall mechanism was displayed in Fig. 3.18.

From this sensor system, the expected FRET process for sensing purpose was unsuccessful. However, this system based on intermolecular of two fluorophore enabled to enhance the specific detection of DA and NE from other biogenic amines.

### 3.3.3 Complexation studies of SNPs-OPTA\_CTAB and ZnC2 with biogenic amines

To develop histidine detection, **ZnC2** was expected to be the acceptor fluorophore. As our assumption, Zn (II) based **ZnC2** would bind with the imidazole in histidine base. We proposed that histidine, acting as a proper guest linker between two self-recognition sensing elements namely isoindole product based on SNPs-OPTA and **ZnC2**, induced the energy transfer from the isoindole part to **ZnC2** part to give the fluorescence spectrum of **ZnC2** called FRET-on process.

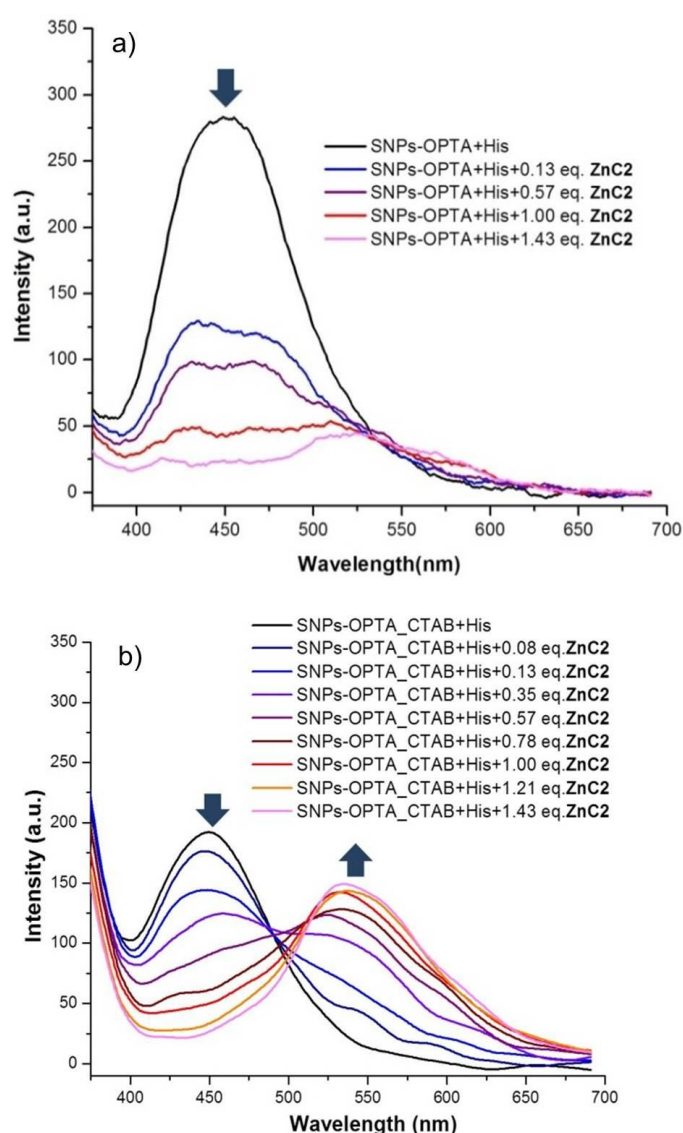


**Figure 3.19** Emission bands of various amount of **ZnC2** a) in SNPs-OPTA and b) in SNPs-OPTA\_CTAB with 125  $\mu\text{M}$  histidine in 10 mM phosphate buffer solution, pH 7.4,  $\lambda_{\text{ex}} = 345 \text{ nm}$



The **ZnC2** complex was a complementary receptor to specifically detect histidine in the possessing of SNPs-OPTA in phosphate buffer solution, pH 7.4. To optimize the proper amount of **ZnC2**, the fluorescence responses with various amount of **ZnC2** were investigated. Fluorescence quenching at 450 nm was observed upon the addition of **ZnC2** in the solution as depicted in Fig. 3.19 (a). From the result, it was proposed that the fluorescence self-quenching at 550 nm was observed as a result of orderly packing of naphthalimide based **ZnC2** on the surface of silica under strong interaction between positive charge of Zn(II) on the **ZnC2** and negative charge on silica surface. To avoid this effect, cationic surfactant cetyltrimethylammonium bromide (CTAB) was applied as a neutralizing molecule. Interestingly, the system consisting of CTAB (SNPs-OPTA\_CTAB) examined by various amount of **ZnC2** showed the promoting of energy transfer which exhibited decreasing fluorescence intensity at 450 nm and increasing fluorescence intensity at 550 nm as shown in Fig. 3.19 (b).

In conclusion, CTAB as positive charge neutralizing silica surface could reduce self-packing of **ZnC2** on the silica surface and **ZnC2** enabled to interact with isoindole product. Therefore, energy transfer from the isoindole product to **ZnC2** was performed and consequently, the emission band at 550 nm corresponding to **ZnC2** complex was demonstrated. Therefore, the proper amount of **ZnC2** for this approach is 0.2 M, which is used in all manipulations.

Remarkably, the fluorescence responses of SNPs-OPTA toward biogenic amines including primary amine namely dopamine, norepinephrine, tyramine, L-glutamic acid, L-lysine, histidine, and histamine displayed emission bands at 450 nm ( $\lambda_{\text{ex}} = 345 \text{ nm}$ ) as shown in Fig. 3.15 (a), while the fluorescence response of SNPs-OPTA\_CTAB showed a strong fluorescent intensity at 450 nm ( $\lambda_{\text{ex}} = 345 \text{ nm}$ ) only in the case of histidine as depicted in Fig. 3.20 (a). This revealed that CTAB incorporated on SNP-OPTA enables to enhance the selectivity of histidine.

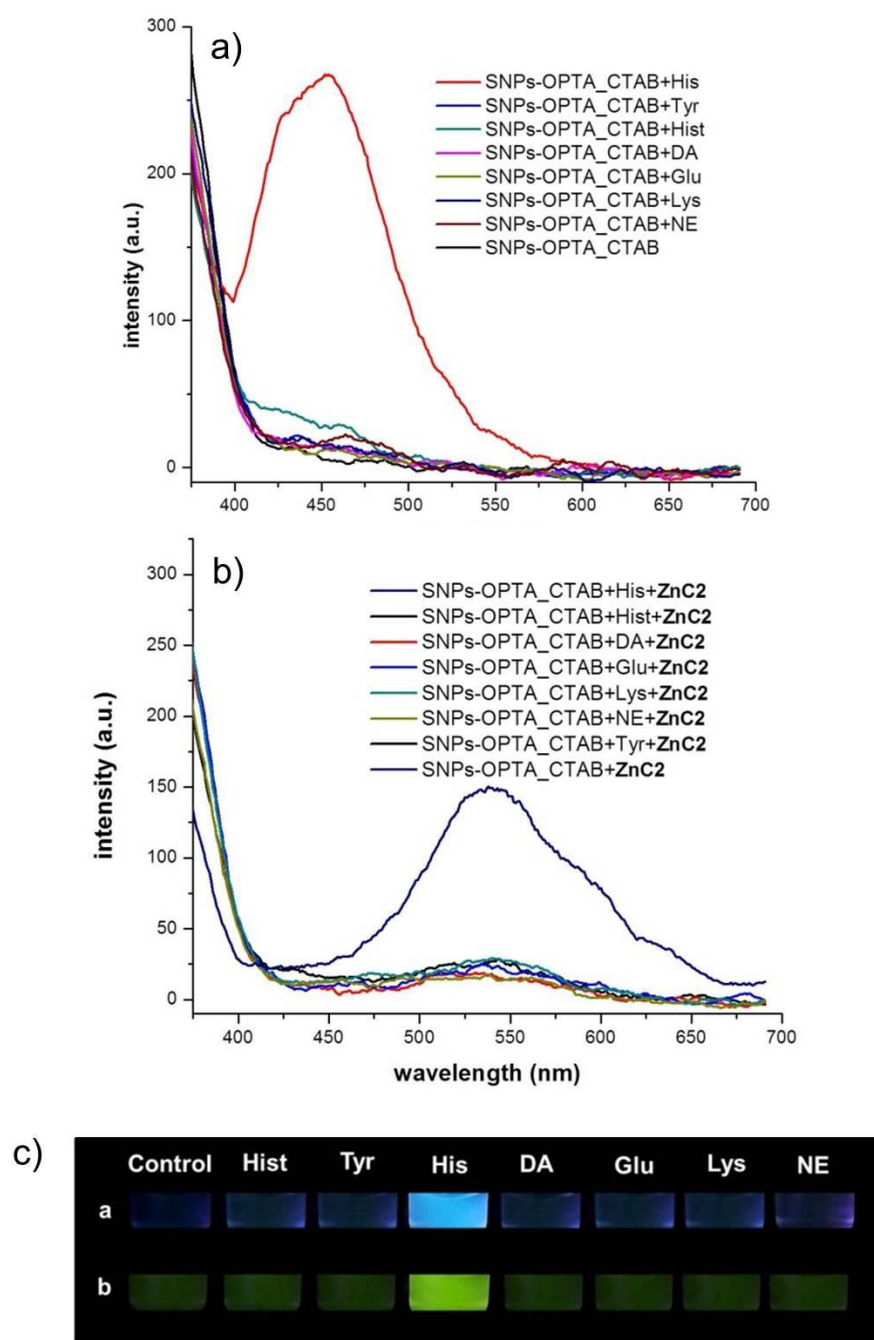


**Figure 3.20** Fluorescence emission responses of 1.5 mg/mL SNPs-OPTA\_CTAB a) in the absence and b) in the presence of 0.2 M **ZnC2** toward various biogenic amines at the concentration of 125  $\mu$ M, in 10 mM phosphate buffer solution, pH 7.4,  $\lambda_{\text{ex}} = 345$  nm c) Naked-eye studies under UV light of (a) and (b)

Moreover, the detection of the guest molecules by SNPs-OPTA\_CTAB solution possessing **ZnC2** showed high fluorescence intensity at 550 nm in case of histidine as shown in Fig. 3.20 (b). This suggested that this system offered the specific binding with histidine. It was proposed that the energy transfer occurred between isoindole and **ZnC2** molecule inserted in space of hydrocarbon chain of CTAB on silica surface. Furthermore, the solutions of the sensors in guest molecules were investigated with naked-eye study under UV-light found that only in the case of histidine showed high fluorescence brightness of blue and green color regarding isoindole product and **ZnC2**, respectively (Fig. 3.20(c)). It is clear that the SNPs-OPTA\_CTAB system possessing **ZnC2** showed high selectivity for the detection of histidine in water solution and the system enabled to apply and study by naked-eye sensor under UV-light.

Notably, the detection of biogenic amine by SNPs-OPTA\_CTAB system with and without **ZnC2** also provided high selectivity in case of histidine detection by appearance of emission bands at 550 and 450 nm, respectively. However, higher emission wavelength enables to reduce matrix interference from biological system. Therefore, the system consisting of **ZnC2** is more suitable for detection of histidine in body fluid such as blood and urine for diagnosis of histidinemia.

#### 3.3.4 Complexation studies of MSNs-OPTA with various biogenic amines

Moreover, mesoporous silica nanoparticles were also utilized as supporting matrix incorporated with amine-sensitive *o*-phthalic hemithioacetal (OPTA) group on the pore-surface. The pore of the particles takes advantage of the size-sieving ability that only small molecules can diffuse into the pores and react with the OPTA group.

Fluorescent responses of MSNs-OPTA with various amino acids exhibited the strong fluorescence at 450 nm in the case of histidine. Moreover, histidine induced the brightness of luminescence of isoindole product underneath UV lamp as shown in Fig. 3.21 (b).

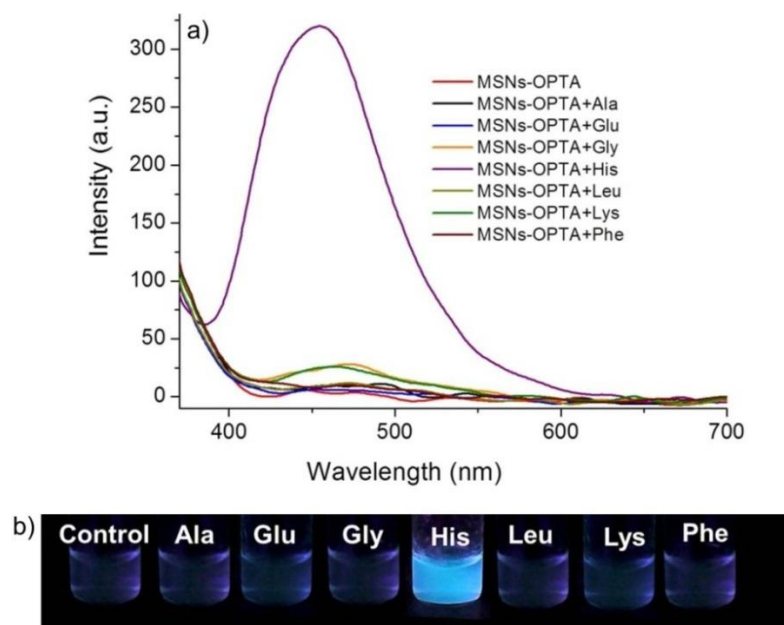


**Figure 3.21** a) Fluorescence responses and b) images under UV light of the solution consisting of 0.75 mg/mL MSNs-OPTA toward various amino acids (125  $\mu$ M) namely alanine (Ala), glutamic acid (Glu), glycine (Gly), histidine (His), leusine (Leu), lysine (Lys) and phenylalanine (Phe) in 10 mM phosphate buffer solution, pH 7.4,  $\lambda_{\text{ex}} = 345$  nm stirred for 20 minutes

To study quantitative detection of histidine, the change of the fluorescent spectra was observed upon increment of histidine in 10 mM phosphate buffer solution pH 7.4 as shown in Fig. 3.22 (a). The calibration plots showed a good linear relationship between the fluorescent intensity at 450 nm and the logarithm of the histidine concentration as depicted in Fig. 3.22 (c).

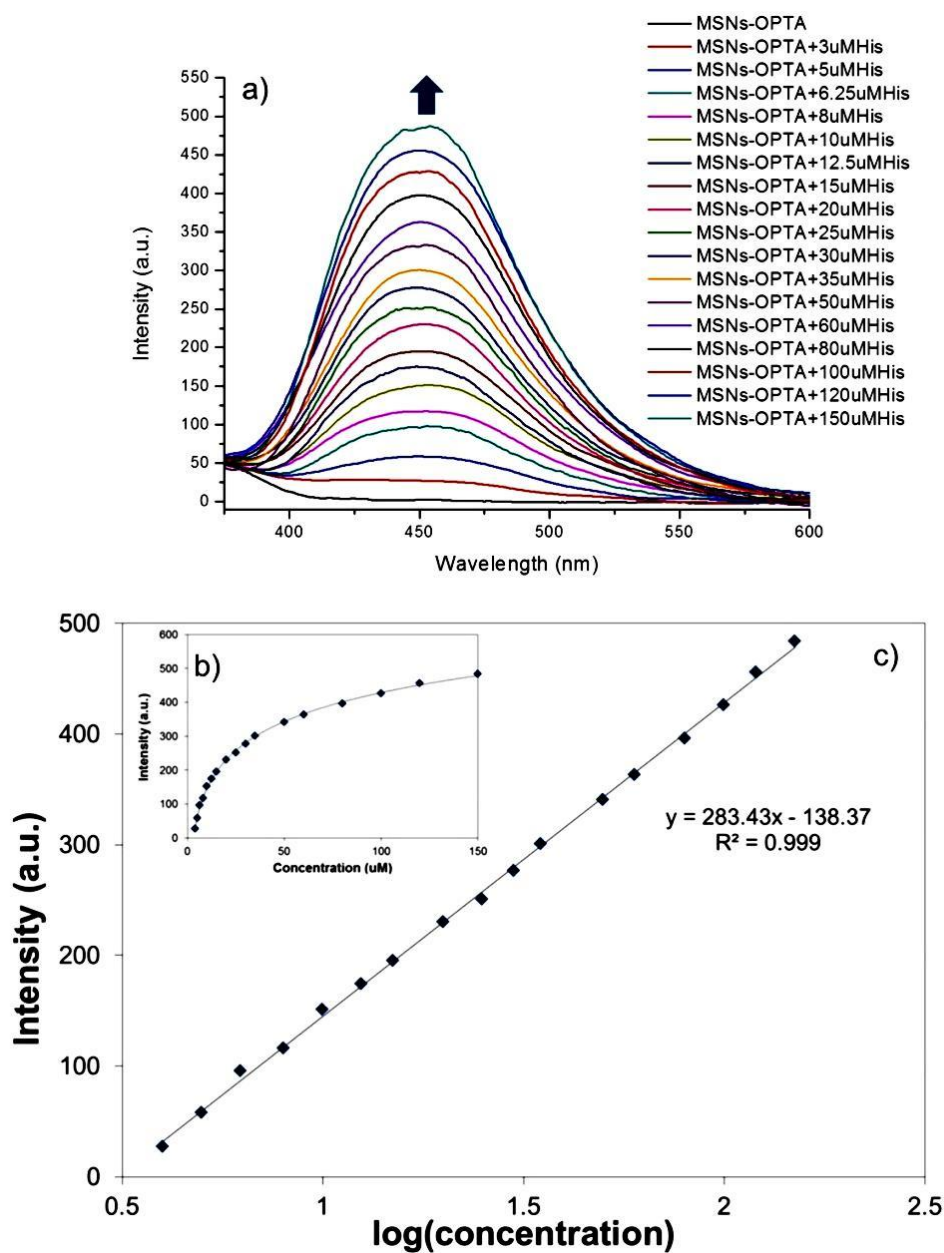


**Figure 3.22** a) Fluorescence titration of MSNs-OPTA with histidine concentration (5-150  $\mu\text{M}$ ), b) calibration curve plotted between fluorescence intensity and histidine concentration and c) plotted on a semi-log scale at emission intensity changing at 450 nm in 1.0 mg/mL MSNs-OPTA diluted in 10 mM phosphate buffer solution pH 7.4 stirred for 40 minutes,  $\lambda_{\text{ex}} = 345$  nm

The linear regression equation was  $F(\text{a.u.}) = 283.43\log(C_{\text{histidine}(\mu\text{M})}) - 138.37$  with a linear regression coefficient of 0.9990. The detection limit and quantification limit were calculated to be 17.7 nM and 59.22 nM, respectively [56].

Furthermore, the kinetic studies of isoindole product formation in 150  $\mu\text{M}$  of various amino acids including histidine (His), glycine (Gly), leucine (Leu), L-glutamic acid (Glu), alanine (Ala), phenylalanine (Phe), threonine (Thre), lysine (Lys) and methionine (Met) were carried out by monitoring the emission band at 450 nm upon excitation wavelength of 345 nm and the plot per time unit was shown in Fig. 3.23.

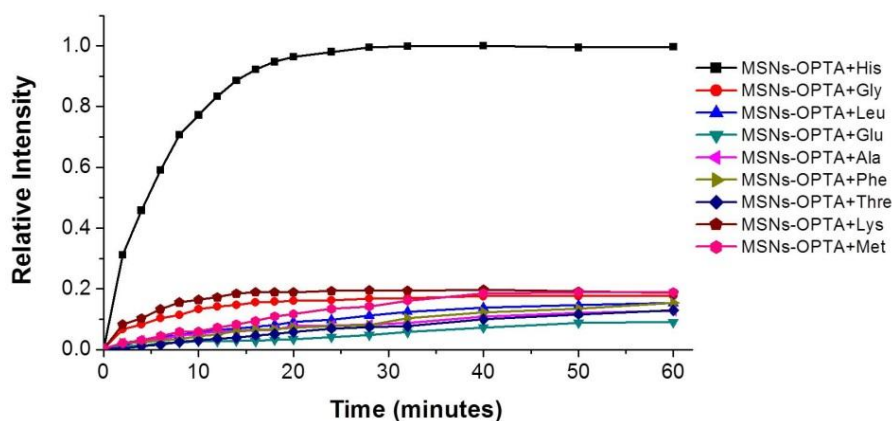


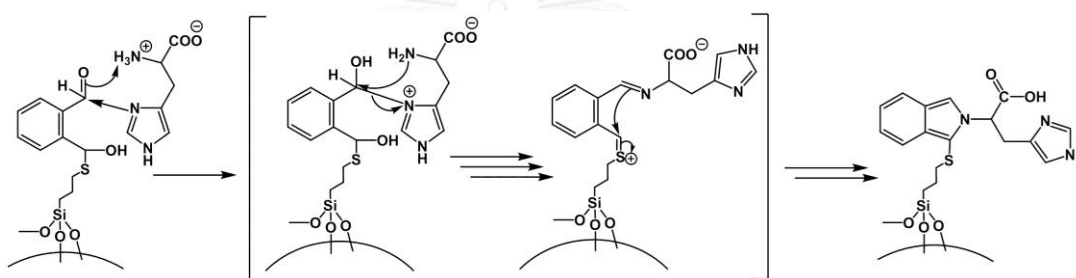
**Figure 3.23** Kinetic measurements of the fluorescence detection of OPTA-derivatized mesoporous silica (MSNs-OPTA) toward 150  $\mu\text{M}$  of various amino acid in 0.01 M phosphate buffer solution, excited wavelength of 345 nm

The result obviously illustrated that histidine exhibited high relative intensity change of isoindole product which is constant after 20 minutes, while other amino acids showed a small fluorescent change and spent long time to reach the constant except Lys and Gly which spent around 15 minutes. From the result, it was proposed that the reaction rates of biogenic amines did not be influenced by the size-sieving approach of these mesoporous materials because the similar sizes of the biogenic amines performed similarly reaction rates except histidine. Considerably, glycine possesses the smallest molecule, while others are insignificant difference in molecular sizes. Furthermore, the fluorescence responses of SNPs-OPTA with various biogenic amines showed the similar trend with those of MSNs-OPTA with various biogenic amines. This is indicative of size-sieving independence toward the reaction rate.

Apart of charge interest of the biogenic amines, pI values of them were considered [57, 58]. Most of biogenic amines including Gly, Leu, Ala, Phe, Thr and

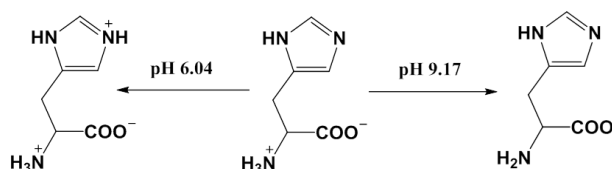
Met show negative charge, while Glu, Lys and His shows positive charge at pH 7.4. However, difference of molecular charge did not show the different fluorescence response as well. Therefore, it could be concluded that charges and molecular sizes of biogenic amines did not significantly effect on the reaction rate and the binding affinity.

From Kielland's research, imidazole on histamine acting as a self-catalyst for binding to Histamine Blue was reported [59]. According to this report, role of imidazole on histidine was proposed as a self-catalyst and carboxylate group was served as a powerful neutralization of intermediates to promote the formation of isoindole product as a proposed mechanism in Scheme 3.13.



**Scheme 3.13** Proposed mechanism for a self-catalyst of histidine to form isoindole product

To prove the mechanism, fluorescence responses of isoindole product in various pHs were examined. We hypothesized that if the imidazole group in histidine base showed ability to be a self-catalyst, the amount of isoindole product will be declined at acidic condition because of the protonated form of the imidazole group.



**Scheme 3.14** Proposed structures of histidine at different pH [60]

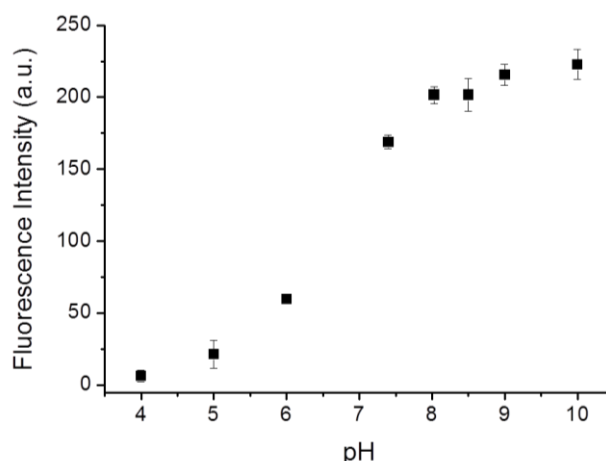


**Figure 3.24** Effects of pH on fluorescence intensity of isoindole products

The relationship of the pH and the fluorescence intensity of isoindole products was illustrated in Fig. 3.24. The fluorescence intensity of isoindole product decreased dramatically at  $\text{pH} < 7.4$ , while the fluorescence intensity showed slight increase at  $\text{pH} > 7.4$ . The result showed a strong evidence to support the role of a self-catalyst of imidazole in formation of isoindole product.

According to  $\text{p}K_a$  value [60], the positive charge of the imidazole group could be generated at pH lower than 6.04. The self-catalyst capability of imidazole group in protonated imidazole form would be decreased at the  $\text{pH} < 7.4$  causing a decrease of fluorescence intensity. Alternatively, the fluorescence intensity of the sensor system with histidine at  $\text{pH} > 9.00$  was slightly increased. This can be explained that the deprotonated form of amine group based on biogenic amines performs a strong nucleophile to attack carbonyl group of aldehyde to form the isoindole products. The structure of histidine at different pH is shown in Scheme 3.14.

### 3.3.5 Complexation studies of MSNs-OPTA-CTAB and receptor molecules (ZnD2 and E2) with various biogenic amines

#### 3.3.5.1 Particle properties by varying concentration of CTAB

To reduce self-quenching of fluorophore on Zn(II) complexes in histidine detection, MSNs-OPTA coated with CTAB was prepared and studied in buffer solution. CTAB were automatically entrapped on the silica surface by electrostatic interaction between silica and CTAB. To verify the physical properties of MSNs-



OPTA-CTAB system by varying the amount of CTAB, **E2** was employed as an optical probe.

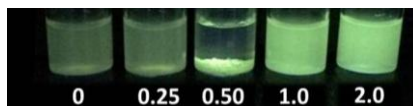
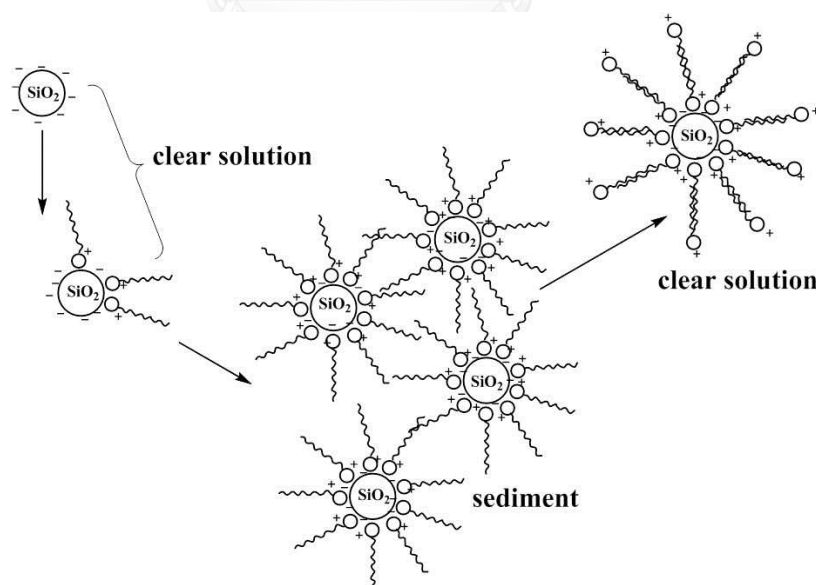


**Figure 3.25** Naked-eye fluorescence studies of MSNs-OPTA-E2-CTAB at various concentration of CTAB (0, 0.25, 0.5, 1 and 2 mM, respectively) in the presence of 0.1 mM **E2**, 0.01 M phosphate buffer solution at pH 7.4 under UV light

Naked-eye fluorescence studies at various concentration of CTAB (0, 0.25, 0.5, 1 and 2 mM, respectively) in the solution of 0.45 mg/mL MSNs-OPTA and 0.1 mM **E2** dissolved in 0.01 M phosphate buffer solution pH 7.4 were observed under UV-light as illustrated in Fig. 3.25. A well-dissolved silica materials in water was observed in the presence of CTAB less than 0.25 mM, while the sediment of silica materials in water appeared at the concentration of CTAB at 0.5 mM. Alternatively, the clear suspension of solution was observed at the concentration of CTAB around 1-2 mM. The phenomenon was proposed following the knowledge of Liu's research [61] (Scheme 3.15).



**Scheme 3.15** Possible scheme of CTAB mono- and bilayers on  $\text{SiO}_2$ /water interface, when the CTAB concentration was increased [61]

The observation of the aggregation form of MSNs-OPTA-CTAB was possibly caused by the perfect monolayer formation of CTAB on surface of MSNs. At higher concentration of CTAB, the bilayer formation of the surfactant around silica surface arranged the hydrophilic head to point out resulting in the well-dissolved particles in water. The possible scheme of CTAB mono- and bilayers on SiO<sub>2</sub>/water interface in various amount of CTAB was illustrated in Scheme 3.15.

To prove this phenomenon, zeta potential and particle size of MSNs-OPTA at various concentrations of CTAB were investigated to elucidate the formation between silica nanoparticles and CTAB in each condition. It was found that at low concentration of CTAB (0.125 mM), zeta potential values of the particles showed negative charge around -13.03 mV which is indicative of free negative charge on the silica surface addressing the monolayer formation of CTAB on some part of silica surface. Surprisingly, the particles were hydrated by water molecules resulting in well-dissolved particles in water solution and the proposed formation was shown in Scheme 3.15. The aggregation of particles at 0.5 mM CTAB showed the zeta potential at +3.93 mV, which corresponded to the complete monolayer formation of CTAB on silica surface. Therefore, surface of particles possessed the hydrophobic property which was insoluble in water. At the concentration of CTAB about 0.75 and 1 mM, zeta potential showed positive charge values at +14.89 and +24.07, respectively. These conditions showed well suspension of the particles as demonstrated in Fig. 3.25. Owing to high concentration of CTAB, formation of bilayer of CTAB on silica surface was induced through hydrophobic interaction of hydrocarbon tails. The surfactant bilayer formation enhanced water solubility due to positive charge on nano-SiO<sub>2</sub>/CTAB/water systems as shown in Scheme 3.15 (clear solution).

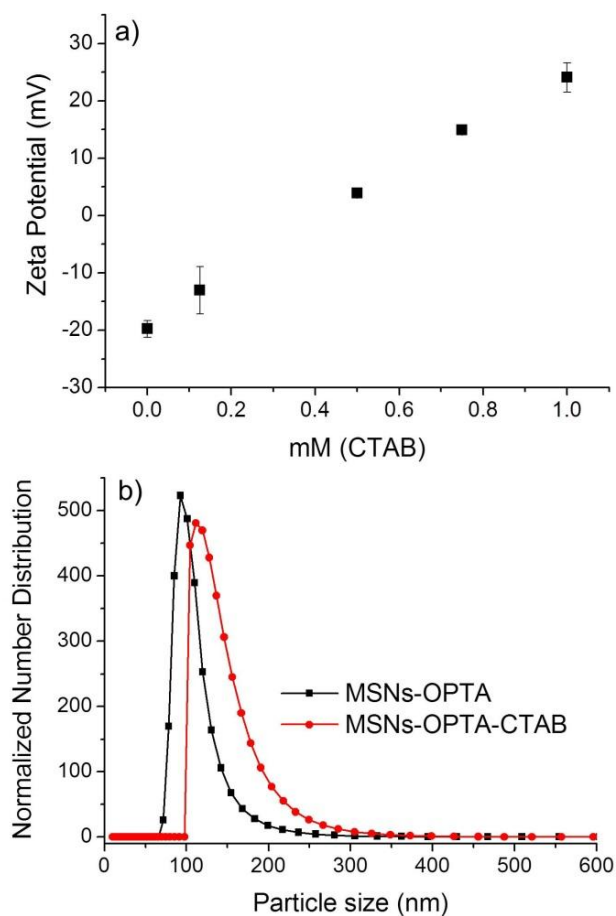


**Figure 3.26** a) Zeta potential of the MSNs-OPTA 0.45 mg/mL at different concentrations of CTAB (0–1 mM) b) size distributions of MSNs-OPTA and MSNs-OPTA-CTAB at 1.0 mM CTAB analyzed by laser diffraction

Furthermore, size distribution was examined to verify the particle formation. Size distributions of the particles at 0 and 1 mM CTAB were measured by dynamic light scattering (DLS) showing the particle size of 92.64 and 111.57 nm, respectively (Fig. 3.26 (b)). This result confirmed the swelling particles by the formation of CTAB bilayer around the particles. In this research, the MSNs-OPTA-CTAB system at 1 mM CTAB was applied to classify biogenic amine which showed high dispersion of particles in the system. Because of the surfactant bilayer formation, water solubility of the system was enhanced.

### 3.3.5.2 Complexation studies

At first design, we took an attempt to prepare the **ZnD2** complex. Unfortunately, **ZnD2** complex cannot be obtained. To solve this problem, **D2** was studied the complexation abilities with various metal cations. The formation between **D2** and different metal ions in buffer solution such as phosphate and HEPES buffer solution, pH 7.4, was investigated. It was found that **D2** in HEPES buffer solution showed different responses in detection of metal ions, especially Zn (II) ion as shown in Fig. 3.27.

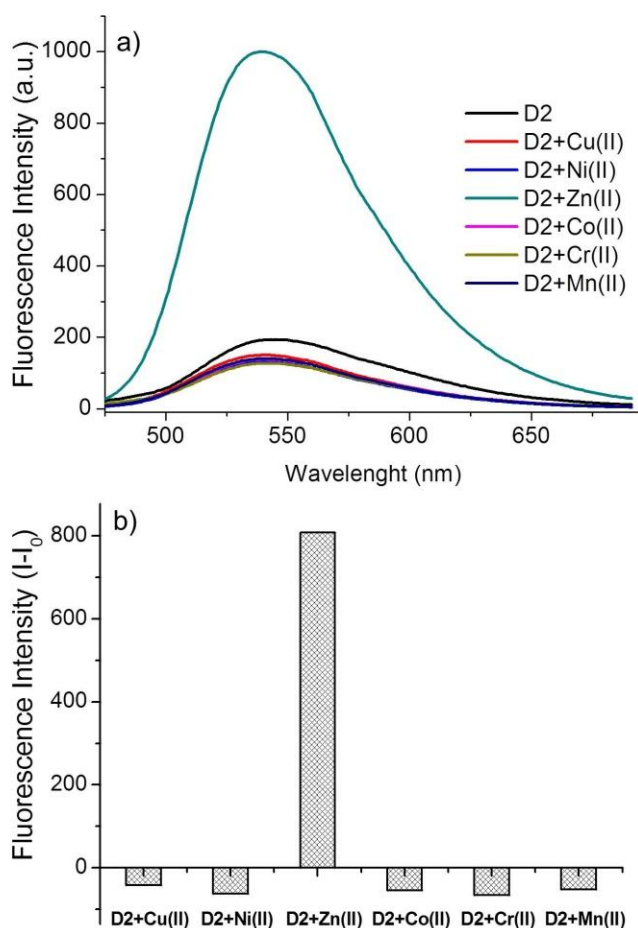


**Figure 3.27** Fluorescence responses of **D2** toward different metal ions namely Cu (II), Ni (II), Zn (II), Co (II), Cr (II) and Mn (II) in 1% DMSO:HEPES buffer (0.01M, pH7.4) with excitation at 450 nm

The fluorescence responses of ligand **D2** in the presence of various metal ions in HEPES buffer solution showed the fluorescent enhancement at 530 nm for Zn (II)

ion. This is indicative of the specific binding of **D2** toward Zn (II) ion, while other metal ions including Cu (II), Ni (II), Co (II), Cr (II) and Mn (II) did not affect to the fluorescence responses of **D2**. The mechanism of the binding event was proposed that the dipicolylamine of the **D2** preferred to coordinate to Zn (II) ion. The electron density of the fluorophore was reduced because of sharing electron density to Zn (II) atom. The consequent inhibition of PET process on **D2** fluorophore was observed. As a result, the fluorescence intensity of the fluorophore was increased upon binding with Zn (II) ion.

**ZnD2** complex was applied to detect histidine in MSNs-OPTA-CTAB system. The system consisting of MSNs-OPTA, CTAB, Zn (II) and **D2** was further used for histidine sensing. Firstly, MSNs-OPTA-CTAB and **ZnD2** was separately prepared by stirring at room temperature. After that, the mixture solution of MSNs-OPTA-CTAB and **ZnD2** was mixed. Upon addition of **ZnD2**, which was prepared by stirring the solution of Zn(II) and **D2** in HEPES solution, to the solution of MSNs-OPTA and CTAB, the clear solution of MSNs-OPTA-CTAB became turbid that can be detected by naked eye. This was proposed that free Zn (II) in solution acts as competitive CTAB-binding silica surface and consequently obstructs the CTAB to form interaction with silica surface. Therefore, **ZnD2** was not experienced to detect histidine in the system.

In our hypothesis, we proposed that the interaction between **D2** and MSNs-OPTA-CTAB could be occurred by hydrophobic interaction. To prove this hypothesis, the complexation studies of MSNs-OPTA-CTAB and **D2** were carried out in the presence of histidine with varying the concentration of **D2**.

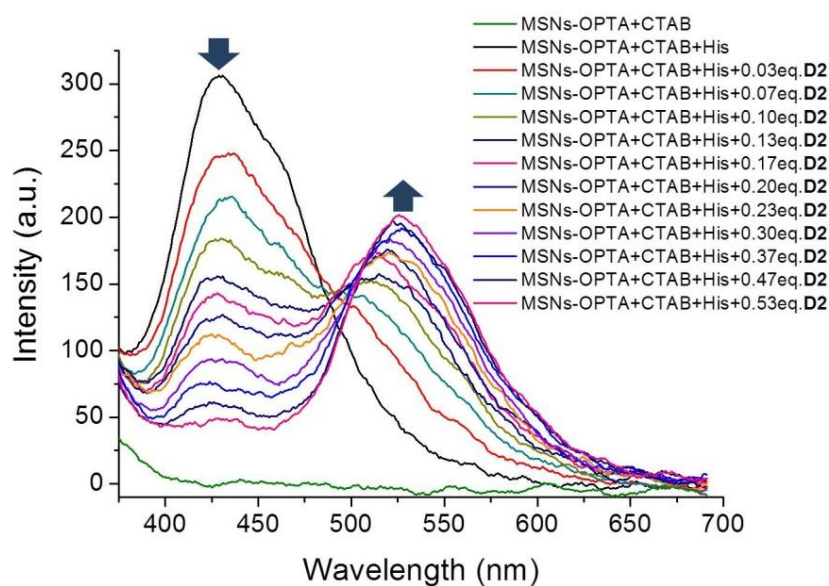


**Figure 3.28** Fluorescence responses of isoindole product in the presence of **D2** at various concentrations in MSNs-OPTA (0.45 mg/mL), 1 mM CTAB dispersed in phosphate buffer solution, pH 7.4,  $\lambda_{\text{ex}} = 345 \text{ nm}$

Fluorescence responses of isoindole product which was generated from the reaction of histidine and MNPs-OPTA-CTAB system toward various concentration of **D2** were investigated. The fluorescent intensity at 425 nm was decreased upon the increment of **D2** with a concomitant increase of emission band at 530 nm as shown in Fig. 3.28. This signified that energy transfer between isoindole product and the naphthalimide of **D2** was occurred. It can be explained that the receptor molecule (**D2**) was preferentially inserted in the hydrocarbon chain of CTAB without specific binding between donor and acceptor molecules.

The system consisting of MSNs-OPTA, CTAB and **D2** was applied to study a specific detection of various biogenic amines including alanine (Ala), glutamic acid (Glu), glycine (Gly), histidine (His), leusine (Leu), lysine (Lys) and phenylalanine (Phe) in phosphate buffer solution. For this study, we employed the concentration of **D2** at 75  $\mu\text{M}$ . It was found that only histidine exhibited the fluorescent enhancement at 425 and 530 nm as shown in Fig. 3.29.

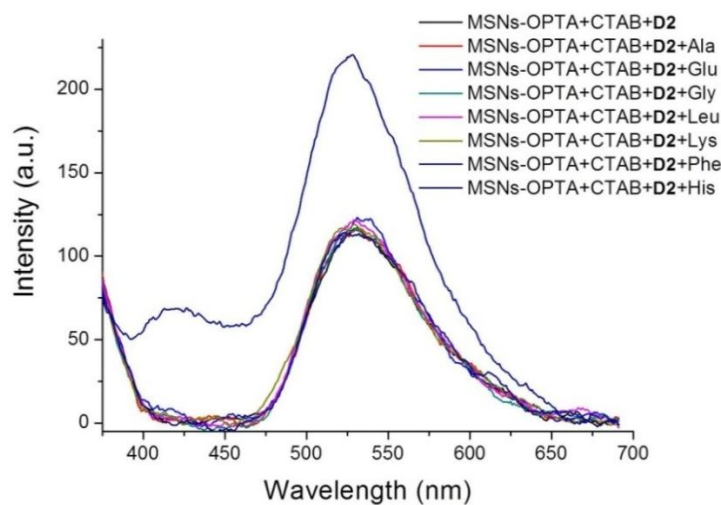


**Figure 3.29** Fluorescence responses of sensor MSNs-OPTA (0.45 mg/mL), 1 mM CTAB and 75  $\mu\text{M}$  **D2** in 1% DMSO:phosphate buffer solution (0.01 M, pH 7.4) in the presence of 150  $\mu\text{M}$  of various amino acids,  $\lambda_{\text{ex}} = 345 \text{ nm}$

Moreover, the fluorophore **E2** consisting of naphthalene dicarboxylic acid anhydride and hydrocarbon chain was designed and synthesized to be a control molecule without Zn (II) binding site. Moreover, it was expected that the hydrocarbon chain as hydrophobic part could induce better insertion of **E2** in hydrocarbon of CTAB on silica surface and the system could be more efficient in energy transfer.

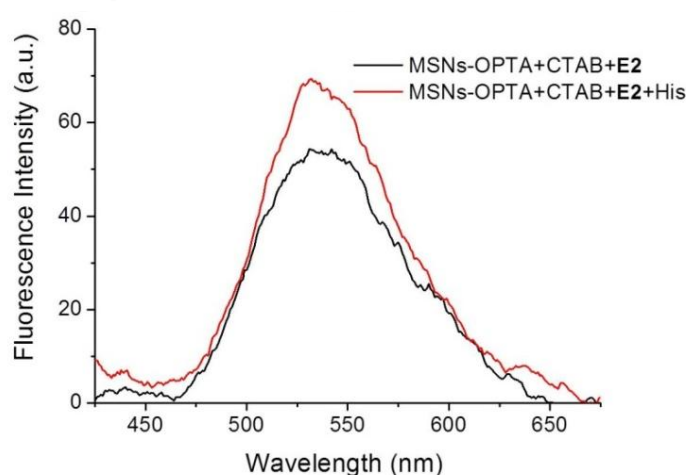
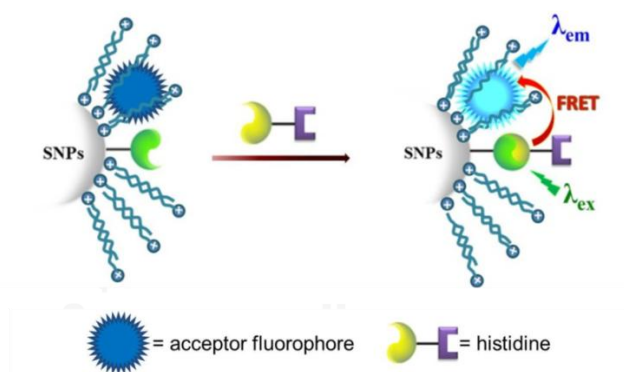


**Figure 3.30** Fluorescence responses of sensor MSNs-OPTA (0.45 mg/mL), 1 mM CTAB and 75  $\mu\text{M}$  **D2** in 1% DMSO: phosphate buffer solution (0.01 M, pH 7.4) in the presence of 150  $\mu\text{M}$  histidine

However, the result showed that a small change in fluorescence response after adding histidine in the solution. It was implied that the hydrocarbon chain of **E2** could be packed very well with hydrocarbon chain of CTAB. Thus, this approach showed a highly steric hindrance towards histidine to react with OPTA unit attached on MSNs. As the result, the system did not be continue to study.

Definitely, it has been concluded that the energy transfer was occurred through space interaction between isoindole product to **D2** and **E2**. These results gave a strong evidence that the energy transfer between donor and acceptor fluorophores entrapped in MSNs-OPTA-CTAB system can occur without the direct interaction between two fluorophores but it stemmed thought space of close proximity of the donor and acceptor fluorophores encapsulated in MSNs/CTAB system. The proposed intermolecular energy transfer through non-binding interaction was depicted in Scheme 3.16.



**Scheme 3.16** Binding event between MSNs-OPTA-CTAB and acceptor fluorophores (**D2** or **E2**)

Based on the intermolecular energy transfer, a longer emission band of this approach offers the high benefits for biological sensing diagnosis. Definitely, the system of MSNs-OPTA-CTAB and **D2** served as a highly promising sensitivity and selectivity of histidine detection via FRET process.



## CHAPTER IV

### CONCLUSION

The design and synthesis of new fluorescence sensor systems for determination of biogenic amine have been performed. In this research, silica nanoparticles (SNPs) and mesoporous silica nanoparticles (MSNs) applied as solid support to enhance water solubility was modified by primary amine sensitive *o*-phthalic hemithioacetal (OPTA) to yield SNPs-OPTA and MSNs-OPTA, respectively. The modified silica materials were applied to detect primary amines which enable to generate isoindole product as a donor fluorophore in the detection systems.

Coumarin derivative containing a boronic acid (**CB**) has been designed and synthesized to classify catecholamine. This sensory molecule was a complementary sensor to discriminate biogenic amines in SNPs-OPTA. It was found that in SNPs-OPTA solution, all biogenic amines enabled to form an isoindole product which displayed the emission band at 450 nm ( $\lambda_{\text{ex}} = 345\text{nm}$ ) due to the reaction between OPTA and primary amine. Interestingly, the case of histidine showed the highest fluorescence intensity at 450 nm while other biogenic amines showed low fluorescence intensity. To discriminate the catecholamine, the addition of **CB** as acceptor fluorescence sensor providing the emission band at 500 nm in SNPs-OPTA system induced the reaction of dopamine (DA) and norepinephrine (NE) with boronic acid based **CB** resulting in the fluorescence quenching of coumarin at 500 nm. Therefore, we have successfully developed a new fluorescence sensory system to discriminate the catecholamine of DA and NE from other biogenic amines under PET process.

To determine histidine, Zn (II) fluorophore namely **ZnC2** and **ZnD2** as receptor fluorophores were designed and synthesized. Only **ZnC2** was successfully synthesized. The use of **ZnC2** in SNPs-OPTA system provided the fluorescence quenching of isoindole product at 450 nm and disappearance of emission band at 550 nm belonging to **ZnC2**. As our hypothesis, the fluorescence self-quenching was possibly caused by orderly packing of naphthalimide based **ZnC2** on the surface of silica under strong interaction between positive charge of Zn (II) on the **ZnC2** and

negative charge on silica surface. To avoid this effect, cationic surfactant cetyltrimethylammonium bromide (CTAB) was applied as a neutralizing molecule. Interestingly, the system of SNPs-OPTA\_CTAB upon increment of the **ZnC2** showed a decrease of fluorescence intensity at 450 nm and an increase of fluorescence intensity at 550 nm in case of histidine. This is indicative of the favorite energy transfer process. Moreover, the solutions of the sensors in the presence of guest molecules were investigated with naked-eye study under UV-light. In case of histidine, it exhibited a high fluorescence brightness of blue and green colors regarding isoindole product and **ZnC2**, respectively. It was clear that the SNPs-OPTA\_CTAB system possessing **ZnC2** showed high selectivity for the detection of histidine in water solution and this system offered an excellently naked-eye sensor of histidine under UV-light.

Moreover, mesoporous silica nanoparticles (MSNs) were also utilized as supporting matrix incorporated with amine-sensitive *o*-phthalic hemithioacetal (OPTA) group on the pore-surface. Fluorescence responses of MSNs-OPTA with various amino acids exhibited the strong fluorescence at 450 nm in the case of histidine. Furthermore, the kinetic studies of isoindole product illustrated that histidine exhibited high relative intensity change of isoindole product, while other amino acids showed a small fluorescence change. The factors of molecular size and *pKa* of guests did not influence on binding ability between MSNs-OPTA and biogenic amines because all biogenic amines bearing a similar molecular size showed a similar performance of fluorescence responses except histidine, and the difference of molecular charge did not affect the fluorescence response. From study on isoindole product at various pH values, the result showed a strong evidence to support the role of imidazole as a self-catalyst in formation of isoindole product. For analytical application, the calibration plots showed a good linear relationship between the fluorescence intensity at 450 nm and the logarithm of the histidine concentration. The linear regression equation was  $F(\text{a.u.}) = 283.43 \log (\text{Histidine}(\mu\text{M})) - 138.37$  with a linear regression coefficient of 0.9990. The detection limit and quantification limit were calculated to be 17.7 nM and 59.22 nM, respectively.

To reduce self-quenching of fluorophore in histidine detection, MSNs-OPTA coated with CTAB was prepared and studied in buffer solution. Due to the surfactant bilayer formation on MSNs-OPTA, water solubility of MSNs-OPTA-CTAB system was enhanced. To confirm the energy transfer caused by non-interaction between guest linker bound on MSNs-OPTA-CTAB and the acceptor dyes, **D2** and **E2** acted as the model dyes which have no specific binding site to interact with imidazole based histidine. The results still showed a fluorescence enhancement of dyes in the presence of histidine in these systems. These gave strong evidences that the energy transfer between donor and acceptor fluorophores entrapped in MSNs-OPTA-CTAB system can occur without the direct interaction between two fluorophores.



## REFERENCES



- [1] Pradhan, T., Jung, H.S., Jang, J.H., Kim, T.W., Kang, C., and Kim, J.S. Chemical sensing of neurotransmitters. Chemical Society Reviews 43(13) (2014): 4684-4713.
- [2] Hettie, K.S., Liu, X., Gillis, K.D., and Glass, T.E. Selective Catecholamine Recognition with NeuroSensor 521: A Fluorescent Sensor for the Visualization of Norepinephrine in Fixed and Live Cells. ACS Chemical Neuroscience 4(6) (2013): 918-923.
- [3] Feng, J.-J., Guo, H., Li, Y.-F., Wang, Y.-H., Chen, W.-Y., and Wang, A.-J. Single Molecular Functionalized Gold Nanoparticles for Hydrogen-Bonding Recognition and Colorimetric Detection of Dopamine with High Sensitivity and Selectivity. ACS Applied Materials & Interfaces 5(4) (2013): 1226-1231.
- [4] Stewart, A.J., Hendry, J., and Dennany, L. Whole Blood Electrochemiluminescent Detection of Dopamine. Analytical Chemistry 87(23) (2015): 11847-11853.
- [5] Mercante, L.A., et al. Electrospun Polyamide 6/Poly(allylamine hydrochloride) Nanofibers Functionalized with Carbon Nanotubes for Electrochemical Detection of Dopamine. ACS Applied Materials & Interfaces 7(8) (2015): 4784-4790.
- [6] Zhang, X., et al. Highly Sensitive and Selective Detection of Dopamine Using One-Pot Synthesized Highly Photoluminescent Silicon Nanoparticles. Analytical Chemistry 87(6) (2015): 3360-3365.
- [7] Lenders, J.W.M., Eisenhofer, G., Mannelli, M., and Pacak, K. Pheochromocytoma. The Lancet 366(9486): 665-675.
- [8] Schifferdecker, B., Kodali, D., Hausner, E., and Aragam, J. Adrenergic Shock - An Overlooked Clinical Entity? Cardiology in Review 13(2) (2005): 69-72.
- [9] Hughes, A.J., Daniel, S.E., Kilford, L., and Lees, A.J. Accuracy of clinical diagnosis of idiopathic Parkinson's disease: a clinico-pathological study of 100 cases. Journal of Neurology, Neurosurgery & Psychiatry 55(3) (1992): 181-184.
- [10] Kawai, Y., et al. Molecular characterization of histidinemia: identification of four missense mutations in the histidase gene. Hum Genet 116(5) (2005): 340-6.
- [11] Taylor, R.G., Levy, H.L., and McInnes, R.R. Histidase and histidinemia. Clinical and molecular considerations. Mol Biol Med 8(1) (1991): 101-16.

- [12] Holmes, C., Eisenhofer, G., and Goldstein, D.S. Improved assay for plasma dihydroxyphenylacetic acid and other catechols using high-performance liquid chromatography with electrochemical detection. Journal of Chromatography B: Biomedical Sciences and Applications 653(2) (1994): 131-138.
- [13] Wu, Y.-B., Wu, J.-H., Shi, Z.-G., and Feng, Y.-Q. Simultaneous determination of 5-hydroxyindoles and catechols from urine using polymer monolith microextraction coupled to high-performance liquid chromatography with fluorescence detection. Journal of Chromatography B 877(20–21) (2009): 1847-1855.
- [14] dos Santos, M.P., Rahim, A., Fattori, N., Kubota, L.T., and Gushikem, Y. Novel amperometric sensor based on mesoporous silica chemically modified with ensal copper complexes for selective and sensitive dopamine determination. Sensors and Actuators B: Chemical 171–172 (2012): 712-718.
- [15] Yu, D., Zeng, Y., Qi, Y., Zhou, T., and Shi, G. A novel electrochemical sensor for determination of dopamine based on AuNPs@SiO<sub>2</sub> core-shell imprinted composite. Biosensors and Bioelectronics 38(1) (2012): 270-277.
- [16] Liu, S., et al. A novel label-free electrochemical aptasensor based on graphene–polyaniline composite film for dopamine determination. Biosensors and Bioelectronics 36(1) (2012): 186-191.
- [17] Paugam, M.-F., Valencia, L.S., Boggess, B., and Smith, B.D. Selective Dopamine Transport Using a Crown Boronic Acid. Journal of the American Chemical Society 116(24) (1994): 11203-11204.
- [18] Kim, J., Raman, B., and Ahn, K.H. Artificial Receptors That Provides a Preorganized Hydrophobic Environment: A Biomimetic Approach to Dopamine Recognition in Water. The Journal of Organic Chemistry 71(1) (2006): 38-45.
- [19] Ishizu, T., Hirayama, J., and Noguchi, S. Complex Formation of Cyclo(L-Phe-L-Pro)<sub>4</sub> with Noradrenaline Hydrochloride. CHEMICAL & PHARMACEUTICAL BULLETIN 42(5) (1994): 1146-1148.
- [20] Campayo, L., et al. A Proton-Ionizable Ester Crown of 3,5-Disubstituted 1H-Pyrazole Able To Form Stable Dinuclear Complexes with Lipophilic Phenethylamines. The Journal of Organic Chemistry 62(9) (1997): 2684-2693.
- [21] Gavin, J.A., Garcia, M.E., Benesi, A.J., and Mallouk, T.E. Chiral Molecular Recognition in a Tripeptide Benzylviologen Cyclophane Host. The Journal of Organic Chemistry 63(22) (1998): 7663-7669.

- [22] Molt, O., Rübeling, D., and Schrader, T. A Selective Biomimetic Tweezer for Noradrenaline. Journal of the American Chemical Society 125(40) (2003): 12086-12087.
- [23] Odashima, K., Yagi, K., Tohda, K., and Umezawa, Y. Dopamine-selective response in membrane potential by homooxalix[3]arene triether host incorporated in PVC liquid membrane. Bioorganic & Medicinal Chemistry Letters 9(16) (1999): 2375-2378.
- [24] Molt, O. and Schrader, T. Highly Sensitive Recognition of Substrates of Adrenergic Receptors at the Air/Water Interface. Angewandte Chemie International Edition 42(44) (2003): 5509-5513.
- [25] Makote, R. and Collinson, M.M. Template Recognition in Inorganic–Organic Hybrid Films Prepared by the Sol–Gel Process. Chemistry of Materials 10(9) (1998): 2440-2445.
- [26] Mannironi, C., Di Nardo, A., Fruscoloni, P., and Tocchini-Valentini, G.P. In Vitro Selection of Dopamine RNA Ligands. Biochemistry 36(32) (1997): 9726-9734.
- [27] Lin, V.S.Y., Lai, C.-Y., Huang, J., Song, S.-A., and Xu, S. Molecular Recognition Inside of Multifunctionalized Mesoporous Silicas: Toward Selective Fluorescence Detection of Dopamine and Glucosamine. Journal of the American Chemical Society 123(46) (2001): 11510-11511.
- [28] Radu, D.R., Lai, C.-Y., Wiench, J.W., Pruski, M., and Lin, V.S.Y. Gatekeeping Layer Effect: A Poly(lactic acid)-coated Mesoporous Silica Nanosphere-Based Fluorescence Probe for Detection of Amino-Containing Neurotransmitters. Journal of the American Chemical Society 126(6) (2004): 1640-1641.
- [29] Raymo, F.M. and Cejas, M.A. Supramolecular Association of Dopamine with Immobilized Fluorescent Probes. Organic Letters 4(19) (2002): 3183-3185.
- [30] Feng, P., Bu, X., and Pine, D.J. Control of Pore Sizes in Mesoporous Silica Templated by Liquid Crystals in Block Copolymer–Cosurfactant–Water Systems. Langmuir 16(12) (2000): 5304-5310.
- [31] Mbaraka, I.K., McGuire, K.J., and Shanks, B.H. Acidic Mesoporous Silica for the Catalytic Conversion of Fatty Acids in Beef Tallow. Industrial & Engineering Chemistry Research 45(9) (2006): 3022-3028.
- [32] Goel, S., et al. VEGF121-Conjugated Mesoporous Silica Nanoparticle: A Tumor Targeted Drug Delivery System. ACS Applied Materials & Interfaces

- 6(23) (2014): 21677-21685.
- [33] Tan, J., Wang, H.-F., and Yan, X.-P. Discrimination of Saccharides with a Fluorescent Molecular Imprinting Sensor Array Based on Phenylboronic Acid Functionalized Mesoporous Silica. Analytical Chemistry 81(13) (2009): 5273-5280.
- [34] Hoffmann, F., Cornelius, M., Morell, J., and Fröba, M. Silica-Based Mesoporous Organic–Inorganic Hybrid Materials. Angewandte Chemie International Edition 45(20) (2006): 3216-3251.
- [35] Secor, K.E. and Glass, T.E. Selective Amine Recognition: Development of a Chemosensor for Dopamine and Norepinephrine. Organic Letters 6(21) (2004): 3727-3730.
- [36] Coskun, A. and Akkaya, E.U. Three-Point Recognition and Selective Fluorescence Sensing of L-DOPA. Organic Letters 6(18) (2004): 3107-3109.
- [37] Jang, Y.J., et al. Fluorescence Sensing of Dopamine. ChemInform 37(14) (2006): no-no.
- [38] Harding, M.M. and Cole, S.J. The crystal structure of di(histidino)zinc pentahydrate. Acta Crystallographica 16(7) (1963): 643-650.
- [39] Fabbrizzi, L., Licchelli, M., Parodi, L., Poggi, A., and Taglietti, A. The Molecular Design of Fluorescent Sensors for Ionic Analytes. Journal of Fluorescence 8(3) (1998): 263-271.
- [40] Fabbrizzi, L., Francese, G., Licchelli, M., Perotti, A., and Taglietti, A. Fluorescent sensor of imidazole and histidine. Chemical Communications (6) (1997): 581-582.
- [41] Xu, Y., et al. Switch-on Fluorescence Sensing of Glutathione in Food Samples Based on a Graphitic Carbon Nitride Quantum Dot (g-CNQD)–Hg<sup>2+</sup> Chemosensor. Journal of Agricultural and Food Chemistry 63(6) (2015): 1747-1755.
- [42] Nguyen, D.M., Frazer, A., Rodriguez, L., and Belfield, K.D. Selective Fluorescence Sensing of Zinc and Mercury Ions with Hydrophilic 1,2,3-Triazolyl Fluorene Probes. Chemistry of Materials 22(11) (2010): 3472-3481.
- [43] Peng, X., Wu, Y., Fan, J., Tian, M., and Han, K. Colorimetric and Ratiometric Fluorescence Sensing of Fluoride: Tuning Selectivity in Proton Transfer. The Journal of Organic Chemistry 70(25) (2005): 10524-10531.
- [44] Yuan, L., Lin, W., Zheng, K., and Zhu, S. FRET-Based Small-Molecule



Fluorescent Probes: Rational Design and Bioimaging Applications. Accounts of Chemical Research 46(7) (2013): 1462-1473.

- [45] Jisha, V.S., Thomas, A.J., and Ramaiah, D. Fluorescence Ratiometric Selective Recognition of Cu<sup>2+</sup> Ions by Dansyl–Naphthalimide Dyads. The Journal of Organic Chemistry 74(17) (2009): 6667-6673.
- [46] Chaicham, A., Sahasithiwat, S., Tuntulani, T., and Tomapatanaget, B. Highly effective discrimination of catecholamine derivatives via FRET-on/off processes induced by the intermolecular assembly with two fluorescence sensors. Chemical Communications 49(81) (2013): 9287-9289.
- [47] Sanguansap, Y., Ruangpornvisuti, V., Tuntulani, T., Promarak, V., and Tomapatanaget, B. Highly promising discrimination of various catecholamines using ratiometric fluorescence probes with intermolecular self-association of two sensing elements. RSC Advances 5(96) (2015): 78468-78475.
- [48] Roth, M. Fluorescence reaction for amino acids. Analytical Chemistry 43(7) (1971): 880-882.
- [49] Stöber, W., Fink, A., and Bohn, E. Controlled growth of monodisperse silica spheres in the micron size range. Journal of Colloid and Interface Science 26(1) (1968): 62-69.
- [50] Yang, Z., Xia, Y., and Mokaya, R. High Surface Area Silicon Carbide Whiskers and Nanotubes Nanocast Using Mesoporous Silica. Chemistry of Materials 16(20) (2004): 3877-3884.
- [51] Yee, J.K., Parry, D.B., Caldwell, K.D., and Harris, J.M. Modification of quartz surfaces via thiol-disulfide interchange. Langmuir 7(2) (1991): 307-313.
- [52] Kim, H., Kim, S., Park, C., Lee, H., Park, H.J., and Kim, C. Glutathione-Induced Intracellular Release of Guests from Mesoporous Silica Nanocontainers with Cyclodextrin Gatekeepers. Advanced Materials 22(38) (2010): 4280-4283.
- [53] Cui, Y., Dong, H., Cai, X., Wang, D., and Li, Y. Mesoporous Silica Nanoparticles Capped with Disulfide-Linked PEG Gatekeepers for Glutathione-Mediated Controlled Release. ACS Applied Materials & Interfaces 4(6) (2012): 3177-3183.
- [54] Schneider, P. Adsorption isotherms of microporous-mesoporous solids revisited. Applied Catalysis A: General 129(2) (1995): 157-165.

- [55] Maue, M. and Schrader, T. A Color Sensor for Catecholamines. Angewandte Chemie 117(15) (2005): 2305-2310.
- [56] Zhu, Y.-D., Peng, J., Jiang, L.-P., and Zhu, J.-J. Fluorescent immunosensor based on CuS nanoparticles for sensitive detection of cancer biomarker. Analyst 139(3) (2014): 649-655.
- [57] Jack, K.S., Vizcarra, T.G., and Trau, M. Characterization and Surface Properties of Amino-Acid-Modified Carbonate-Containing Hydroxyapatite Particles. Langmuir 23(24) (2007): 12233-12242.
- [58] Bodner, G.M. Assigning the pKa's of polyprotic acids. Journal of Chemical Education 63(3) (1986): 246.
- [59] Kielland, N., Vendrell, M., Lavilla, R., and Chang, Y.-T. Imaging histamine in live basophils and macrophages with a fluorescent mesoionic acid fluoride. Chemical Communications 48(59) (2012): 7401-7403.
- [60] Zubavichus, Y., et al. Surface Chemistry of Ultrathin Films of Histidine on Gold As Probed by High-Resolution Synchrotron Photoemission. The Journal of Physical Chemistry B 109(2) (2005): 884-891.
- [61] Liu, Y., Tourbin, M., Lachaize, S., and Guiraud, P. Silica nanoparticles separation from water: Aggregation by cetyltrimethylammonium bromide (CTAB). Chemosphere 92(6) (2013): 681-687.



**APPENDIX**

จุฬาลงกรณ์มหาวิทยาลัย  
CHULALONGKORN UNIVERSITY

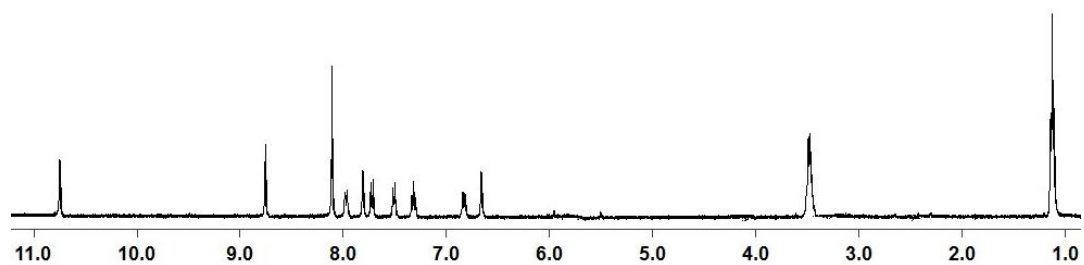


**Figure A1** The  $^1\text{H}$ -NMR spectrum of sensor **CB** in  $\text{DMSO-}d_6$  at 400 MHz

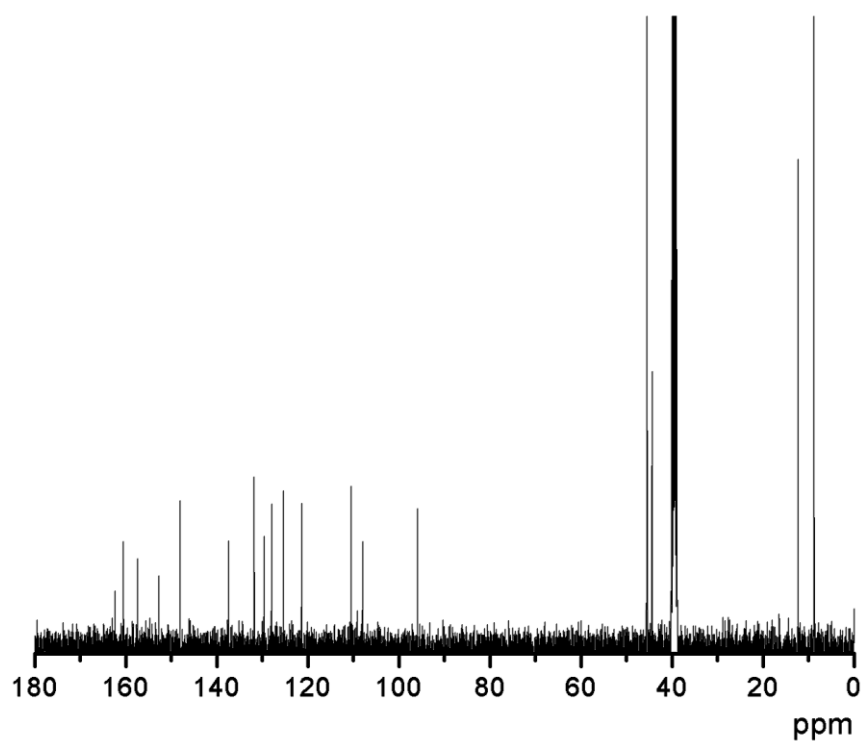


**Figure A2** The  $^{13}\text{C}$ -NMR spectrum of sensor **CB** in  $\text{DMSO-}d_6$  at 400 MHz

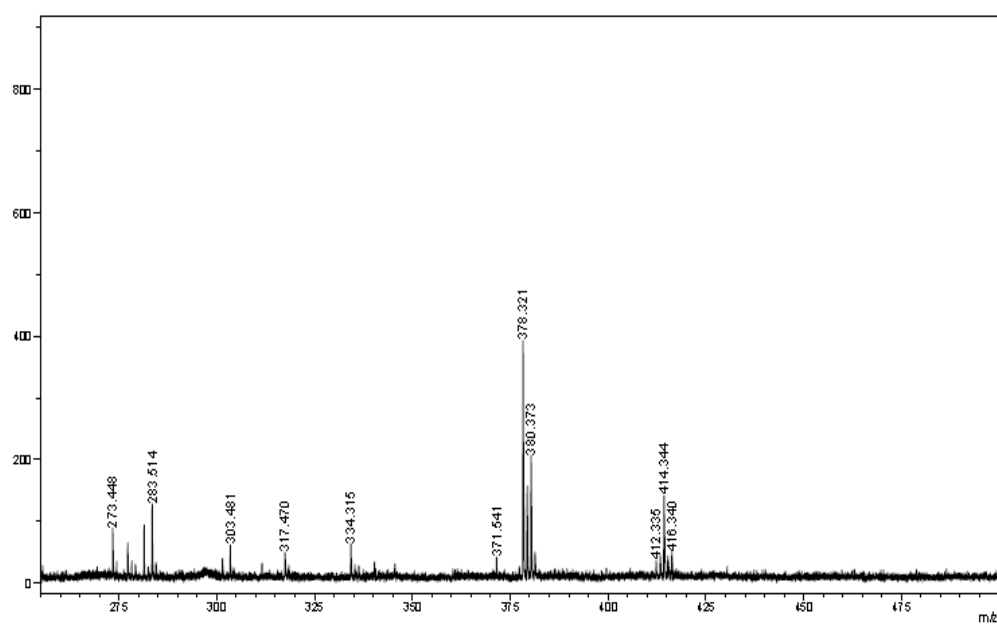


**Figure A3** MALDI-TOF mass spectrum of sensor **CB** shown at 380.373 m/z

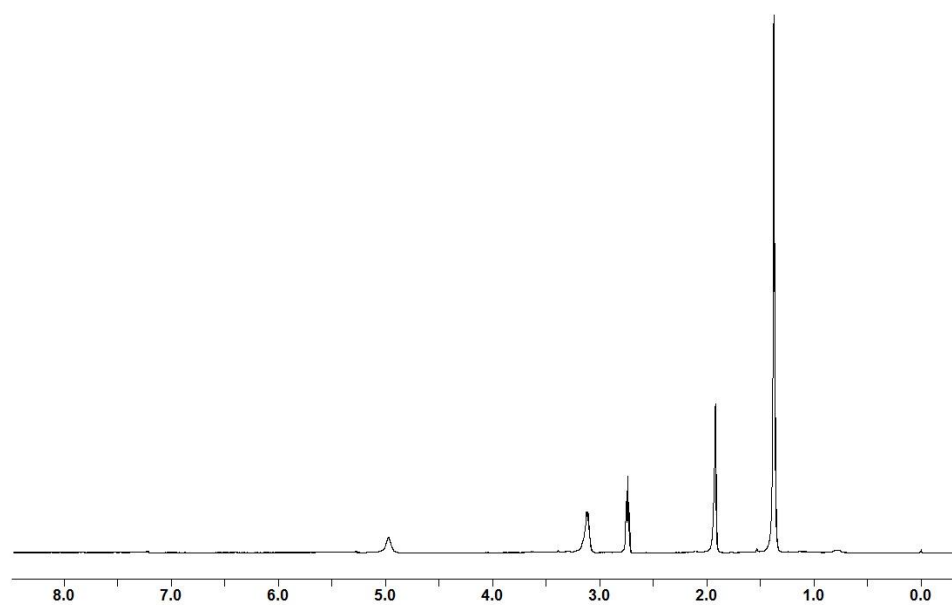


**Figure A4** The  $^1\text{H}$ -NMR spectrum of **B1** in  $\text{CDCl}_3$  at 400 MHz

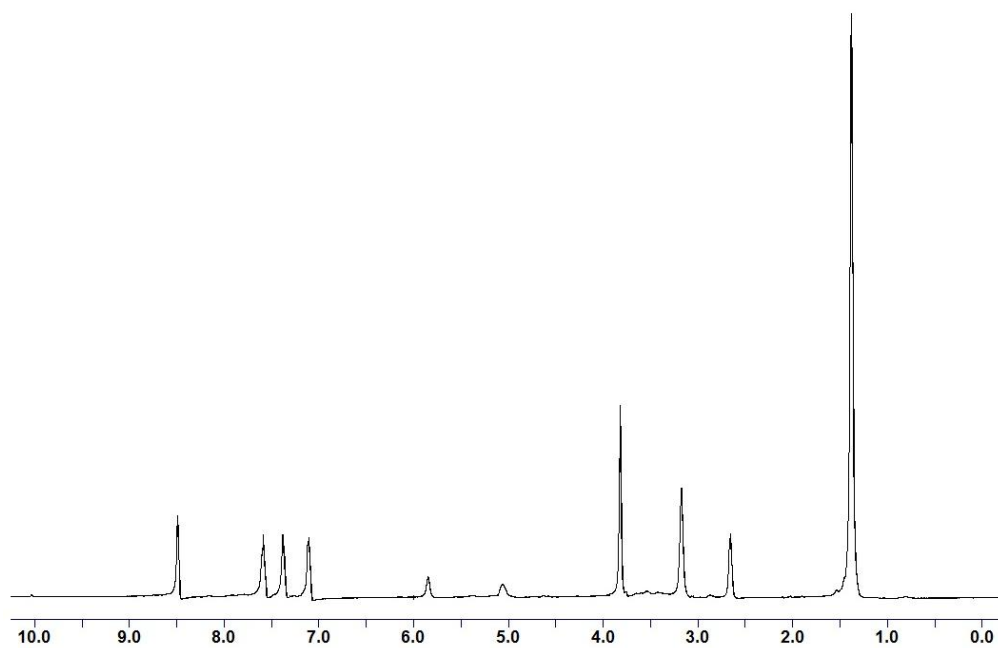


**Figure A5** The <sup>1</sup>H-NMR spectrum of **B2** in CDCl<sub>3</sub> at 400 MHz

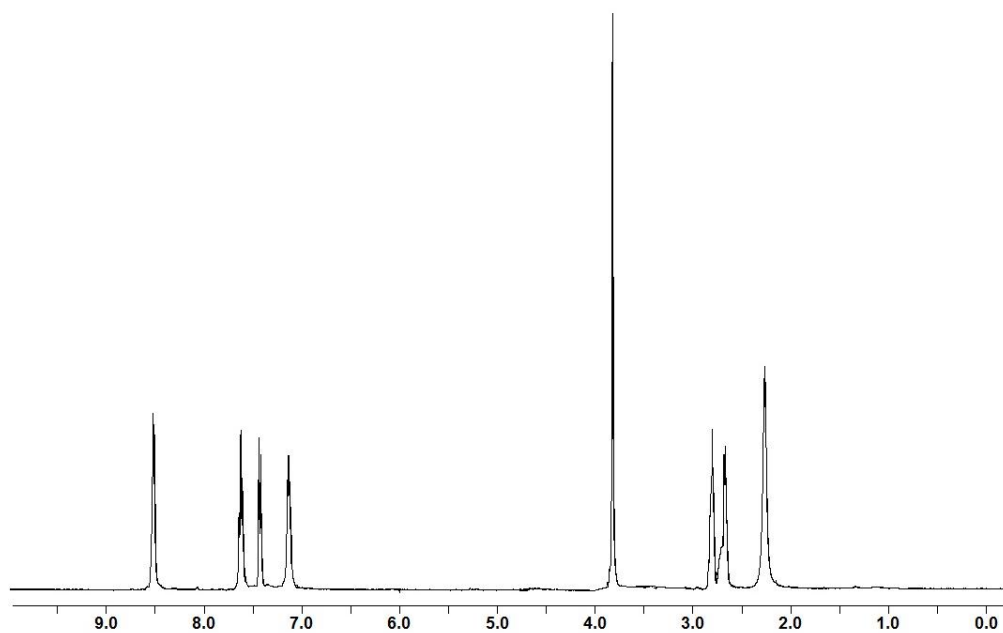


**Figure A6** The <sup>1</sup>H-NMR spectrum of **B3** in CDCl<sub>3</sub> at 400 MHz

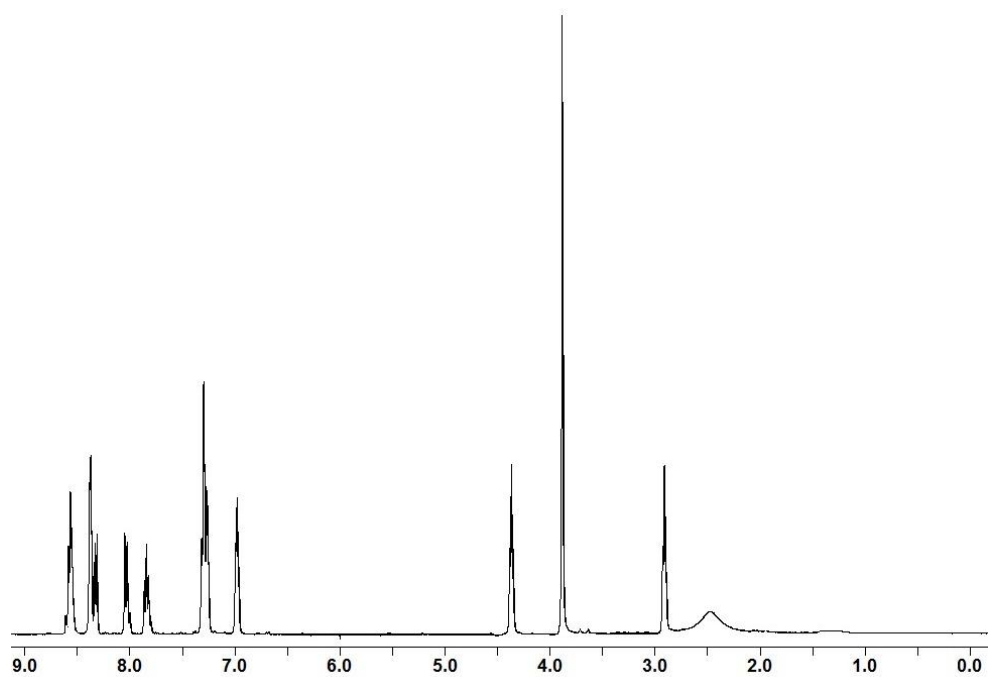


**Figure A7** The  $^1\text{H-NMR}$  spectrum of **C1** in  $\text{CDCl}_3$  at 400 MHz

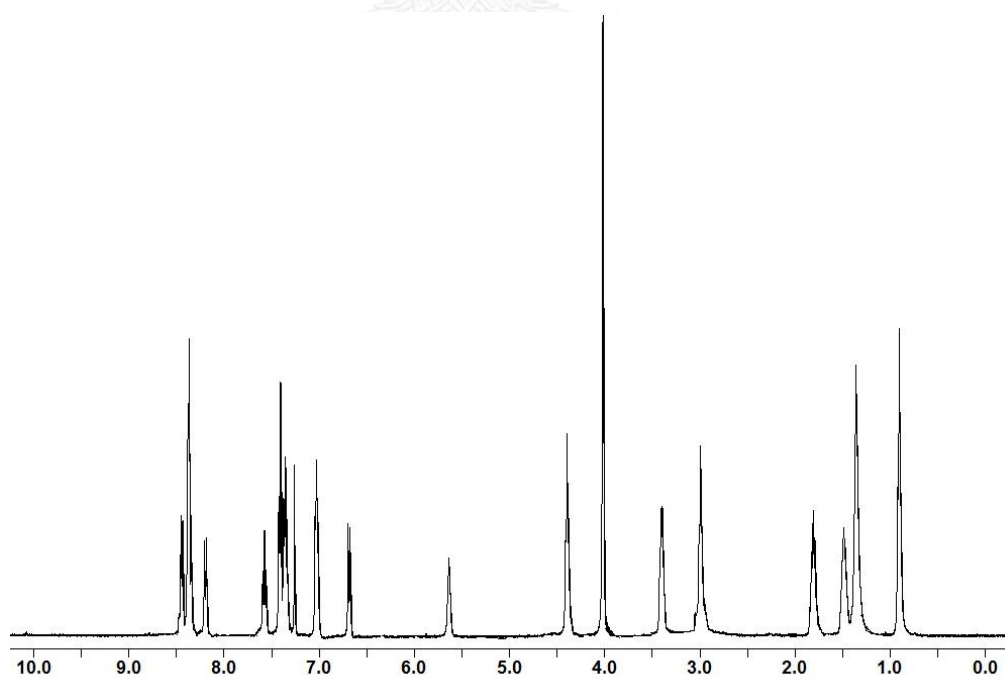


**Figure A8** The  $^1\text{H-NMR}$  spectrum of **C2** in  $\text{CDCl}_3$  at 400 MHz

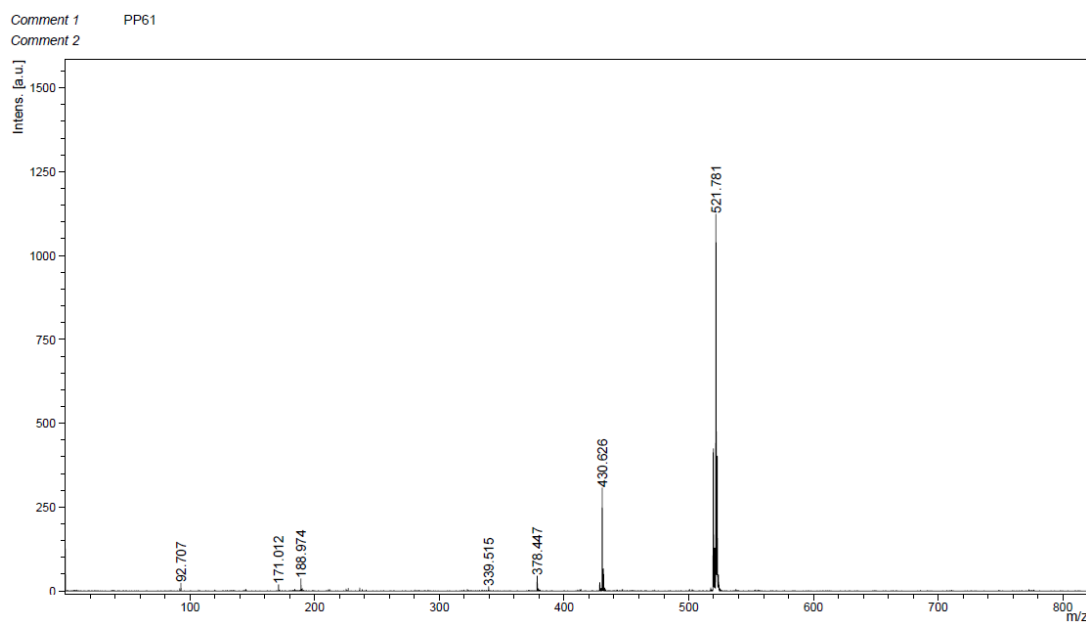


**Figure A9** The ESI-High Resolution Mass spectrum of sensor **C2** shown at 521.781 m/z

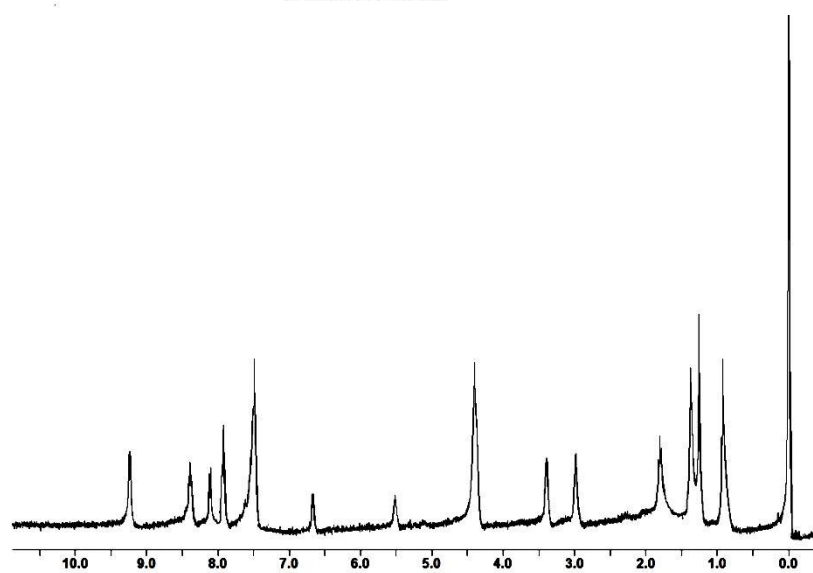


**Figure A10** The  $^1\text{H}$ -NMR spectrum of **ZnC2** in  $\text{CDCl}_3$  at 400 MHz



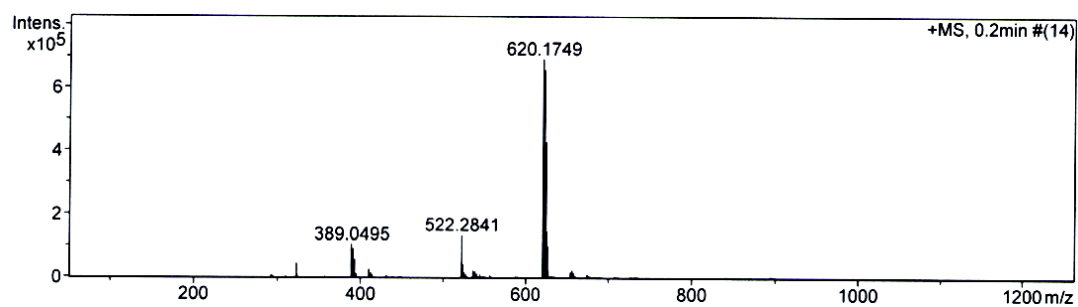


**Figure A11** The ESI-High Resolution Mass spectrum of sensor **ZnC2** shown at 620.1749 m/z

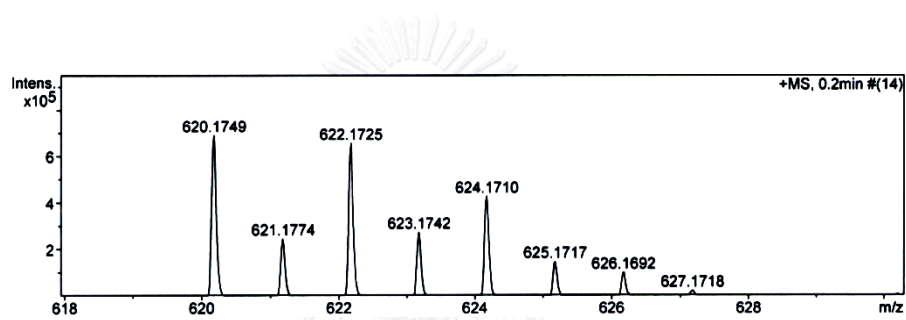


**Figure A12** The ESI-High Resolution Mass spectrum of isotope peak of Zn (II) in sensor **ZnC2**

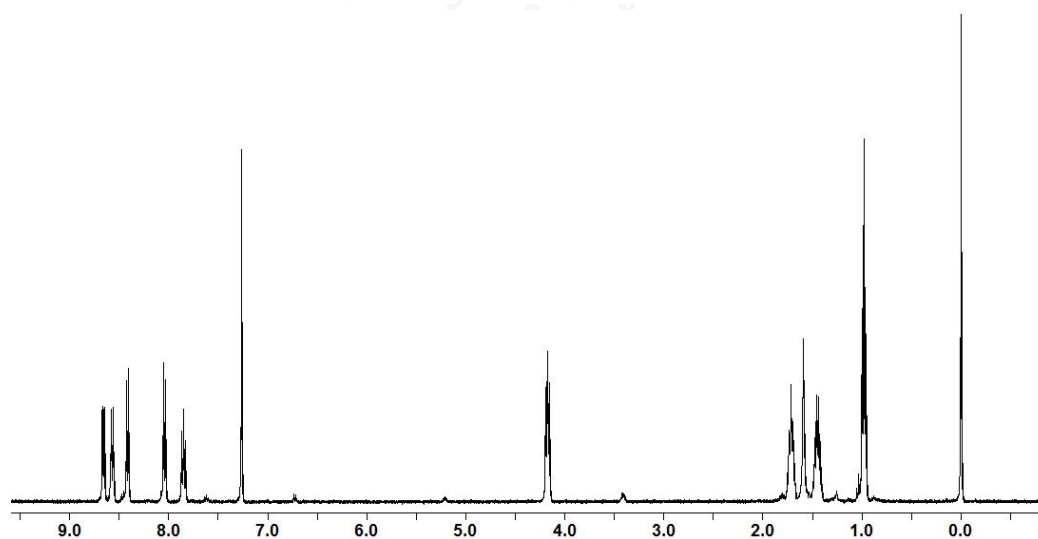


**Figure A13** The <sup>1</sup>H-NMR spectrum of **D1** in CDCl<sub>3</sub> at 400 MHz

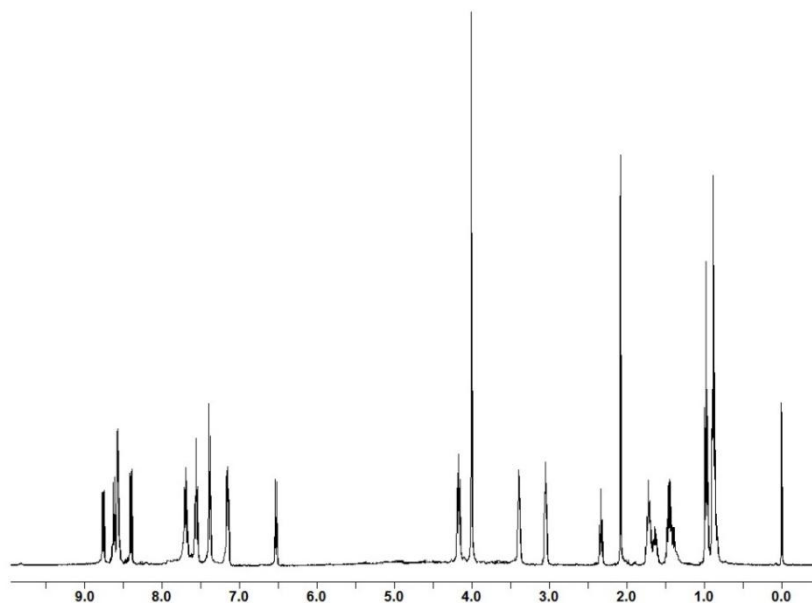


**Figure A14** The  $^1\text{H}$ -NMR spectrum of **D2** in  $\text{CDCl}_3$  at 400 MHz

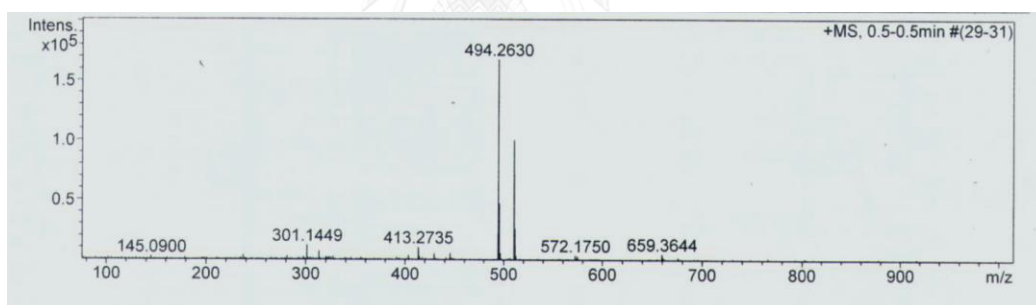


**Figure A15** The ESI-High Resolution Mass spectrum of sensor **D2**

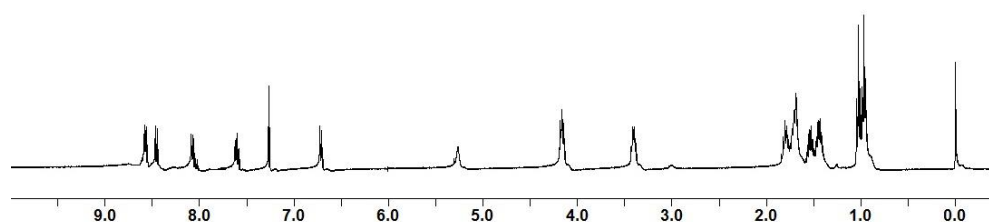


**Figure A16** The  $^1\text{H}$ -NMR spectrum of **E2** in  $\text{CDCl}_3$  at 400 MHz

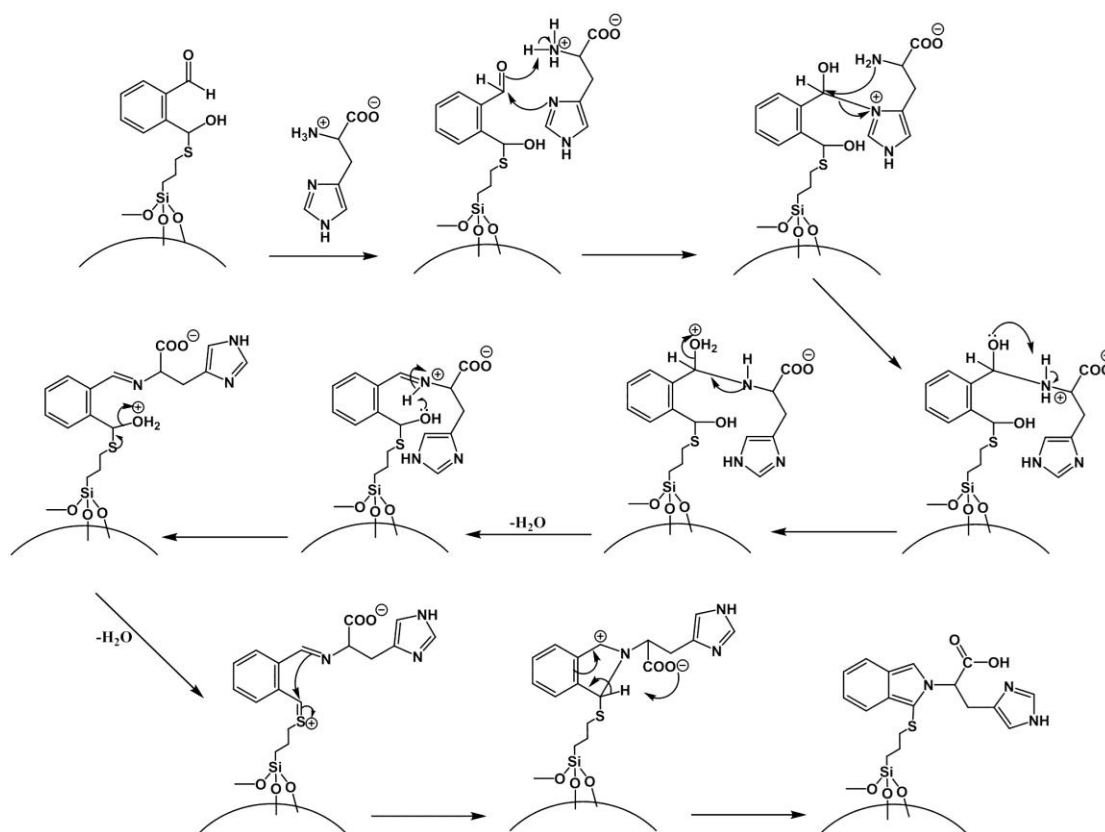


**Figure A17** Proposed mechanism for a self-catalyst of histidine to form isoindole product in physiological solution.

## VITA

Miss Premrudee Promdet was born on July 9th, 1989 in Nakorn Sri Thammarat province, Thailand. She finished secondary school at Triam Udom Suksa School of the South. She was a student under The Development and Promotion of Science and Technology Talent Project (DPST) from 2008-until now. She graduated and received a B.Sc. (Chemistry) 1st class honor from Department of Chemistry, Faculty of Science, Prince of Songkla University and completed the program in academic year 2015.



